Copy
RM SL54C24

This document consists of 73 pages
No. 5 of 5 Copies, Series B

RESEARCH MEMORANDUM

for the

Atomic Energy Commission

AN INVESTIGATION OF THE LONGITUDINAL STABILITY AND AFTERBODY PRESSURE CHARACTERISTICS OF SPECIALIZED STORE CONFIGURATIONS AT TRANSONIC SPEEDS

By John A. Braden and Beverly Z. Henry, Jr.

Langley Aeronautical Laboratory
Langley Field, Va.

[redacted]

NATIONAL ADVISORY COMMITTEE
FOR AERONAUTICS

WASHINGTON

MAR 31 1954

[redacted]

NACA RM SL54C24

[redacted]

NATIONAL ADVISORY COMMITTEE FOR AERONAUTICS

RESEARCH MEMORANDUM

for the

Atomic Energy Commission

AN INVESTIGATION OF THE LONGITUDINAL STABILITY AND AFTERBODY PRESSURE CHARACTERISTICS OF SPECIALIZED STORE CONFIGURATIONS AT TRANSONIC SPEEDS

By John A. Braden and Beverly Z. Henry, Jr.

SUMMARY

An investigation was conducted in the Langley 8-foot transonic pressure tunnel to determine the longitudinal stability and afterbody pressure characteristics of the TX-14 and TX-16 special weapons. The tests were conducted in the Mach number range from about 0.60 to 1.20 at stagnations pressures of 0.40 and 0.60 atmosphere. The Reynolds numbers for the investigation, based on the maximum body diameter, varied from approximately 0.6×10^6 to 0.9×10^6 for 0.40 atmosphere and from 1.10×10^6 to 1.4×10^6 for 0.60 atmosphere.

Dynamic tests of the TX-14 configuration indicated a very low margin of static stability at all Mach numbers whereas the level of dynamic stability was shown to be generally high. Investigations at 0.40 and 0.60 atmosphere indicated that within this Reynolds number range, there was no significant effect of Reynolds number on the longitudinal stability characteristics of the TX-14 configuration.

The TX-16 configuration that was comparable to the TX-14 in fin and spoiler arrangement was unsatisfactory from the standpoint of static stability. The small-finned configurations of the TX-16 displayed large Mach number regions of static instability for all spoiler-band arrangements. Increasing the size and number of spoiler bands as well as fin size on the TX-16 produced substantial improvements in static stability with only small reductions in dynamic stability indicated. A forward movement of the center of gravity on two TX-16 configurations produced improvements in both the dynamic and static stability per[redacted]

Pressure measurements on the TX-14 and TX-16 afterbodies in the angle-of-attack range of $\pm 2^{\circ}$ showed that the equivalent altitude error which may be expected from a pressure-operated fusing device, set for a fusing altitude of 3,000 feet, would be of the order of $\pm 1{,}000$ feet. At greater angles of attack, these errors increased significantly for all model configurations tested.

In general, the longitudinal stability performance of the TX-14 was shown to have been satisfactory through the Mach number range. The TX-16 configuration which displayed the more desirable stability characteristics utilized the large stabilizing fins and the greatest number of large spoiler bands tested with this fin configuration. It was noted that the highly separated flow conditions over these weapons would restrict effective control of the center of pressure by means of minor changes in weapon configuration.

INTRODUCTION

With the attainment of operational aircraft capable of releasing special weapons from high altitudes at Mach numbers near unity, it is probable that weapons so released will obtain supersonic speeds during their descent. As a result, the longitudinal stability problems associated with transonic and supersonic speeds become of major importance to the free-fall characteristics of these bodies.

In accordance with the request of the Atomic Energy Commission and in cooperation with the Sandia Corporation, an investigation was made in the Langley 8-foot transonic pressure tunnel to determine the longitudinal stability characteristics of 0.104-scale models of the TX-14 and TX-16 special weapons. In conjunction with the stability tests, an investigation was made to determine possible pressure port locations which would be suitable for operation of a barometric fusing device. The investigation covered the Mach number range from 0.6 to 1.2 and was conducted at stagnation pressures of approximately 0.40 and 0.60 atmosphere. Because of the highly specialized nature of the special-weapons program and since this investigation constitutes only a portion of the overall performance analysis, the scope of this paper is to evaluate only those results obtained in the 8-foot tunnel.

SYMBOLS

M_o free-stream Mach number

V_o free-stream velocity, ft/sec

[redacted]

ρ_o free-stream density, slugs/cu ft

p_o free-stream static pressure, lb/sq ft

p local static pressure, lb/sq ft

L body length, ft

d maximum body diameter, ft

S body frontal area, sq ft

R Reynolds number, based on d

C_m pitching-moment coefficient, taken about body center of gravity, $\dfrac{\text{Pitching moment}}{\left(\frac{1}{2}\rho_o V_o^2\right)Sd}$

C_L lift coefficient, $\dfrac{\text{Lift}}{\left(\frac{1}{2}\rho_o V_o^2\right)S}$

I transverse moment of inertia of the body about its center of gravity, slug-ft^2

$T_{1/2}$ time to damp to one-half amplitude for a decaying motion, sec

P period of oscillation, sec

α angle of attack, radians or deg

q pitching velocity, radians/sec

C_{m_q} effective rate of change of pitching-moment-curve slope with reduced pitching velocity, $\left.\dfrac{\partial C_m}{\partial\left(\frac{qd}{2V}\right)}\right|_{q \to 0}$

$C_{m_{\dot{\alpha}}}$ effective rate of change of pitching-moment-curve slope with reduced rate of angle of attack, $\left.\dfrac{\partial C_m}{\partial\left(\frac{\dot{\alpha}d}{2V}\right)}\right|_{\dot{\alpha} \to 0}$

[redacted]

$C_{m_q} + C_{m_{\dot{\alpha}}}$ rotational damping coefficient, per radian

C_{m_α} static-longitudinal-stability parameter, $\partial C_m/\partial\alpha$, per deg

APPARATUS AND MODELS

Wind tunnel.- The Langley 8-foot transonic pressure tunnel, the test section of which is shown schematically in figure 1, is a closed system, single-return type and for these tests permitted continuous testing up to a Mach number of about 1.2 at stagnation pressures of about 0.40 and 0.60 atmosphere. The test section is rectangular in shape and is slotted in the axial direction downstream of the effective minimum section with four slots in each of the top and bottom wall panels. The slot width increases from zero at the origin to full open 100 inches downstream from the origin where the combined widths of the slots comprise approximately 10 percent of the inside periphery of the tunnel. The geometric cross-sectional area at the minimum-area station is 50.5 square feet and at a typical model test location 120 inches from the slot origin and 151 inches downstream of the minimum section, the cross-sectional area is about 50.9 square feet. Tunnel calibrations have indicated that the maximum deviation from the average free-stream Mach number was about ±0.008 under supersonic free-stream conditions and about ±0.004 at Mach numbers less than 1.00. Although no specific measurements were available, observation of the dynamic models when allowed to oscillate freely gave no indication of stream misalinement. The Reynolds number for these tests (fig. 2), based on the maximum diameter of the model, varied from about 0.6×10^6 to 0.9×10^6 at approximately 0.40 atmosphere, and from 1.0×10^6 to 1.4×10^6 at about 0.60 atmosphere.

The models were sting-mounted on the tunnel support system, figure 1, which was capable of remotely controlled axial movement to insure the proper location of the models in the test section. Angle-of-attack changes were made by rotation of the downstream end of the support tube along a vertical, circular arc, the center of which was located near the model center of gravity.

Models.- The models tested in this investigation, figure 3, were provided by the Sandia Corporation and consisted of two basic body shapes designated as the TX-14 and the TX-16. The maximum diameter of both bodies was 6.386 inches and represented the full-size weapons to 0.104 scale. The TX-16 model was obtained by lengthening the cylindrical maximum diameter section of the TX-14 by 7.614 inches which increased the overall body length from 22.968 inches (TX-14) to 30.582 inches (TX-16) and the fineness ratio from 3.6 to 4.8. Coordinates for the forebody and afterbody shapes are given in table I.

The models were constructed principally of aluminum and utilized cruciform wedge-type fins attached to the afterbody section at an angle of 45° from the vertical plane. The 6°-14° fins are shown in figure 4 along with the two sizes of spoiler bands used in the investigation. A cutaway drawing of the TX-14 mounted on the dynamic sting assembly is shown in figure 5. The nose and afterbody sections were screw-fastened to the yoke of the dynamic rig and the models were statically balanced about their pitch axis by means of the steel counterweights. Changes in the center-of-gravity positions were made by a longitudinal shift of the model on the yoke. The models were actuated and controlled by the hydraulic pistons for which a fluid pressure of about 1,000 pounds per square inch was used. The attitude of the model was determined by the output of the strain-gage beam.

To obtain pressure measurements over the rear portion of each configuration, separate models were used. These models were identical in external shape to those used for dynamic testing but were fitted with three rows of static pressure orifices over the rear portion. Location of these orifices is shown in table II. These pressure models used a model sting which was instrumented at two axial stations with electrical strain gages which were used to obtain approximate values of lift and pitching moment.

TESTS AND METHODS

The TX-14 was installed in the test section with the model nose-flat located about 113 inches downstream of the slot origin, whereas the nose-flat of the TX-16 was located at about the 106-inch station. The normal center-of-gravity position of the TX-16 was located at the 40.8-percent model station (120 inches, full scale) whereas the TX-14 was tested with the center of gravity located at the 37.1-percent station (81.8 inches, full scale).

The dynamic and static stability data were obtained by deflecting the model from a stream alinement position to an angle of attack of about +7° and locking it in this deflected position. Upon release, the model was allowed to oscillate with one degree of freedom. Three successive records of the time history of this oscillation were recorded on each of two types of instruments: one a photographically recording galvanometer and the other a direct-inking oscillograph.

The natural frequency of the model and support system in the pitch direction was about 16 cycles per second, well in excess of the model frequencies encountered. Continuous monitoring of sting stresses during the stability investigations by means of electrical strain gages attached at the intersection of the cylindrical and conical portions of the model

[redacted]

sting support, indicated negligible deflections of the support system under all loading conditions.

The pressure models were installed in the test section at the same respective tunnel locations as the dynamic models. However, in order to position the top and bottom rows of orifices in the pitch plane, the pressure models were rolled on the support system 22.5° (clockwise, looking upstream).

The TX-14 pressure model was tested at angles of attack from -2° to +2° and the TX-16 was tested from -4° to +12°. All pressure data were photographically recorded from multiple-tube manometers and force data were manually recorded from sensitive-dial potentiometers.

The total temperature and dew point of the tunnel air were automatically controlled to reduce possible humidity effects on the flow in the test section. Stagnation pressures were manually recorded from an automatically compensating mercury-filled manometer. Flow visualization in the vicinity of the model was obtained through the use of standard schlieren photography.

REDUCTION OF DATA

The rotational damping coefficients $C_{m_q} + C_{m_{\dot{\alpha}}}$ and the static-longitudinal-stability parameter C_{m_α} were reduced as in reference 1 according to the following equations:

$$-\left(C_{m_q} + C_{m_{\dot{\alpha}}}\right) = \frac{1.386}{T_{1/2}}\left(\frac{4I}{\rho_o V_o S d^2}\right)$$

$$-C_{m_\alpha} = \frac{1.755\ I/d^3}{P^2 \rho_o V_o{}^2}$$

The time to damp to one-half amplitude $T_{1/2}$ and the period of model motion P were averaged from six successive oscillograph records taken at each test point with the two recording instruments. In the interests of consistency, since the damping rate was nonlinear with amplitude, the damping envelopes were constructed with the amplitude for the initial time as close to ±7° as possible. Static-position

[redacted]

calibrations, made at frequent intervals to determine the output of the strain beam with angle of attack, were sufficiently linear to permit the construction of the damping envelopes directly from the oscillograph records. Model moments of inertia were obtained through the use of a calibrated, torsional pendulum.

Inasmuch as the pressure tests were directed toward the evaluation of the pressure-sensing characteristics of individual orifices, these data have been presented as the variation of the pressure ratio p/p_o with Mach number.

In order to reduce the force data, calibrations were made of the strain gages mounted on the pressure model sting to determine the gage outputs with normal loads and load positions.

ACCURACY

The primary source of error involved in the reduction of these data was the nonrepeatability of the six successive damping envelopes recorded at each test point. Differences between the individual values of the time to damp to one-half of the initial amplitude and the average of the six records varied from about 0 to 50 percent. These differences apparently increased in Mach number regions where the angle of trim of the model increased. In view of these conditions, it would be difficult to determine a particular value which would represent the overall precision of $C_{m_q} + C_{m_{\dot{\alpha}}}$. However, calculations of the probable error involved in the six successive readings indicated that the maximum probable error in $C_{m_q} + C_{m_{\dot{\alpha}}}$ would be about ± 2.0.

Excellent repeatability of the static stability parameter C_{m_α} was shown for all model configurations throughout the Mach number range. The accuracy of C_{m_α}, which is primarily dependent upon measurement of the frequency of model oscillation is considered to be within ± 0.002. It should be pointed out that the value of C_{m_α} as obtained from the dynamic tests represents an integrated average value measured between the oscillatory limits of the model ($\pm 7^\circ$) and is correct or incorrect to the extent that the actual slope of the moment curve is or is not linear. The effects of the strain-beam restoring moment and bearing friction on model oscillations have been discussed in reference 1, wherein the identical dynamic sting was employed. It was concluded from this discussion that neither the strain beam nor frictional forces affected model damping significantly.

At $M_o \approx 1.15$ the pressure models, as well as the dynamic models, were influenced by the model nose shock wave (bow wave) reflecting from the tunnel walls and striking the model base. The effects of this reflection which produced spurious results in comparison to the free-air case is discussed in the section entitled "Results and Discussion."

[redacted]

No attempt has been made to present the limits of accuracy for the force measurements inasmuch as installation of the strain gages to the pressure sting was incorporated in the pressure tests to provide general trends and approximate levels of the lift and pitching-moment coefficients. It is felt that the accuracy of the force data obtained was sufficient for these purposes. It should be noted that the lift coefficient as presented does not include the lift component associated with the axial force which was not obtained. The accuracy of the pressure ratios p/p_o and angle of attack α are considered to be within ± 0.002 and $\pm 0.1^\circ$, respectively.

RESULTS AND DISCUSSION

Longitudinal stability tests of the TX-14 were limited to an investigation of the effects of Reynolds number on the variation of the rotational damping coefficient $C_{m_q} + C_{m_{\dot{\alpha}}}$ and the static-longitudinal-stability parameter C_{m_α} with Mach number. Stability tests of the TX-16, however, included investigations of the effects of spoiler band size and arrangement as well as fin size and center-of-gravity movement on the longitudinal stability characteristics. Typical schlieren photographs (fig. 6) are shown for both models at selected test Mach numbers.

Results of the pressure tests are presented as the variation with Mach number of local static pressure ratios along the TX-14 and TX-16 afterbodies for several angle-of-attack conditions. In addition, force data are presented as the variation of lift and pitching-moment coefficients as a function of angle of attack through the Mach number range.

Dynamic Tests

In the interest of conciseness and in view of the large number of model configurations tested, particularly those of the TX-16, table III is presented as a summary of the major test results for the dynamic models. Included in the table are the spoiler band and fin arrangements used to obtain each model configuration, as well as the general effects on dynamic and static stability of each modification to the fins, spoiler arrangement, and center of gravity.

While the dynamic stability of the TX-14 was shown to be considerably lower than that of the TX-16, both models exhibited a generally high level of dynamic stability throughout the Mach number range and for all test configurations. The major stability problem associated with these bodies was apparently one of static rather than dynamic stability inasmuch as the levels of C_{m_α} were exceptionally low for the majority of the configurations.

[redacted]

The variations of dynamic and static stability with Mach number were essentially the same for both bodies as shown in figures 7 to 14. The effect of Mach number on dynamic stability was a gradual reduction up to $0.80 \geqq M_o \geqq 0.85$ followed by a generally increasing damping rate at the higher Mach numbers. For those configurations that were statically stable, the variation of C_{m_α} with Mach number indicated increasing stability up to $0.85 \leqq M_o \leqq 0.90$ followed by a destabilizing break which leveled off at $M_o \approx 1.00$ to values approximately equal to those shown for the low Mach numbers. Mach number regions in which the models became statically unstable are noted in the figures by gaps in the data.

To observe the body shock patterns and to correlate changes in the body flow fields with variations in the stability data, schlieren photographs were taken at each test Mach number. Figure 6 presents typical photographs of both models for several Mach number conditions. The extensions of the body shock patterns shown were constructed by means of schlieren observations made during the investigation and with the aid of tunnel-wall pressure data. A study of schlieren photographs indicated that compression shocks were formed initially on the nose section at $0.70 \leqq M_o \leqq 0.80$ with apparently detrimental effects to the flow over the afterbody. At $M_o \approx 0.90$ and higher, the oblique shocks on the nose were terminated by a strong normal shock which moved rearward with increases in Mach number (see fig. 6(d) $M_o = 0.931$) and would be expected to have adverse effects on static stability as it moved downstream. Further changes in the body flow fields with increases in Mach number are shown in the figure. At $M_o \approx 1.15$, the base of the model was struck by the model bow wave reflecting from the tunnel wall (figs. 6(c) and (f)). The vertical location of the model center line was 1.625 inches below that of the test section causing the shock reflection to strike the model asymetrically resulting in the model attempting to trim in a nose-down attitude. The actual trim angle as determined by changing the angle of the support system until the model floated free was approximately 17°. The general effect of this shock on both dynamic and static stability was to produce a narrow region of rapidly decreasing followed by suddenly increasing stability as the shock moved across the fins and downstream of the model base. For the majority of the configurations, the initial levels of C_{m_α} were not sufficiently high to prevent the models from becoming statically unstable in this region and dynamic records could not be obtained. The Mach number range over which the stability data may have been seriously affected by this shock reflection was estimated from schlieren photographs to be from about 1.10 to 1.15 for the TX-14 and from 1.10 to 1.17 for the TX-16.

TX-14.- Previous investigations of similar bodies, reference 1, have indicated that Reynolds number may have some effect on the longitudinal stability performance of these specialized body shapes. In an attempt to evaluate possible effects within the Reynolds number range of these tests, the TX-14 was tested at stagnation pressure levels of approximately 0.40 and 0.60 atmosphere with a resulting Reynolds number change

of from 0.6×10^6 to 0.9×10^6 and 1.10×10^6 to 1.4×10^6, respectively, based on the maximum body diameter. The results of this investigation are presented in figure 7. It is seen from the figure that within this Reynolds number range there is no effect of Reynolds number on the static-stability parameter C_{m_α}. Although no large effects on the damping coefficient are indicated, the normal scatter of the data prohibits definite conclusions as to the effects of Reynolds number on $C_{m_q} + C_{m_{\dot{\alpha}}}$. Tests of body shapes of low fineness ratio in reference 1, wherein the Reynolds number was varied from 2.15×10^6 to 2.50×10^6, also indicated no significant changes in the dynamic or static stability performance. However, because of the limited Reynolds number range of the present investigation, these data do not conclusively define the effects of Reynolds number on the longitudinal stability performance of the TX-14.

TX-16.- Configurations 2 to 9 (table III) were tested to evaluate the effects of spoiler band size and arrangement on the dynamic and static stability of the TX-16 with small stabilizing fins. Dynamic records could not be obtained for the clean model (configuration 2) and the configuration comparable in fin and spoiler arrangement to the TX-14 (configuration 3) because of the static instability exhibited by these models over the Mach number range. This was also true of the large-band configurations 4 to 7 for which the 2-band and 7-band arrangements were used.

Configuration 8, utilizing 9 large bands, was statically stable in the Mach number ranges $0.80 \leq M_0 \leq 0.94$ and $1.05 \leq M_0 \leq 1.14$. However, the only spoiler arrangement resulting in positive static stability at all but the highest Mach numbers for the TX-16 with small fins utilized 13 large bands (configuration 9). A comparison of the attainable data of configurations 8 and 9 in figure 8 showed that the addition of bands 4, 6, 9, and 11 to the cylindrical section of the TX-16 yielded a substantial increase in the level of C_{m_α} along with some small reduction in dynamic stability.

Results of investigations of the effects of spoiler bands on the longitudinal stability of the TX-16 with large stabilizing fins are presented in figures 9 and 10. Increasing the number of small bands, figure 9 (configurations 11 to 13) yielded substantial improvements in the static stability performance of the TX-16, especially at Mach numbers above 0.90 with relatively small changes in dynamic stability. These improvements in static stability probably result primarily from changes in the pressure distribution over the body since it would be expected that increasing the spoiler size or number would adversely affect the flow over the afterbody and thus reduce the fin effectiveness. A study of schlieren photographs of configurations 11 and 12 showed that the effect of the additional band (1) on the nose was to decrease the velocities over the forward portion of the body and produce a rearward

[redacted]

shift in the center of pressure. Pressure distributions over the afterbodies also indicated a stabilizing movement of the center of pressure when the size or number of bands on the body was increased. This effect is also shown in figure 10 where the number of large bands were increased over the body midsection (configurations 14 and 15). While further improvements in static stability through use of the large bands are noted at the lower Mach numbers, the largest increases in C_{m_α} occur at Mach numbers above 0.90. Configuration 15, which utilized the greatest number of large bands in conjunction with the large fins, yielded the highest level of static stability for the TX-16 investigations but the lowest level of dynamic stability.

The effect of spoiler band and fin size on the longitudinal stability characteristics of the TX-16 with a specific spoiler arrangement are shown in figures 11 and 12. It is seen in the figures that, for those spoiler arrangements shown, the use of the large bands or fins produced significant improvements in the levels of C_{m_α} while comparatively small reductions in the magnitude of $C_{m_q} + C_{m_{\dot{\alpha}}}$ were indicated. It should be noted, however, that the unusually extensive regions of thick or separated boundary layers evidenced over the major portion of the bodies (see fig. 6) would constitute a highly restrictive influence on stability improvements involving movement of the center of pressure. While use of the large fins is indicated to be a satisfactory means of controlling the center of pressure, this may not necessarily constitute a solution due to the space requirements of these larger fins.

The results of an investigation to determine the effects of center-of-gravity movement on the longitudinal stability characteristics of the TX-16 are presented in figures 13 and 14. As the center of gravity was moved forward 1.6 percent of the body length, there was a definite trend toward a higher level of dynamic stability at all Mach numbers except 0.60. Changes in static stability with center-of-gravity position agreed with calculations from force data with the higher levels of C_{m_α} shown for the more forward center-of-gravity position.

Pressure Tests

A satisfactory pressure-sensing port which could be incorporated in a barometric fusing device for arming these weapons at specified altitudes should maintain the ratio of local to ambient static pressure as near unity as possible. In order to evaluate this characteristic of the pressure ports investigated on the TX-14 and TX-16, the data have been presented in figures 15 to 17 as the variation of the static pressure ratio p/p_o with Mach number for each longitudinal orifice location. The locations of the orifices are given in the figures as the distance from the nose-flat in percentage of body length. Included in each figure is a scale of equivalent altitude error for which a fusing altitude

[redacted]

of 3,000 feet was arbitrarily selected. The rapid fluctuations of the pressures shown in the Mach number range from 1.10 to about 1.15 at nearly all orifice locations was attributed to the bow-wave reflection striking the model base and was disregarded when evaluating the pressure port characteristics. The uniformity of the pressure variations shown for individual orifice stations emphasizes the highly separated flow conditions (see fig. 6) present over the afterbody. This flow condition is further emphasized by the behavior of the bow-shock reflection in that it was widely diffused over the afterbody resulting in a very narrow Mach number region in which the pressure levels were affected.

TX-14.- Pressure tests of the TX-14 were conducted through an angle-of-attack range from -2° to $+2^\circ$, figure 15. At zero angle of attack, the data show that the most favorable location of a pressure port would be from about $x/L = 0.770$ to $x/L = 0.887$. The maximum altitude error for these orifice positions is shown in the figures to be from about $\pm 1{,}000$ feet to $\pm 1{,}200$ feet with the largest errors occurring at Mach numbers of 0.80 and 1.02. Forward of this region, the pressure levels were influenced by flow expansions around the afterbody shoulder and spoiler bands and the development of compression shocks with increases in Mach number.

Dynamic records indicated that the amplitude of free-model oscillations in the wind tunnel were of the order of $\pm 2^\circ$. It is not believed that this amplitude would be exceeded by the weapon when it had descended to its fusing altitude. Angles of attack of $\pm 2^\circ$, figures 15(b) and 15(c), did not appreciably alter the trend of the curves, but at Mach numbers below $M_0 \approx 0.90$, the pressure ratios exhibited a more desirable variation with Mach number than was shown at 0°. Between $x/L = 0.819$ and 0.887, the most favorable location at these angles, the magnitude of altitude error was shown to be about ± 600 feet below $M_0 \approx 1.10$ and about $\pm 1{,}000$ feet at $M_0 \approx 1.2$. Only small differences in pressure levels are indicated at angle of attack of $\pm 2^\circ$ between the top, sides, and bottom of the afterbody.

TX-16.- For tests of the TX-16 pressure model, two spoiler band configurations were investigated. The model with 5 large bands installed, figure 16, was tested through an angle-of-attack range of from -4° to $+12^\circ$ while the configuration with 13 small bands, figure 17, was investigated at angles of attack of from -2° to $+2^\circ$.

At $x/L = 0.831$ on the 5-band configuration, the altitude error was shown to be about 1,000 feet at $M_0 \approx 0.99$ for zero angle of attack. At an angle of attack of $\pm 4^\circ$, the minimum error in altitude for this location was indicated to be 1,800 feet when the top or bottom orifices were considered but only about 1,000 feet for the pressure port on the side of the model. At angles of attack of $+8^\circ$ and $+12^\circ$, the altitude error for the top and bottom orifices became too large for practical

[redacted]

use while the pressure variations for the side orifice showed that the ±1,000 foot error indicated at ±4° would not be exceeded. A study of dynamic records of free-model oscillations of the TX-16 showed that the maximum amplitude in the wind tunnel was about ±2.5°.

Results of the pressure investigation of the 13-band configuration of the TX-16 indicated that while the additional spoiler bands were able to hold the pressure ratios to a constant value of unity at the low Mach numbers ($M_o \leq 0.94$) over a substantial portion of the afterbody ($x/L = 0.745$ to 0.915), reductions in pressure in the Mach number range from 1.00 to 1.10 would result in altitude errors of at least 1,000 feet. These errors would increase to about 1,200 feet at angles of attack of ±2° for the top and bottom as well as sides of the afterbody.

Force measurements.- Results of force measurements made in conjunction with pressure model tests are presented in figures 18 to 20. As there was some indication from these tests that the pitching moments may have been nonlinear at small angles of attack, the data of figures 18 and 20 have been faired to indicate only the effective slopes of the lift and moment curves. Pitching-moment calculations of the TX-14 were made relative to the 81.8-inch (full-scale) center-of-gravity position whereas the 120-inch (full-scale) center-of-gravity position was used for the TX-16.

Force data for the TX-14, figure 18, show that the effect of Mach number on the lift coefficient was small but indicates some reduction in pitching moment at the high Mach numbers. These data support the dynamic tests in that the static stability of the TX-14 was shown to be only marginal through the Mach number range. The effects of shock development over the nose are noted in the Mach number range $0.85 \leq M_o \leq 0.90$ by the reduction in the slope of the moment curve due to a forward shift in the center of pressure.

Tests of the TX-16 with 5 bands, figure 19, reflect the use of the large stabilizing fins in comparatively high values of lift and pitching moment. Although the slopes of the moment curves at low Mach numbers appear reasonably linear, dynamic records did not substantiate the large trim angles shown, indicating a possibly nonlinear moment curve in this angle-of-attack range. The ability of the large fins to maintain the center of pressure well behind the center of gravity is shown by a comparison with the data of figure 20 for which the small fins were used. A substantial reduction in pitching moment is shown for the small-fin, 13-band configuration as compared with the large-fin, 5-band configuration although the lift coefficients are of about the same magnitude.

While previously discussed results indicated that the addition of spoiler bands to these bodies provided an increase in static stability, it should be noted that these increases are considerably smaller than those obtained by the use of larger fins.

[redacted]

A comparison of the effective slopes of the moment curves as obtained from the force data is made with the stability parameter C_{m_α} from dynamic tests in figure 21. It is seen that these data are in good agreement throughout the Mach number range. Those differences shown are believed to result primarily from changes in fin effectiveness when the pressure model was rotated 22.5° as previously mentioned.

CONCLUDING REMARKS

From an investigation of the longitudinal stability and afterbody pressure characteristics of the TX-14 and TX-16 specialized store configurations, the following observations are made:

TX-14.- The level of static stability of the TX-14 was exceptionally low through the Mach number range whereas the dynamic stability performance was generally satisfactory.

Tests of the TX-14 at two Reynolds numbers indicated no significant effects of Reynolds number within the range of these tests on either the dynamic or static stability performance.

Pressure measurements made on the TX-14 afterbody indicated that the most favorable location of a pressure port which could be used in conjunction with a barometric fusing device at ±2° angle of attack was from $x/L = 0.819$ to $x/L = 0.887$. A maximum equivalent altitude error at these locations, for which a fusing altitude of 3,000 feet was arbitrarily selected, of about ±1,000 feet occurred at Mach numbers of 0.80 and 1.02.

TX-16.- The TX-16 configuration comparable in fin and spoiler arrangement to the TX-14 was unsatisfactory from the standpoint of static stability.

Use of the small fins on the TX-16 resulted in large Mach number regions of static instability for all spoiler configurations.

Increasing the size or number of spoiler bands as well as fin size on the TX-16 produced substantial improvements in static stability with only small reduction in dynamic stability indicated.

A forward movement of the center of gravity from 0.408L to 0.392L on two configurations of the TX-16 resulted in improvements for both the dynamic and static stability performance.

[redacted]

Pressure measurements on the afterbody of a 5-band configuration of the TX-16 indicated the most favorable pressure-port location to be in the vicinity of the 83-percent body station. The equivalent altitude error for this location was shown to be about 1,000 feet at 0° angle of attack with an increase to 1,800 feet at ±4°.

Pressure tests at zero angle of attack of a 13-band configuration of the TX-16 indicated an altitude error of about 1,000 feet for orifices located from $x/L = 0.745$ to $x/L = 0.915$. Substantial increases in this error were noted at ±2°.angle of attack.

General.- The longitudinal stability performance of the TX-14 was generally satisfactory at all Mach numbers. The TX-16 configuration displaying the more desirable stability characteristics utilized the large stabilizing fins and the greatest number of large bands tested with this fin configuration.

It was noted that the restrictive influence of the highly separated flow conditions evidenced over the major portions of these weapons would substantially limit effective control of the center of pressure by means of minor changes in weapon configuration.

Langley Aeronautical Laboratory,
National Advisory Committee for Aeronautics,
Langley Field, Va., March 12, 1954.

John A. Braden
Aeronautical Research Scientist

Beverly Z. Henry, Jr.
Aeronautical Research Scientist

Approved:

Eugene C. Draley
Chief of Full-Scale Research Division

cg

[redacted]

REFERENCE

1. Henry, Beverly Z., Jr., and Braden, John A.: An Investigation of the Dynamic and Static Stability Characteristics of a Group of Specialized Store Configurations at Transonic Speeds. NACA RM SL53G09c, 1953.

TABLE I.- COORDINATES FOR THE FOREBODY AND AFTERBODY OF THE TX-14 AND TX-16 MODELS

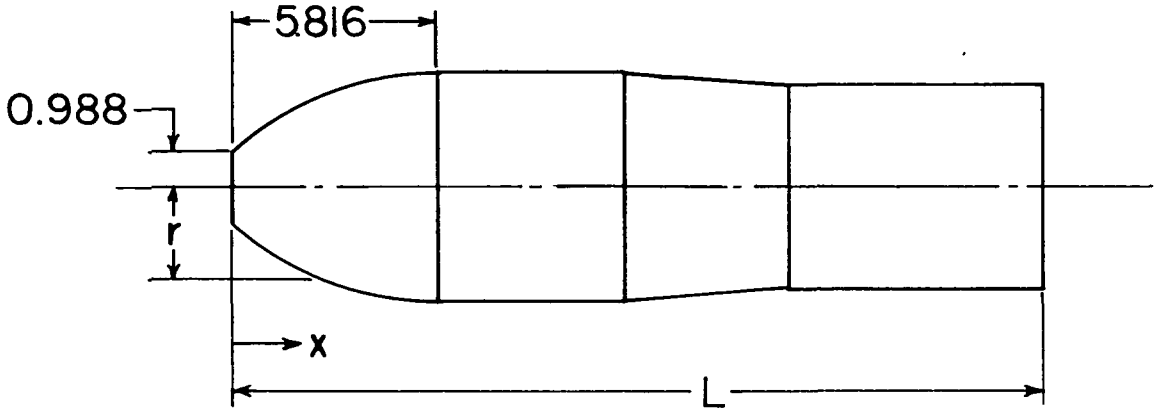

NOSE SECTION
(Identical for Both Bodies)

x, in.	r, in.
.000	.988
.208	1.166
.416	1.334
.624	1.491
.832	1.639
1.040	1.779
1.248	1.910
1.456	2.033
1.664	2.148
1.872	2.256
2.080	2.358
2.288	2.452
2.496	2.540
2.704	2.622
2.912	2.698
3.120	2.768
3.328	2.833
3.536	2.891
3.744	2.945
3.952	2.993
4.160	3.035
4.368	3.073
4.576	3.105
4.784	3.132
4.992	3.154
5.200	3.171
5.408	3.183
5.616	3.191
5.816	3.193

AFTERBODY SECTION
(TX-14)

x, in.	r, in.
5.816	3.193
11.052	3.193
15.779	2.873
22.968	2.873
L = 22.968	

AFTERBODY SECTION
(TX-16)

x, in.	r, in.
5.816	3.193
18.666	3.193
23.394	2.873
30.582	2.873
L = 30.582	

TABLE II

ORIFICE LOCATIONS ON TOP, SIDE, AND BOTTOM OF TX-14 AND TX-16 AFTERBODIES

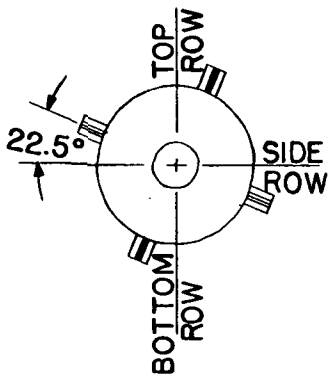

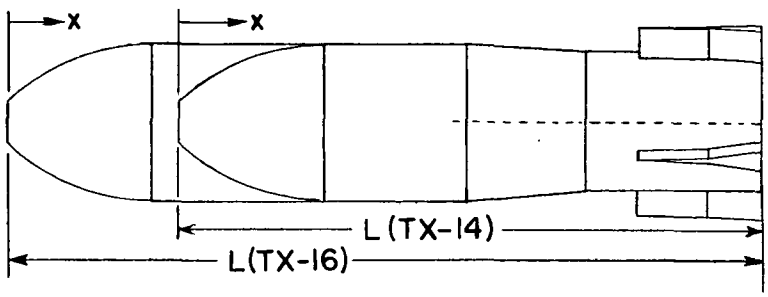

Station Number	TX-14		TX-16	
	x, in.	x/L	x, in.	x/L
1	11.008	0.479	18.622	0.609
2	12.048	.525	19.662	.643
3	12.566	.547	20.180	.660
4	13.088	.570	20.702	.677
5	13.608	.592	21.222	.694
6	14.128	.615	21.742	.711
7	14.648	.638	22.262	.728
8	15.168	.660	22.782	.745
9	15.688	.683	23.302	.762
10	16.208	.706	23.822	.779
11	16.728	.728	24.342	.796
12	17.248	.751	24.862	.813
13	17.768	.770	25.382	.830
14	18.288	.796	25.902	.847
15	18.808	.819	26.422	.864
16	19.328	.842	26.942	.881
17	19.848	.864	27.462	.898
18	20.368	.887	27.982	.915
19	20.888	.909	28.502	.932
20	21.408	.932	29.022	.949
21	21.928	.955	29.542	.966
22	22.240	.968	29.854	.976
23	22.864	.995	30.478	.997
	L = 22.968		L = 30.582	

Note: Orifices omitted at stations 1 - 7 on side row.

[redacted]

TABLE III.- SUMMARY OF MAJOR TEST RESULTS

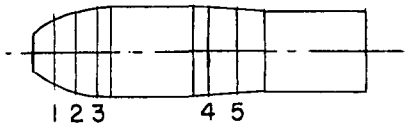

TX-14

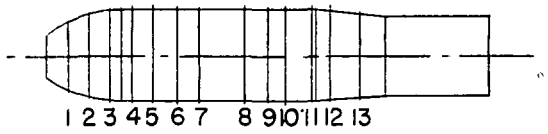

TX-16

Configuration	Model	Spoiler Bands		Fins	CG percent L	I Slug-ft^2	Remarks
		Type	Arrangement				
1	TX-14	Small	1-2-3-4-5	Small	37.1	0.1500	Statically and dynamically stable through M_o range for both 0.40 and 0.60 atmospheres. No effect of Reynolds number noted.
2	TX-16	---	None	↓	40.8	.48818	Model statically unstable through M_o range.
3	↓	Small	1-2-3-12-13	↓	↓	↓	Model statically unstable $0.20 \leq M_o \leq 0.60$.
4	↓	Large	7-8	↓	↓	↓	Model statically unstable through M_o range.
5	↓	↓	1-2-3-5-7-12-13	↓	↓	↓	Model statically unstable through M_o range.
6	↓	↓	1-2-3-5-10-12-13	↓	↓	↓	Model statically unstable through M_o range.
7	↓	↓	1-2-3-8-10-12-13	↓	↓	↓	Model statically unstable through M_o range.
8	↓	↓	1-2-3-5-7-8-10-12-13	↓	↓	↓	Model statically unstable at $M_o \leq 0.75$ and $0.975 \leq M_o \leq 1.02$.
9	↓	↓	1-2-3-4-5-6-7-8-9-10-11-12-13	↓	↓	.4905	Model dynamically and statically stable through Mach-number range.
10	↓	↓	↓	↓	39.2	.5055	Dynamic and static stability improved over configuration 9.
11	↓	Small	2-3	Large	40.8	.50438	Model dynamically and statically stable at all Mach numbers.
12	↓	↓	1-2-3	↓	↓	↓	Static stability improved over configuration 11. Only small changes in dynamic stability noted.
13	↓	↓	1-2-3-12-13	↓	↓	↓	Static stability improved over configuration 12. Only small changes in dynamic stability noted.
14	↓	Large	↓	↓	↓	↓	Large increase in static stability over that of configuration 13 accompanied by slight reduction in dynamic stability.
15	↓	↓	1-2-3-5-7-8-10-12-13	↓	↓	↓	Dynamically and statically stable at all Mach numbers. Highest level of static stability shown for TX-16 with CG at 0.41L.
16	↓	↓	1-2-3-12-13	↓	39.2	.52341	Improvements in both dynamic and static stability noted.

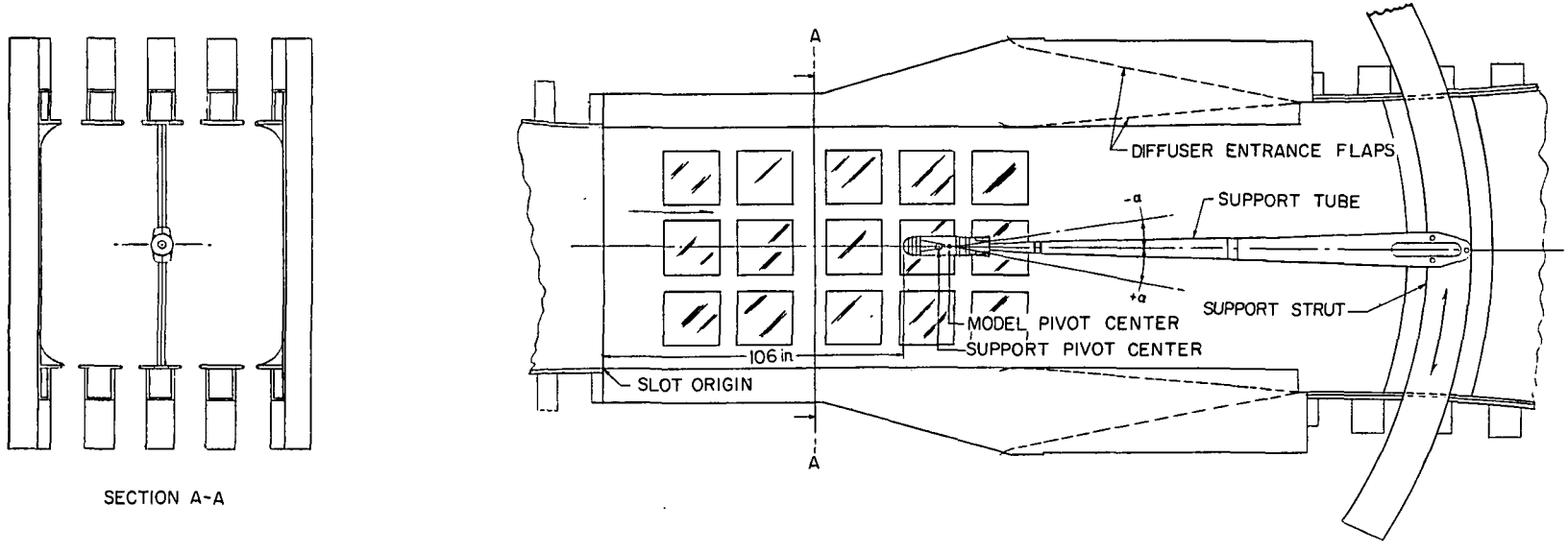

Figure 1.- General arrangement of a typical model installation in the Langley 8-foot transonic pressure tunnel. All dimensions are in inches.

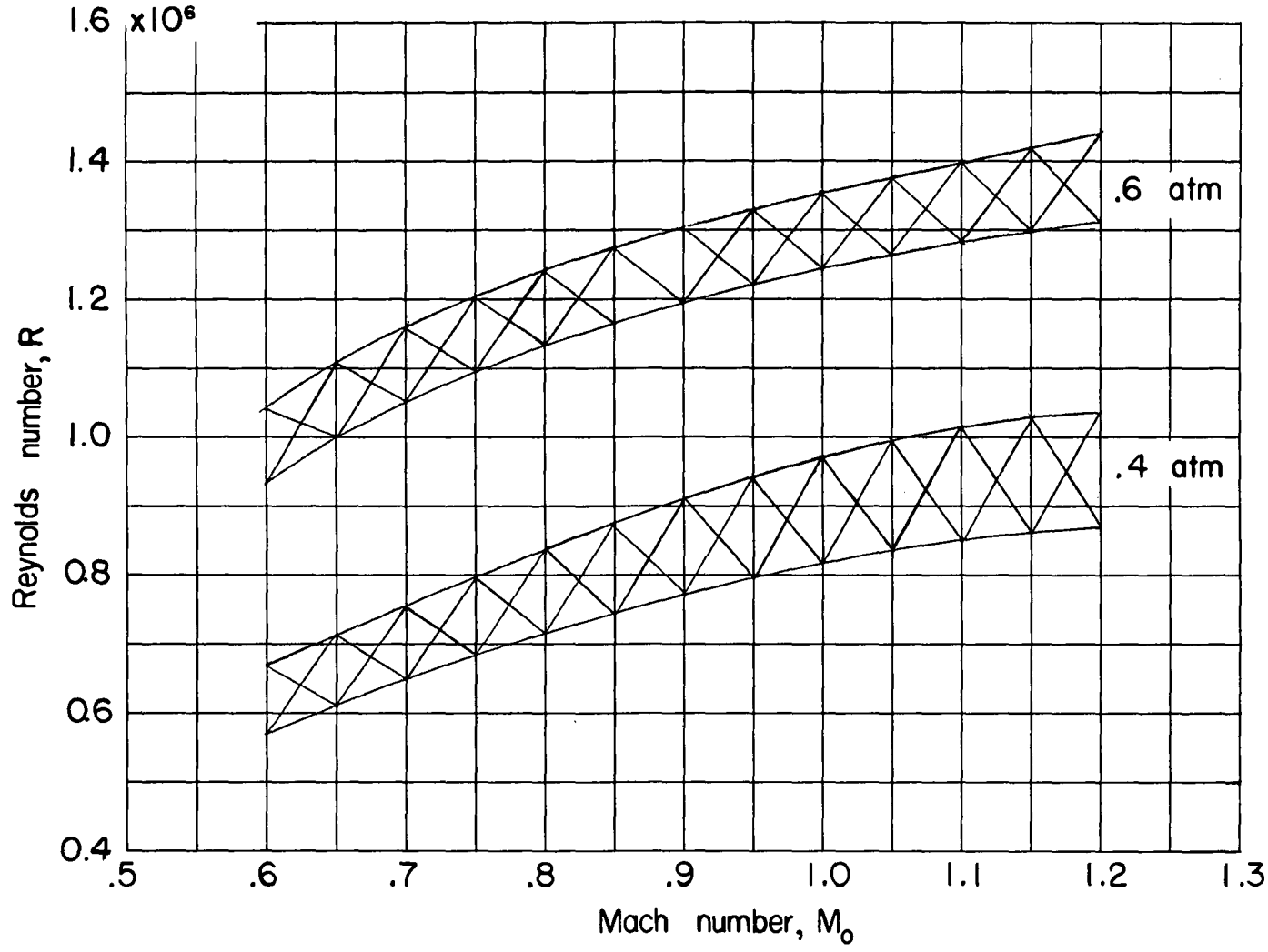

Figure 2.- Variation of Reynolds number in the Langley 8-foot transonic pressure tunnel.

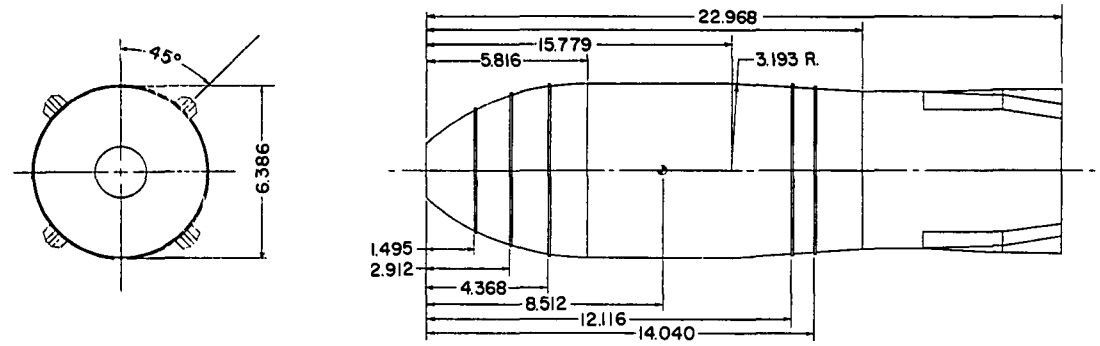

TX-14

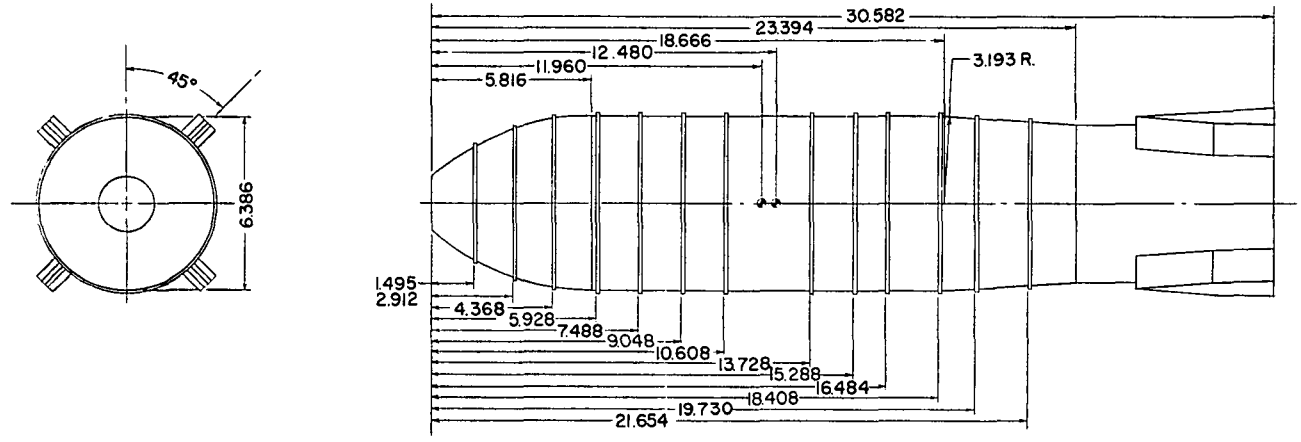

TX-16

Figure 3.- Details of model test configurations. All dimensions are in inches.

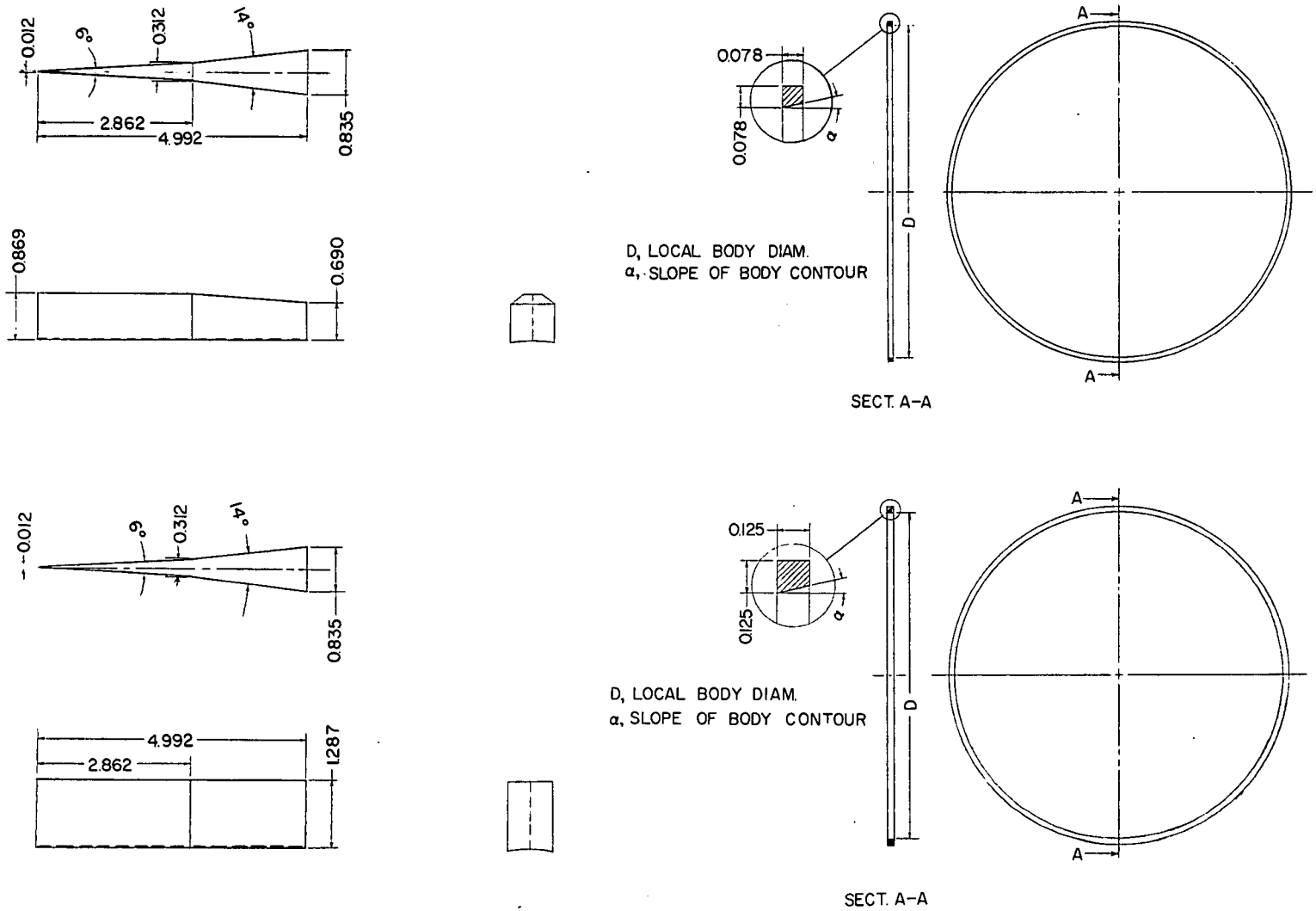

Figure 4.- Details of fins and spoiler bands. All dimensions are in inches.

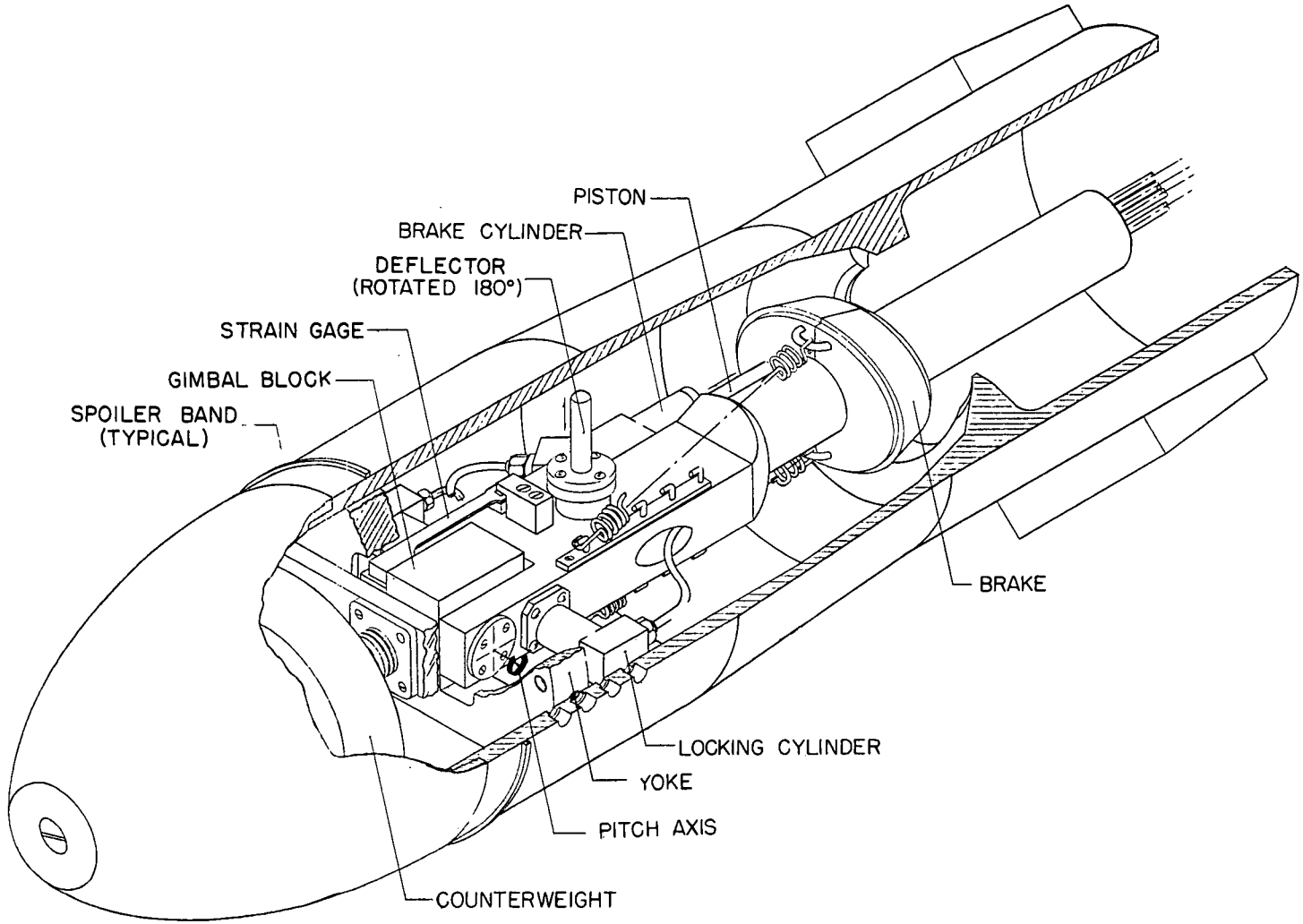

Figure 5.- Details of a typical model installation on the dynamic testing apparatus.

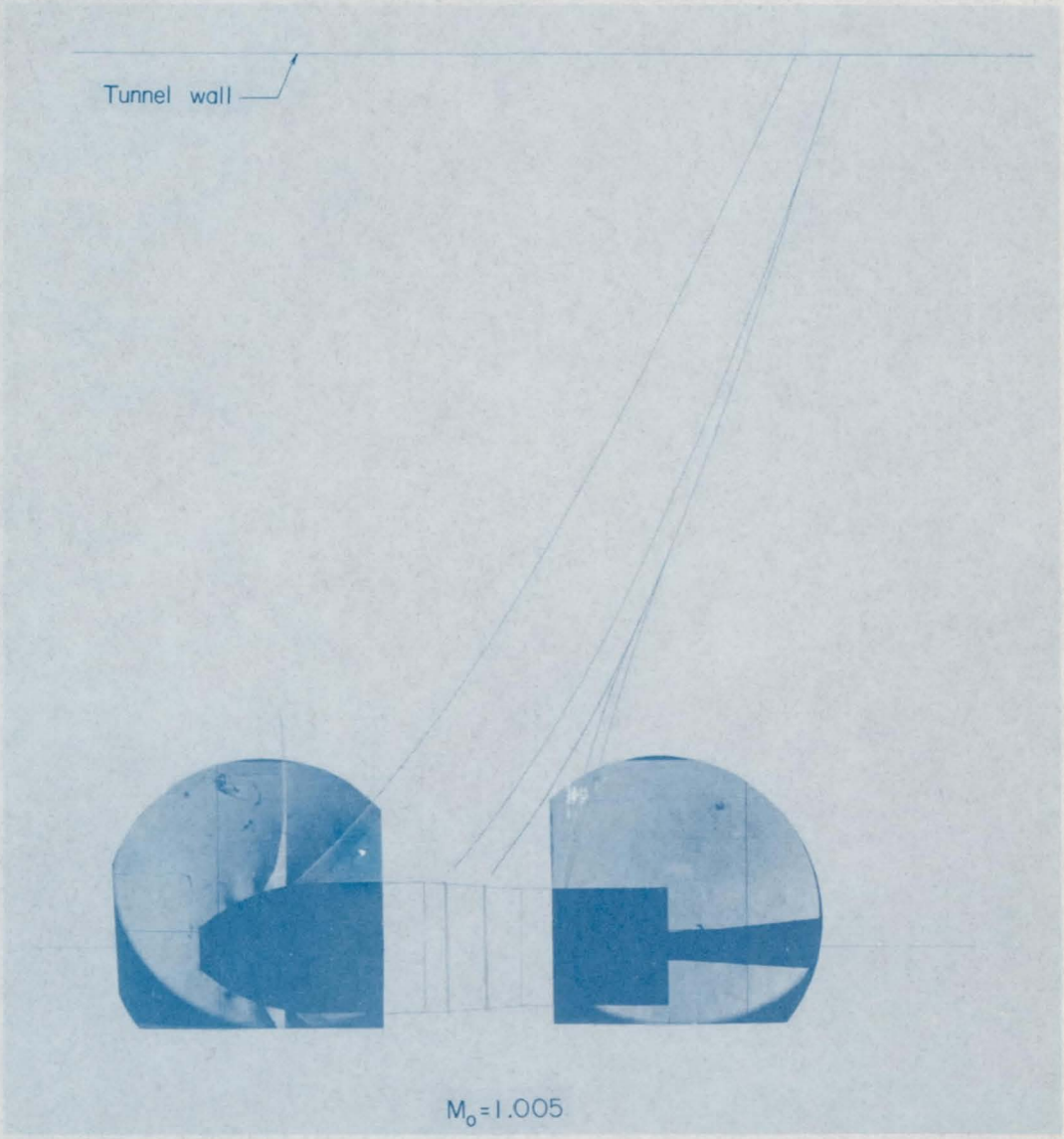

L-83630

(a) TX-14.

Figure 6.- Typical schlieren photographs of the TX-14 and TX-16 models.

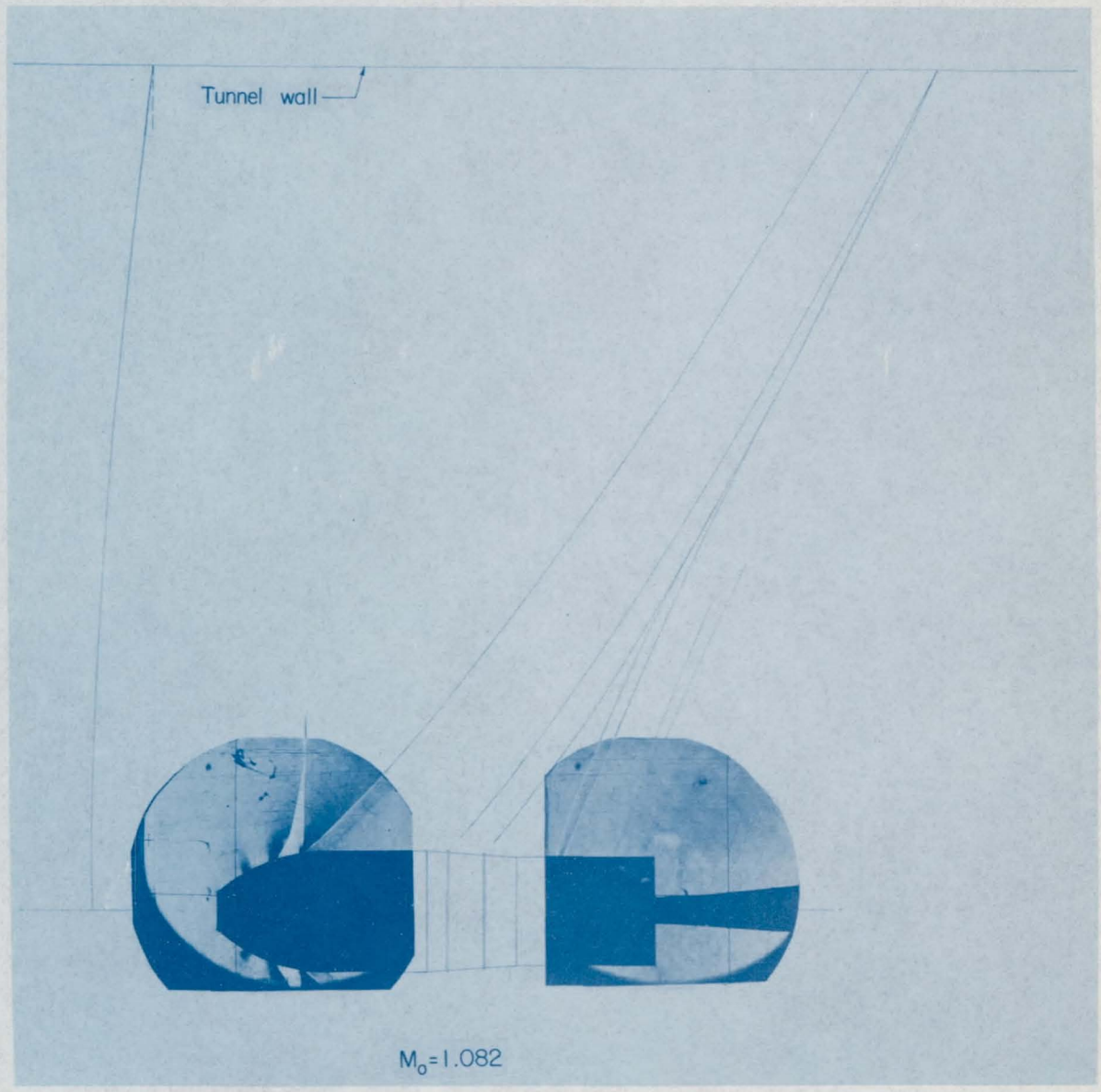

L-83631

(b) TX-16.

Figure 6.- Continued.

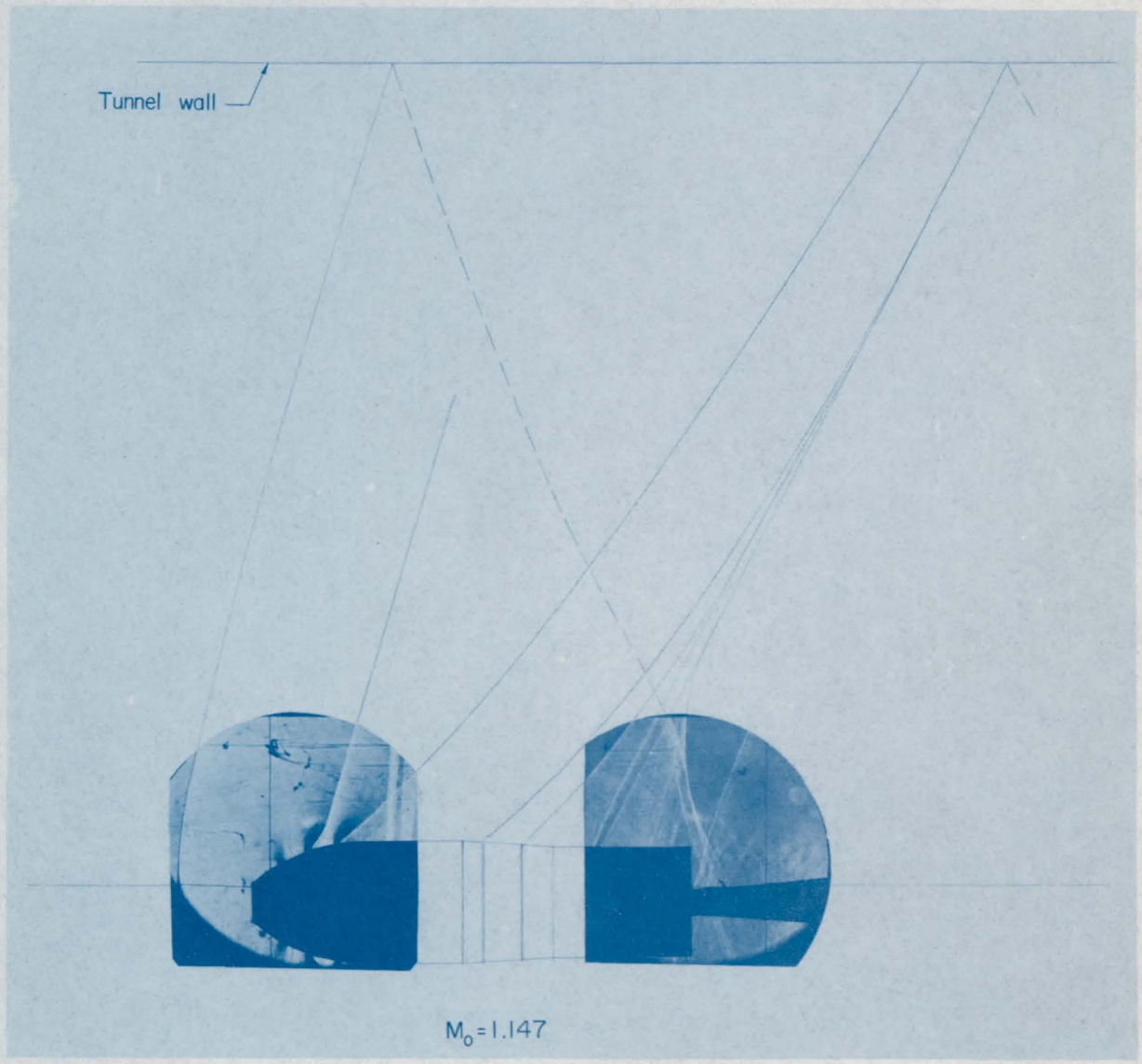

L-83632

(c) TX-14.

Figure 6.- Continued.

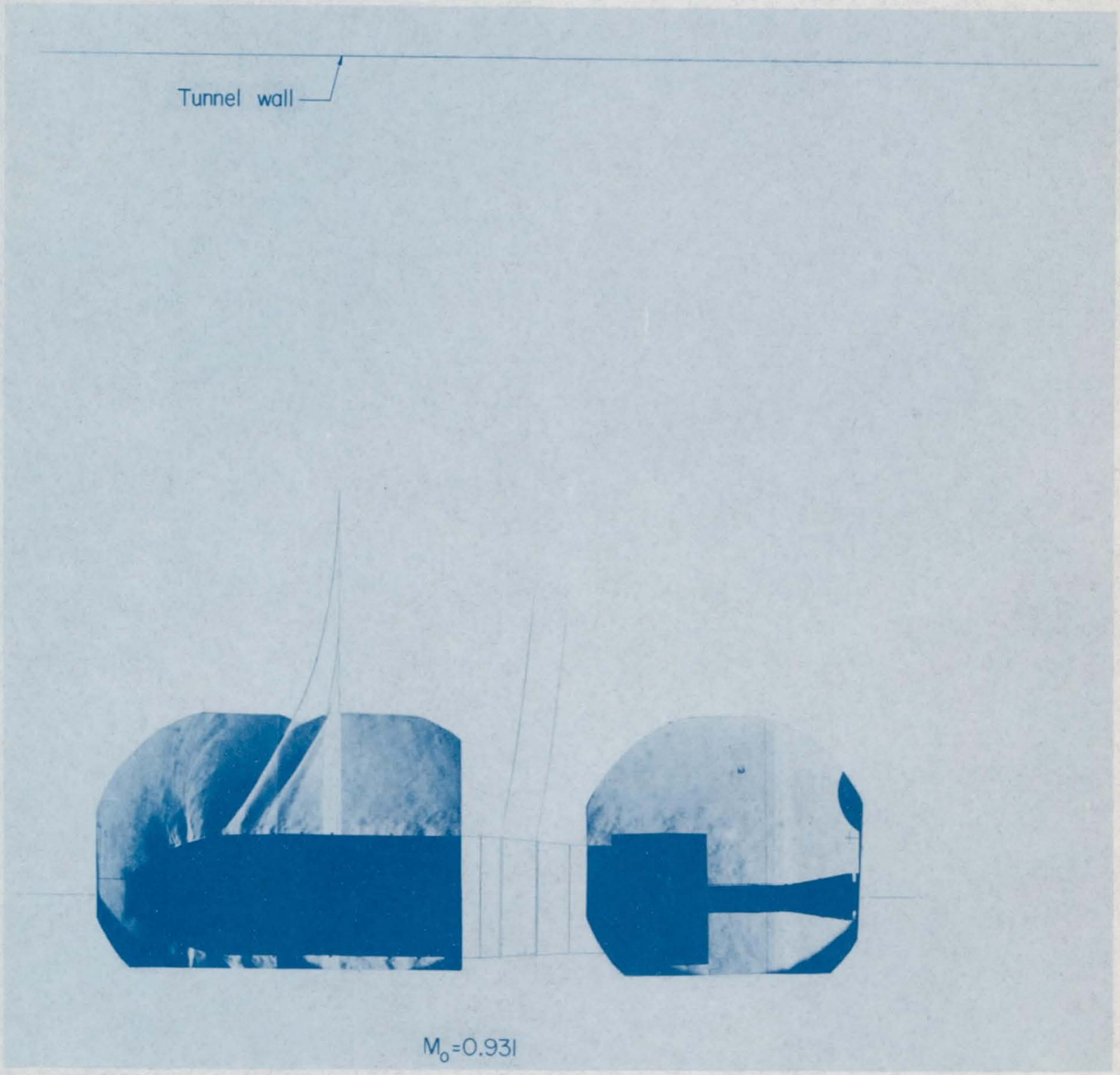

L-83633

(d) TX-16.

Figure 6.- Continued.

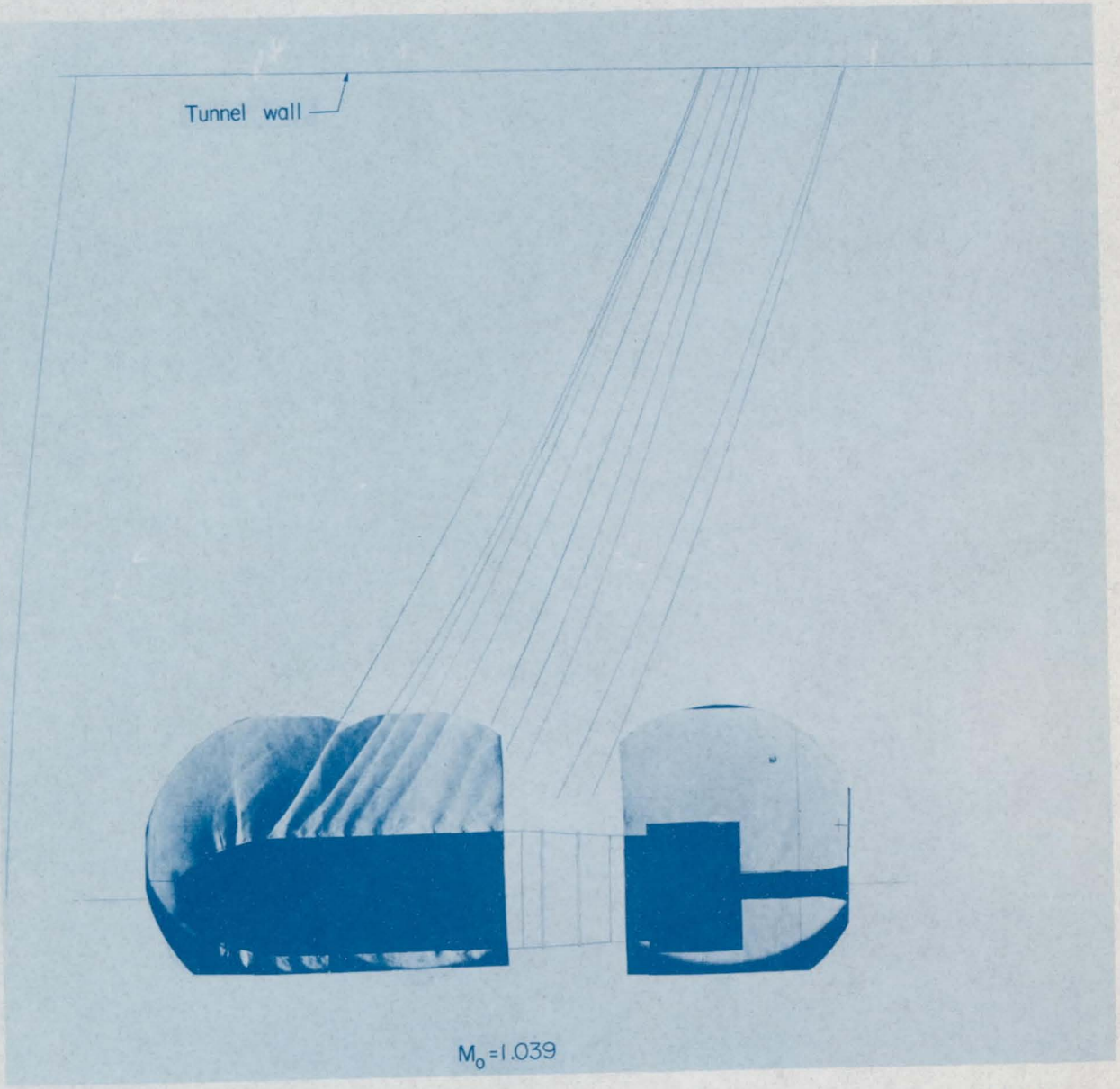

L-83634

(e) TX-16.

Figure 6.- Continued.

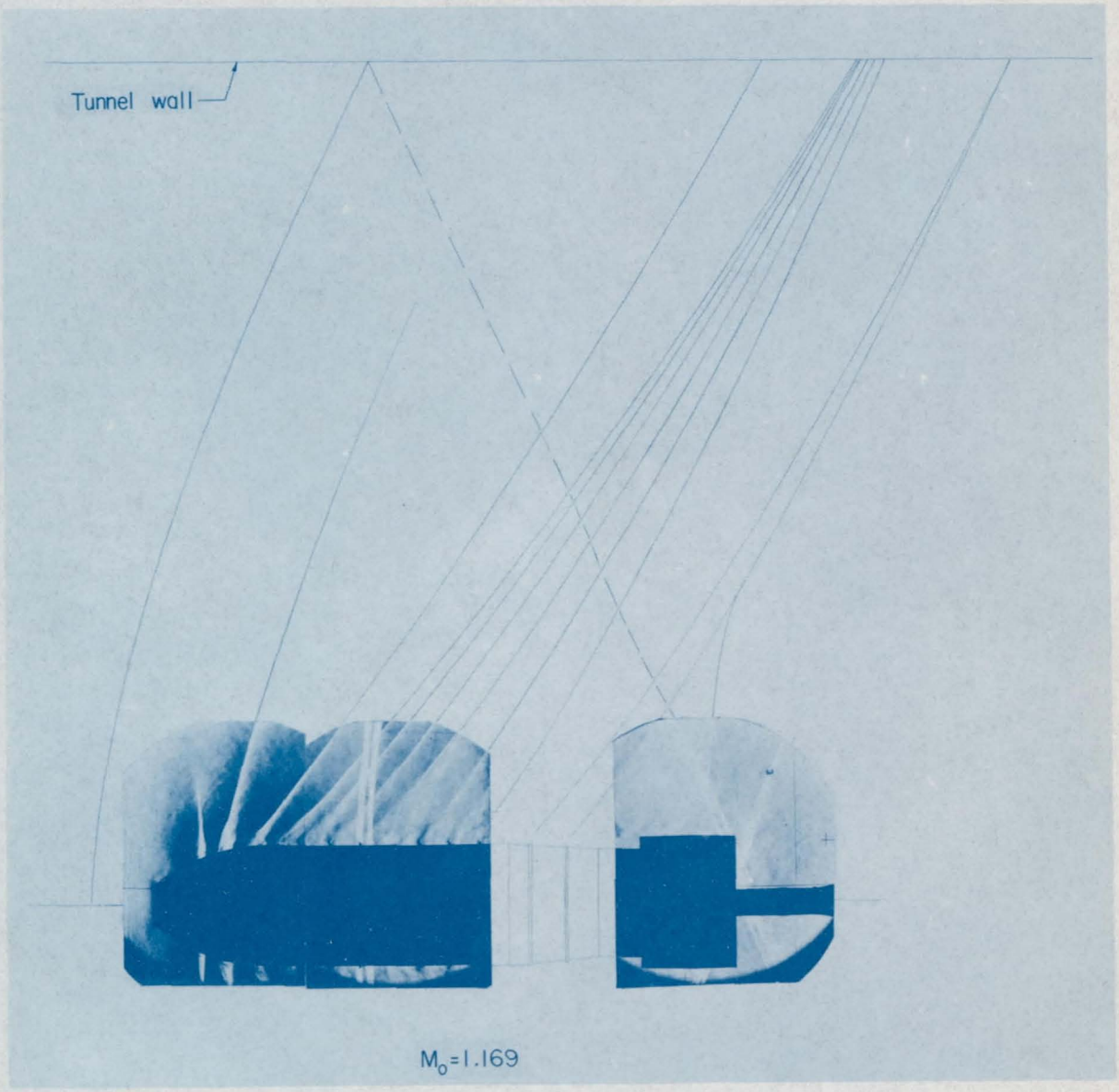

L-83635

(f) TX-16.

Figure 6.- Concluded.

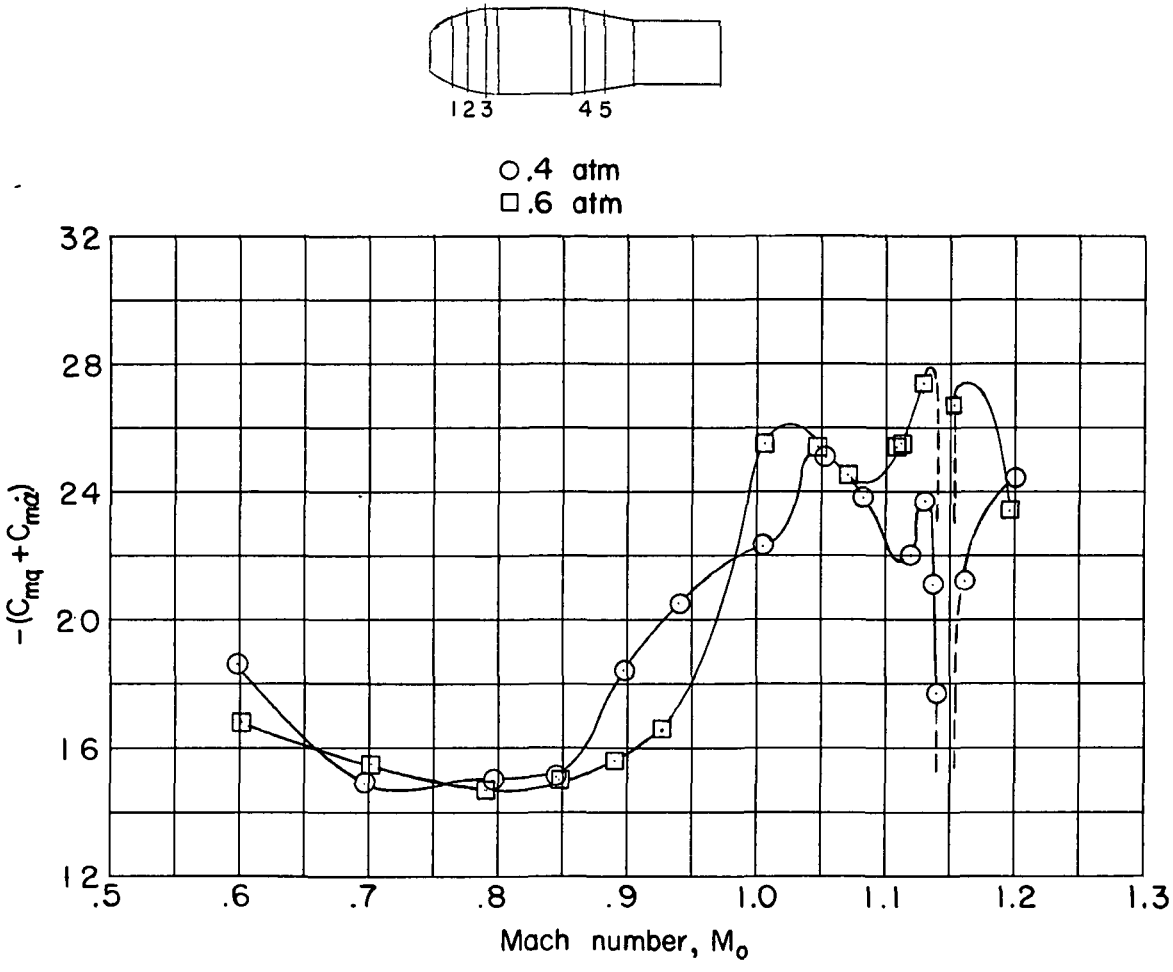

(a) Dynamic stability.

Figure 7.- The effects of Reynolds number variation on the longitudinal stability of the TX-14.

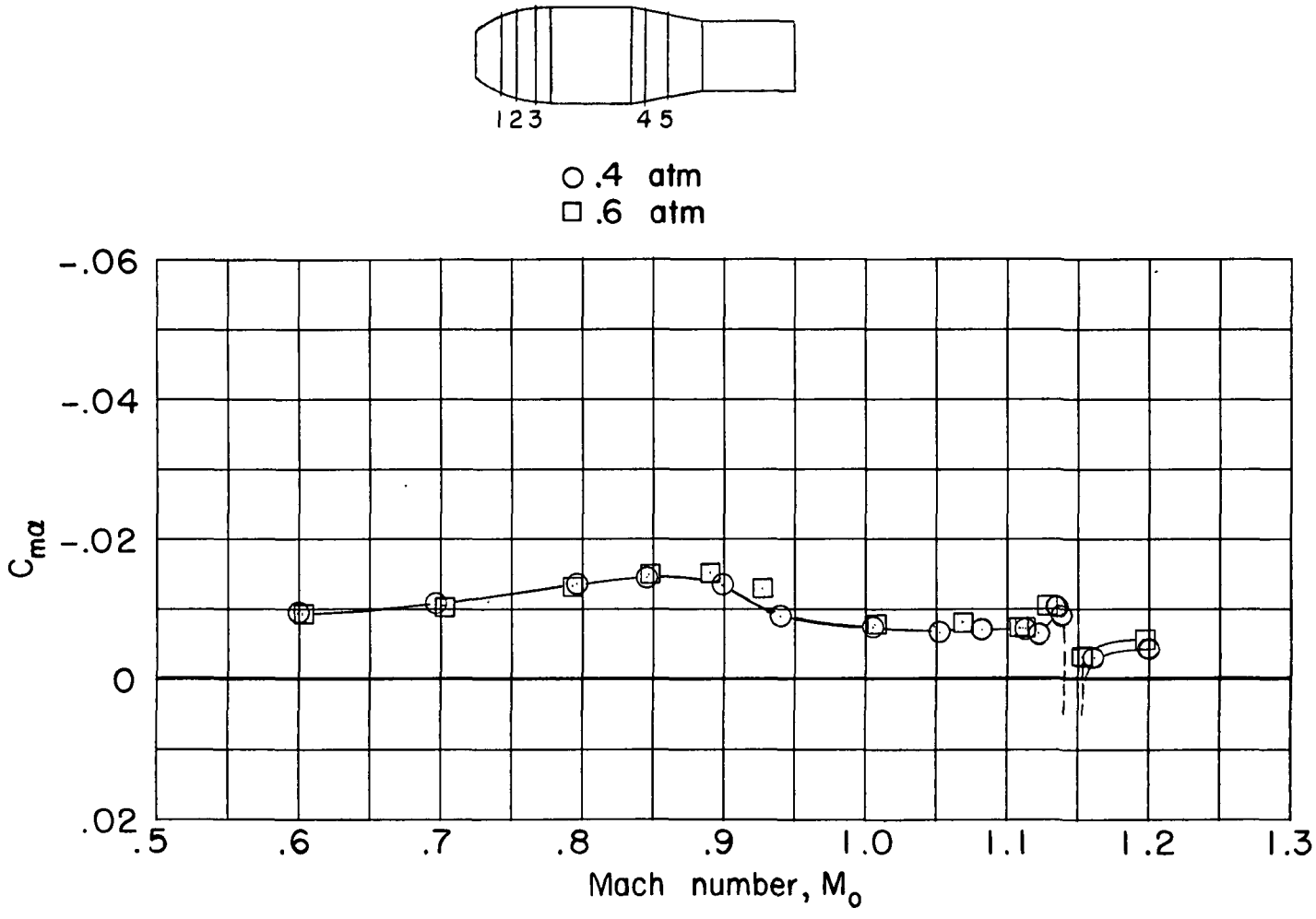

(b) Static stability.

Figure 7.- Concluded.

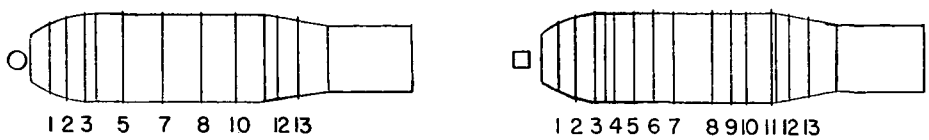

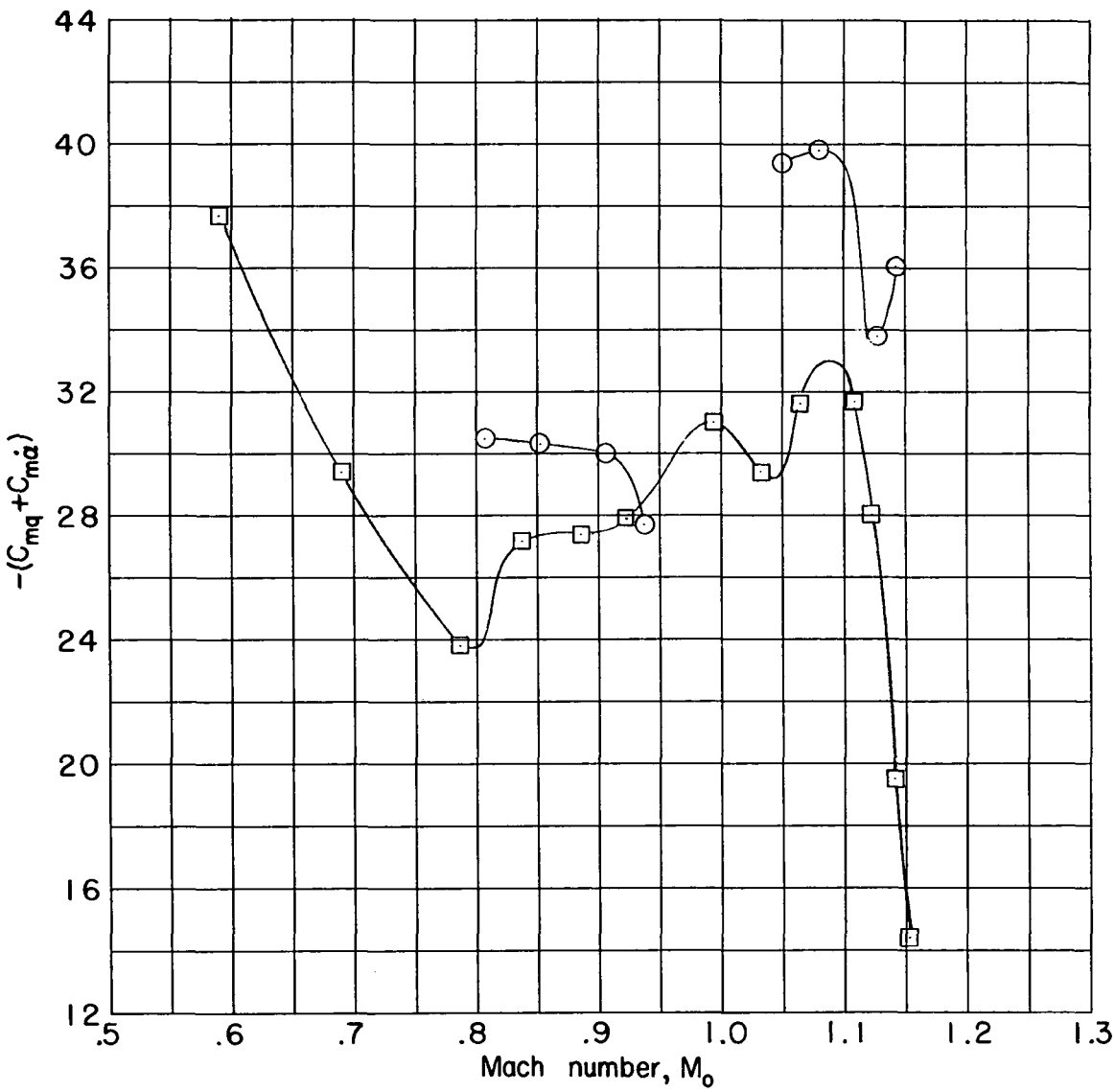

(a) Dynamic stability.

Figure 8.- The effects of variations in large spoiler-band arrangements on the longitudinal stability of the TX-16 with small fins.

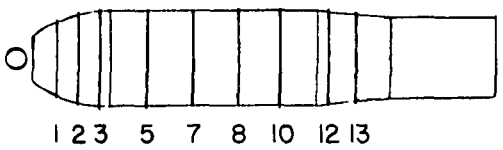

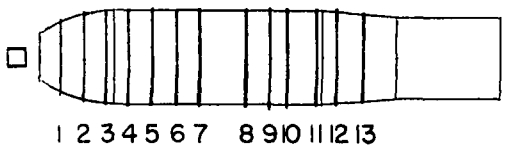

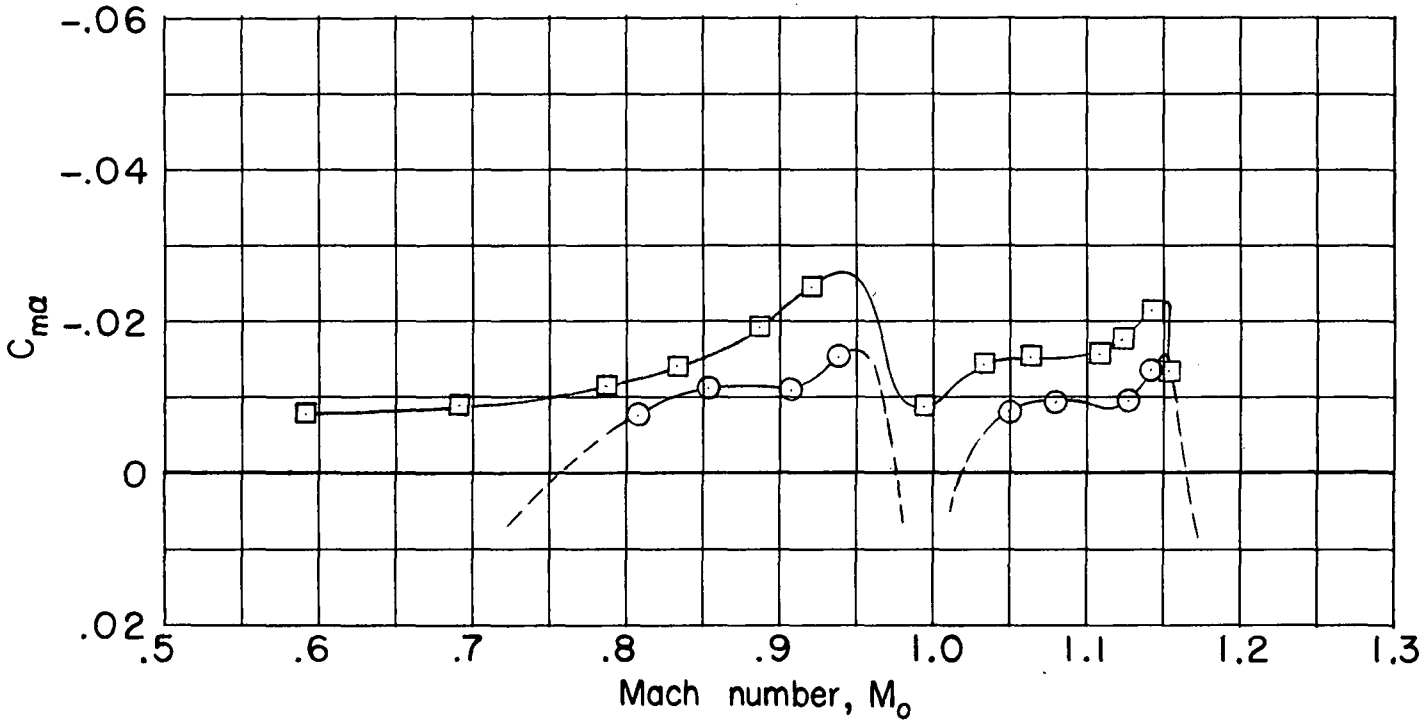

(b) Static stability.

Figure 8.- Concluded.

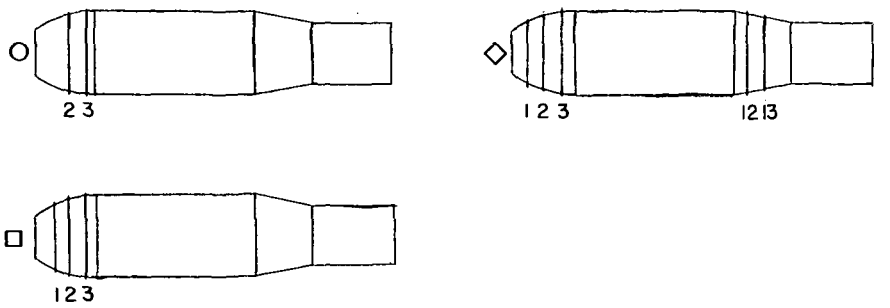

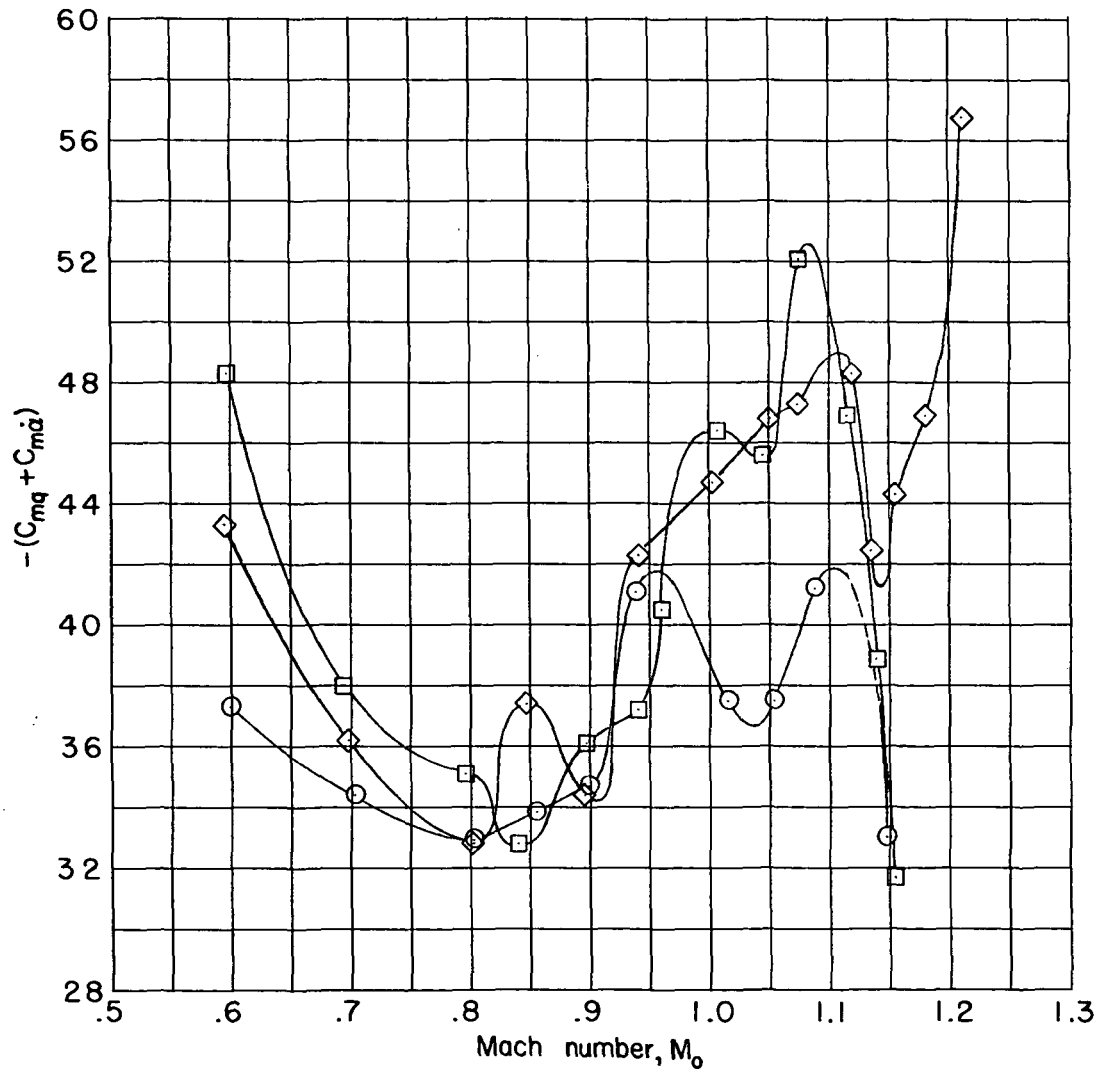

(a) Dynamic stability.

Figure 9.- The effects of variations in small spoiler-band arrangements on the longitudinal stability of the TX-16 with large fins.

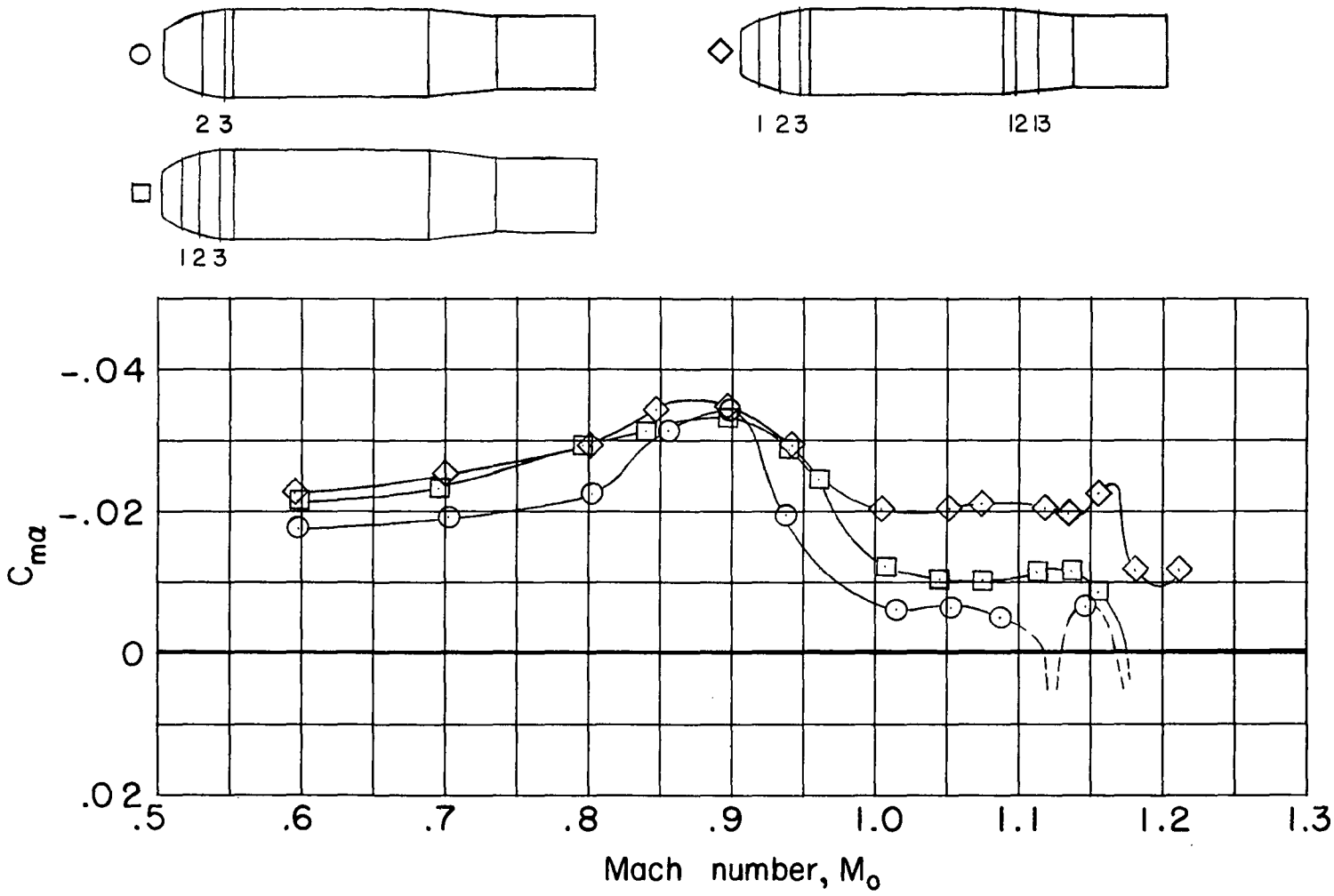

(b) Static stability.

Figure 9.- Concluded.

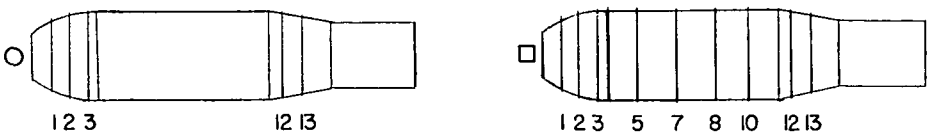

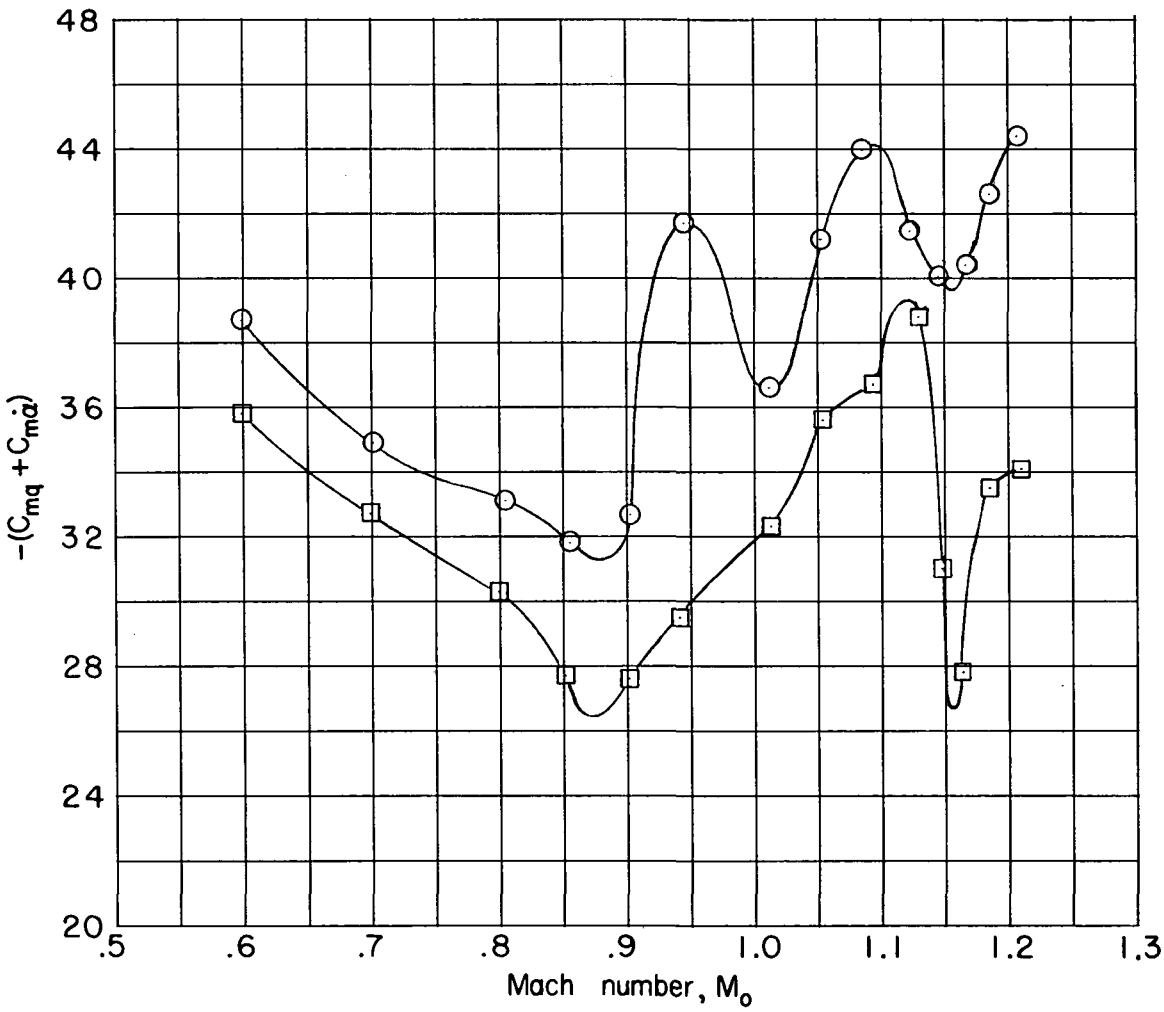

(a) Dynamic stability.

Figure 10.- The effects of variations in large spoiler-band arrangements on the longitudinal stability of the TX-16 with large fins.

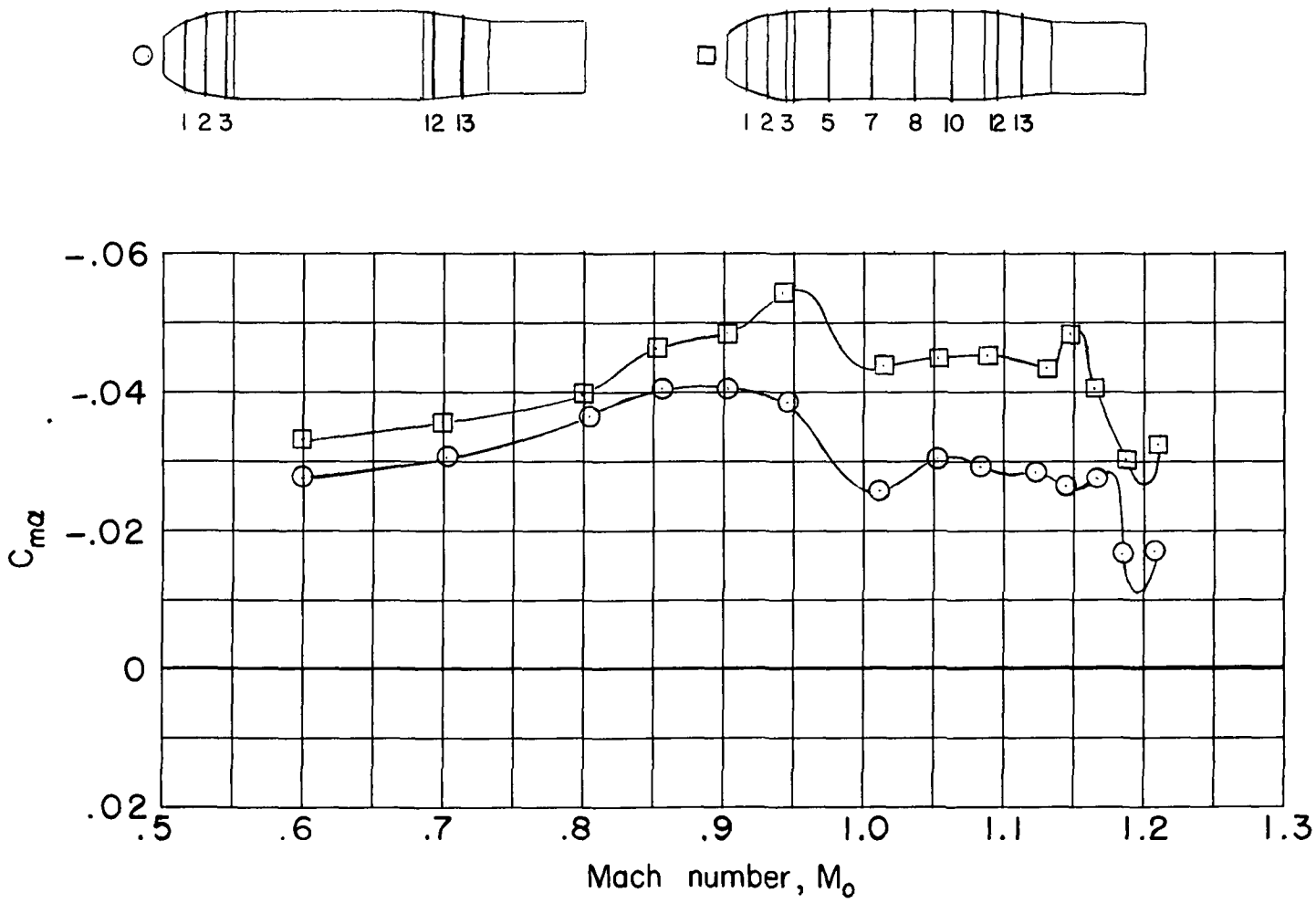

(b) Static stability.

Figure 10.- Concluded.

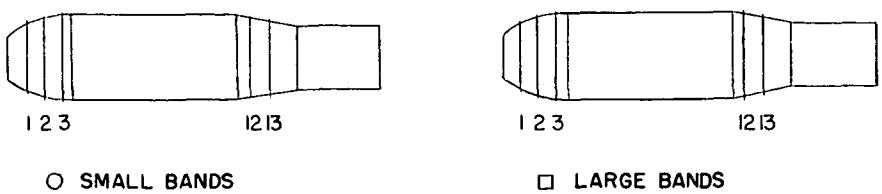

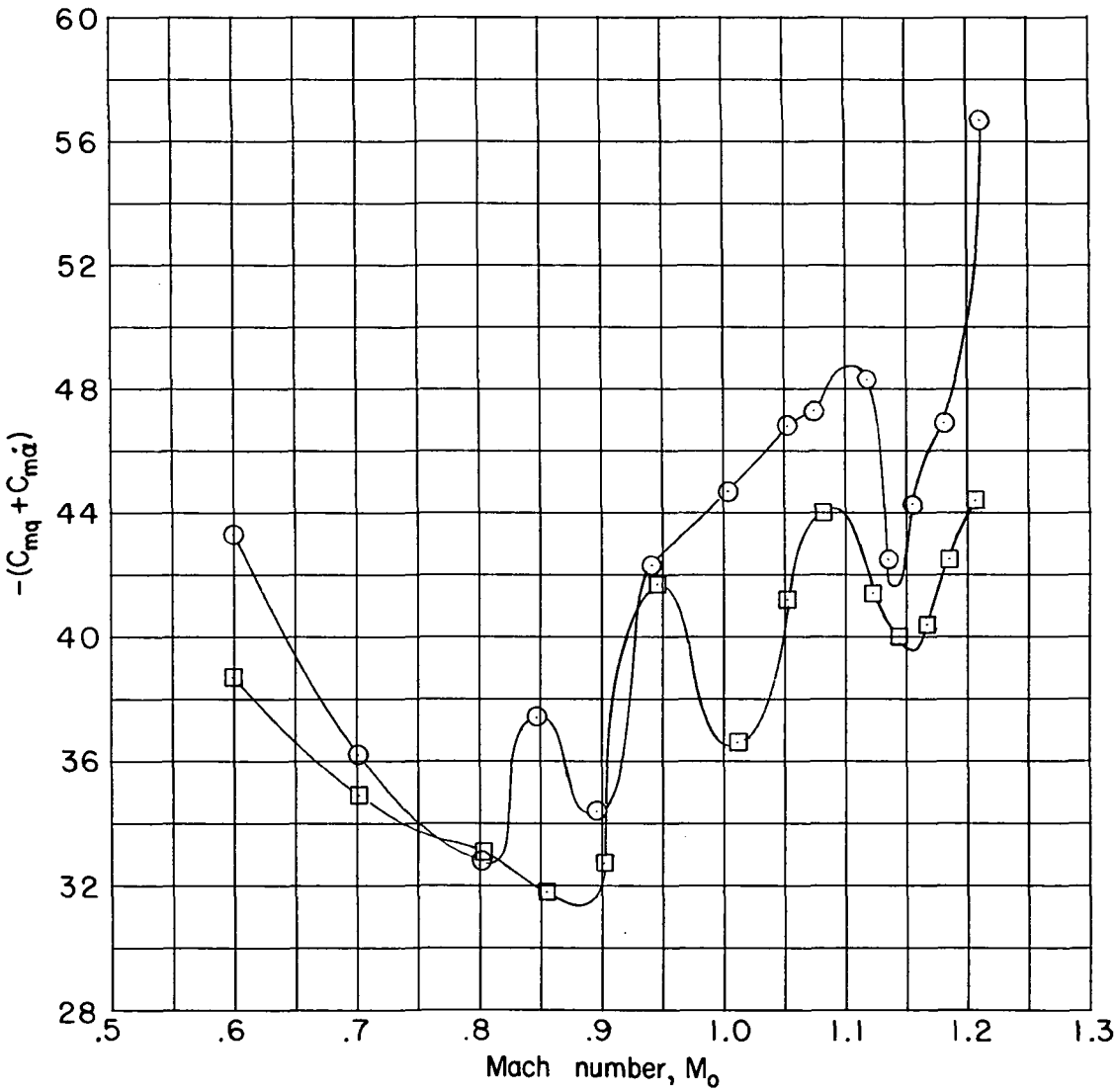

(a) Dynamic stability.

Figure 11.- The effect of spoiler-band size on the longitudinal stability of the TX-16 with large fins.

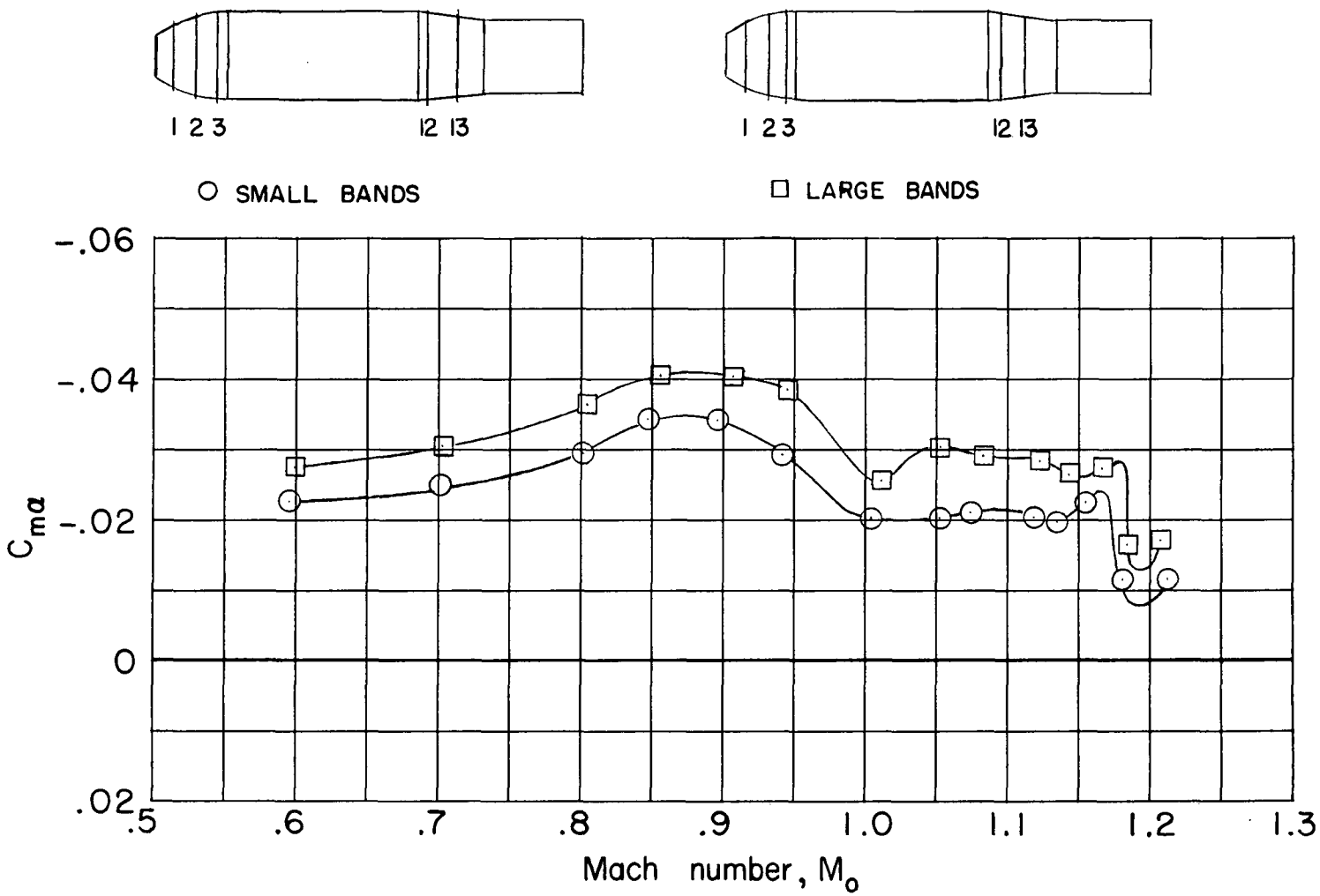

(b) Static stability.

Figure 11.- Concluded.

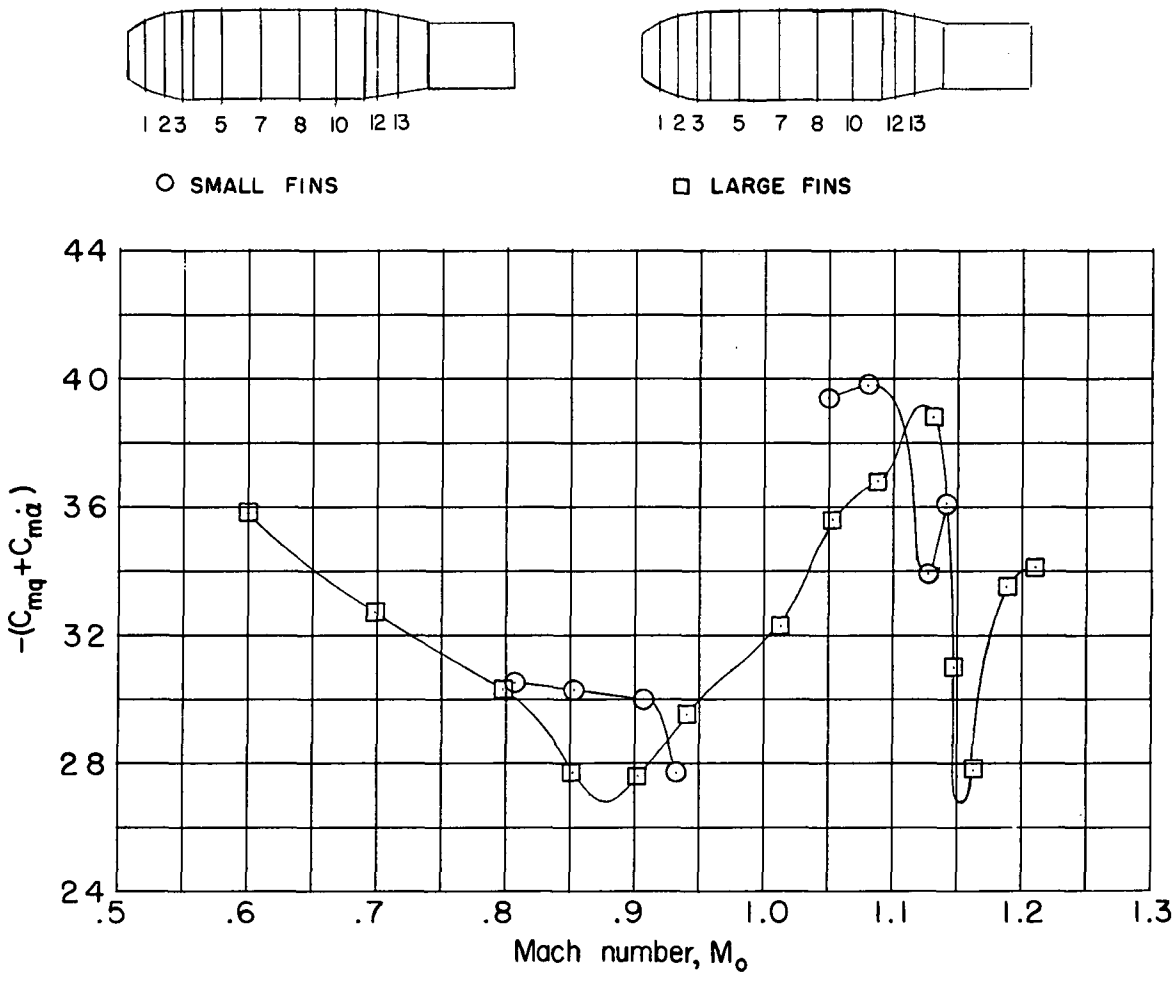

(a) Dynamic stability.

Figure 12.- The effect of fin size on the longitudinal stability of the TX-16 with large bands.

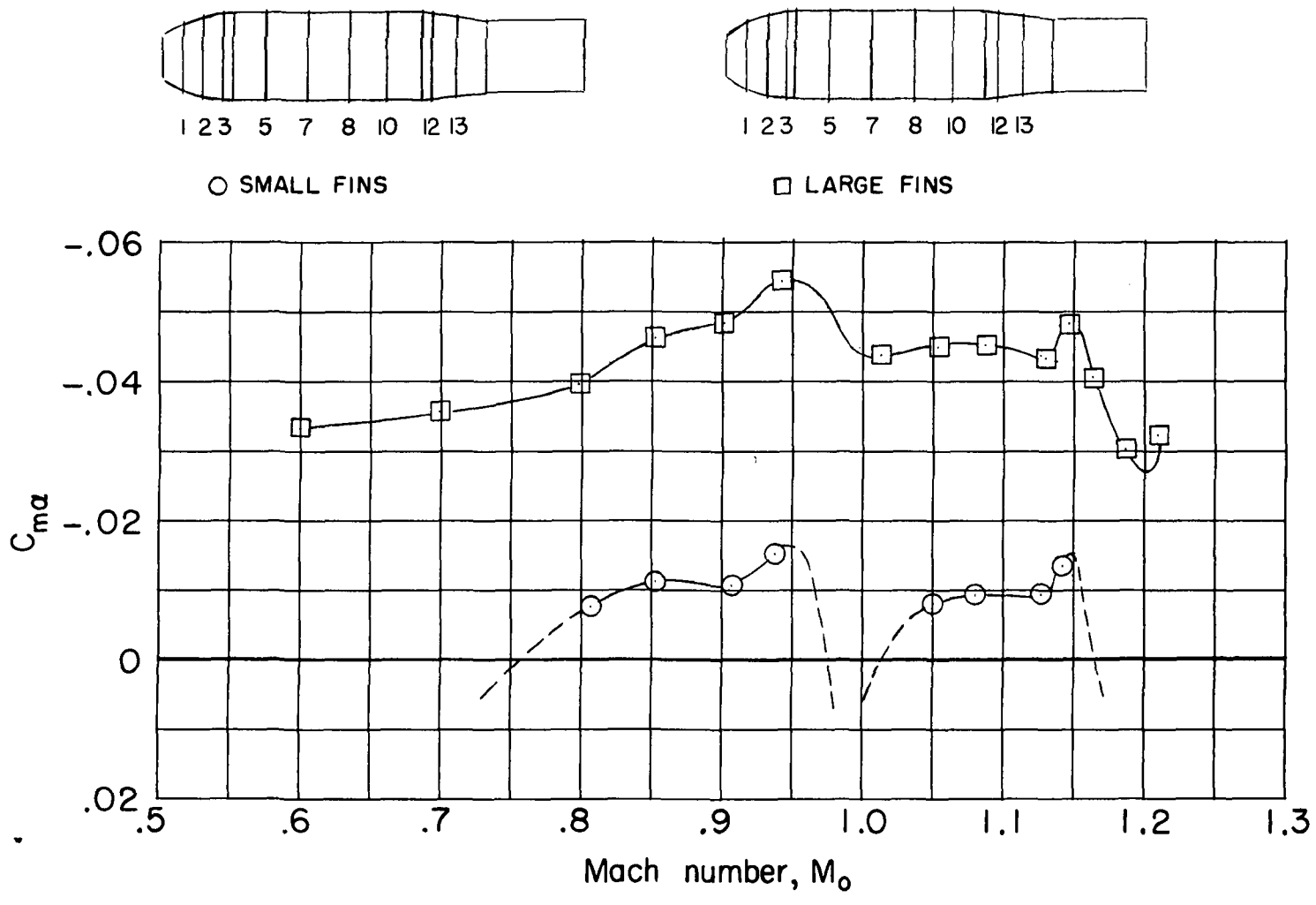

(b) Static stability.

Figure 12.- Concluded.

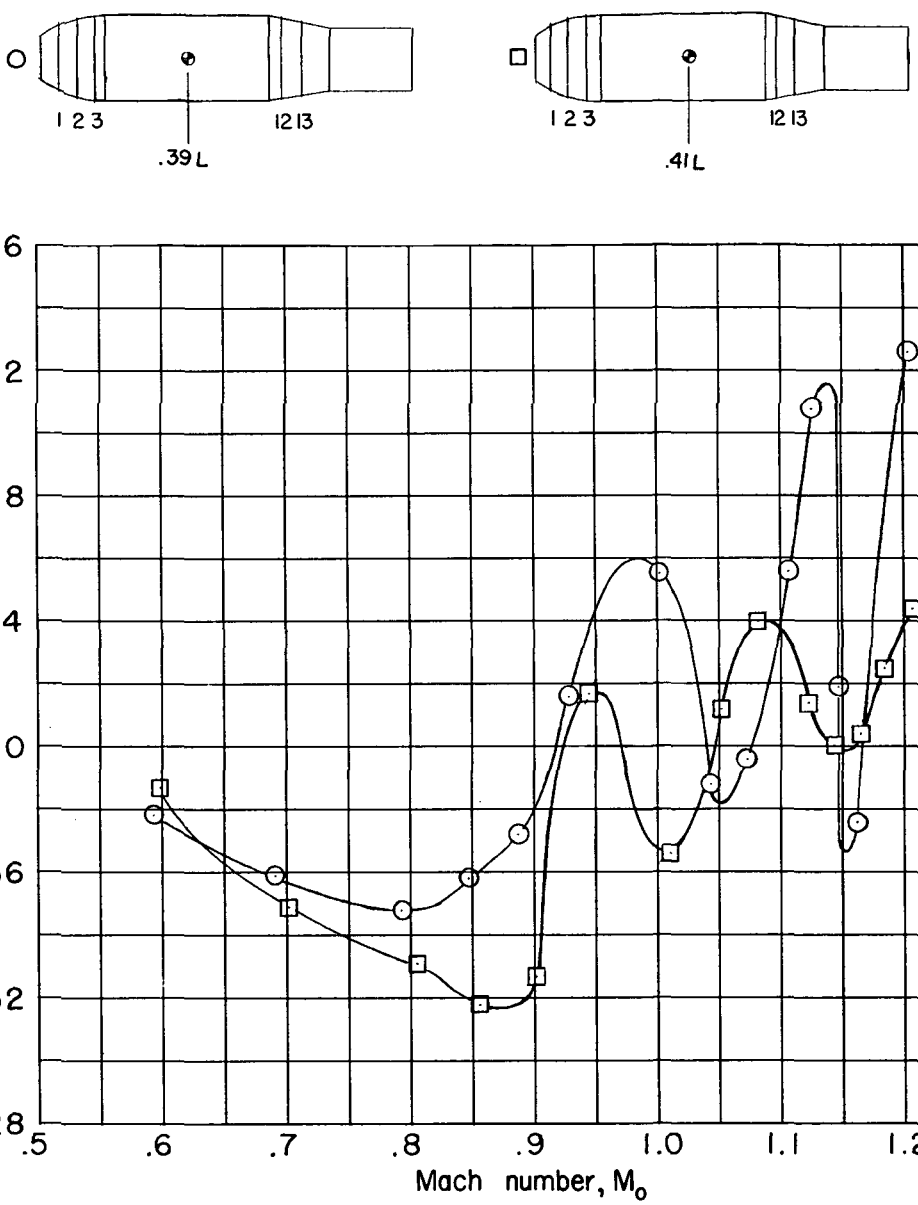

(a) Dynamic stability.

Figure 13.- The effect of center-of-gravity movement on the longitudinal stability of the TX-16 with large fins.

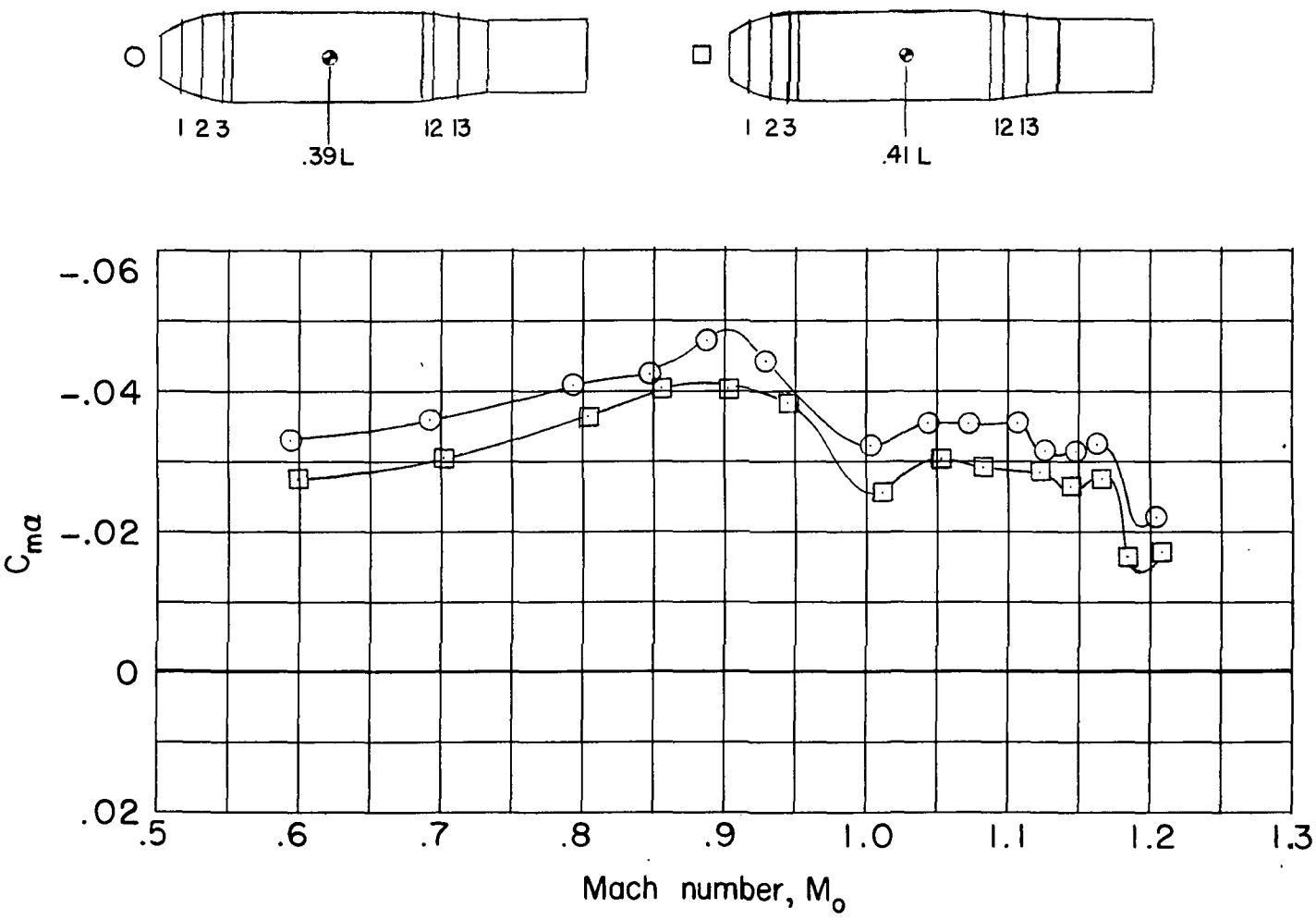

(b) Static stability.

Figure 13.- Concluded.

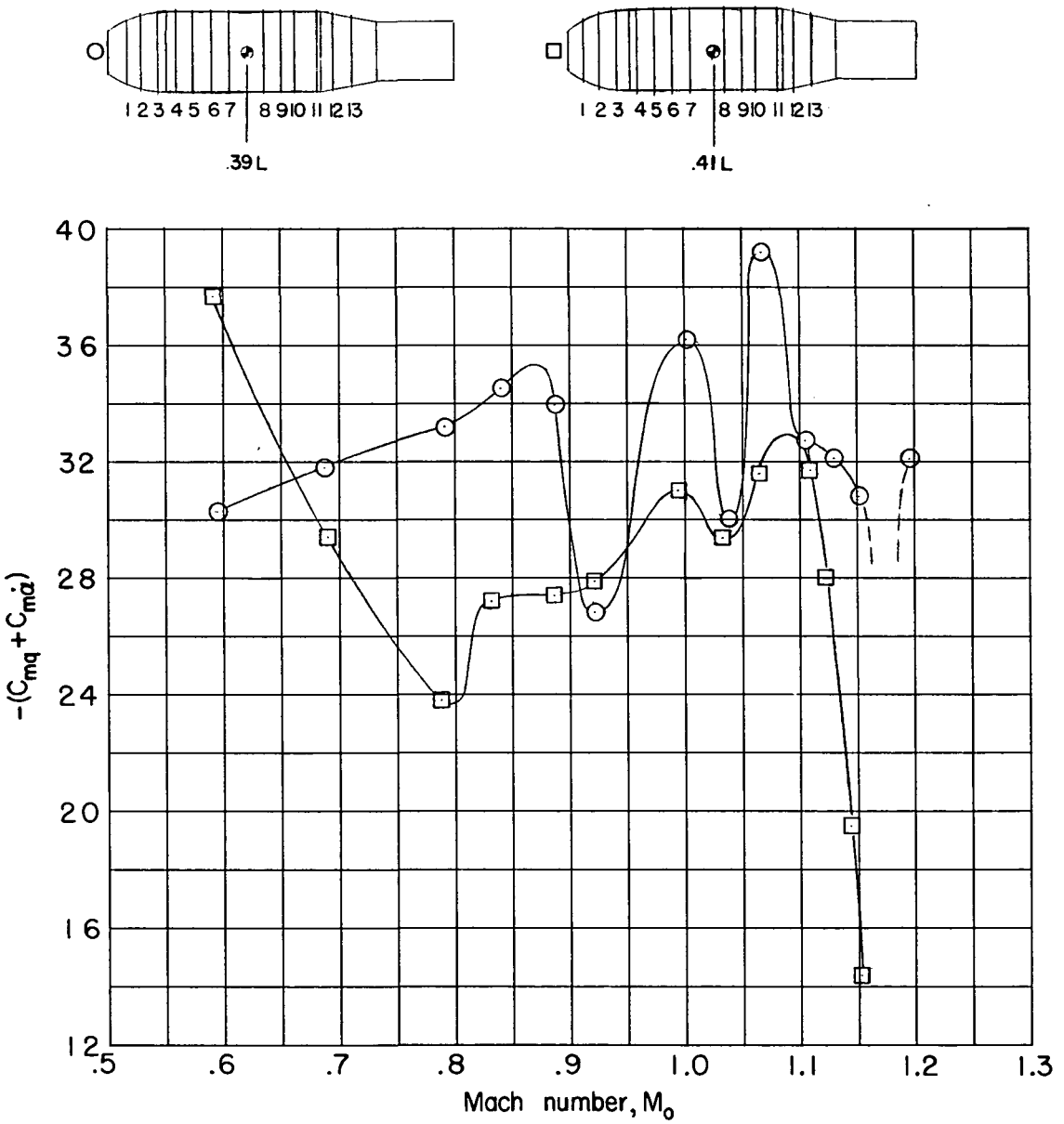

(a) Dynamic stability.

Figure 14.- The effect of center-of-gravity movement on the longitudinal stability of the TX-16 with small fins.

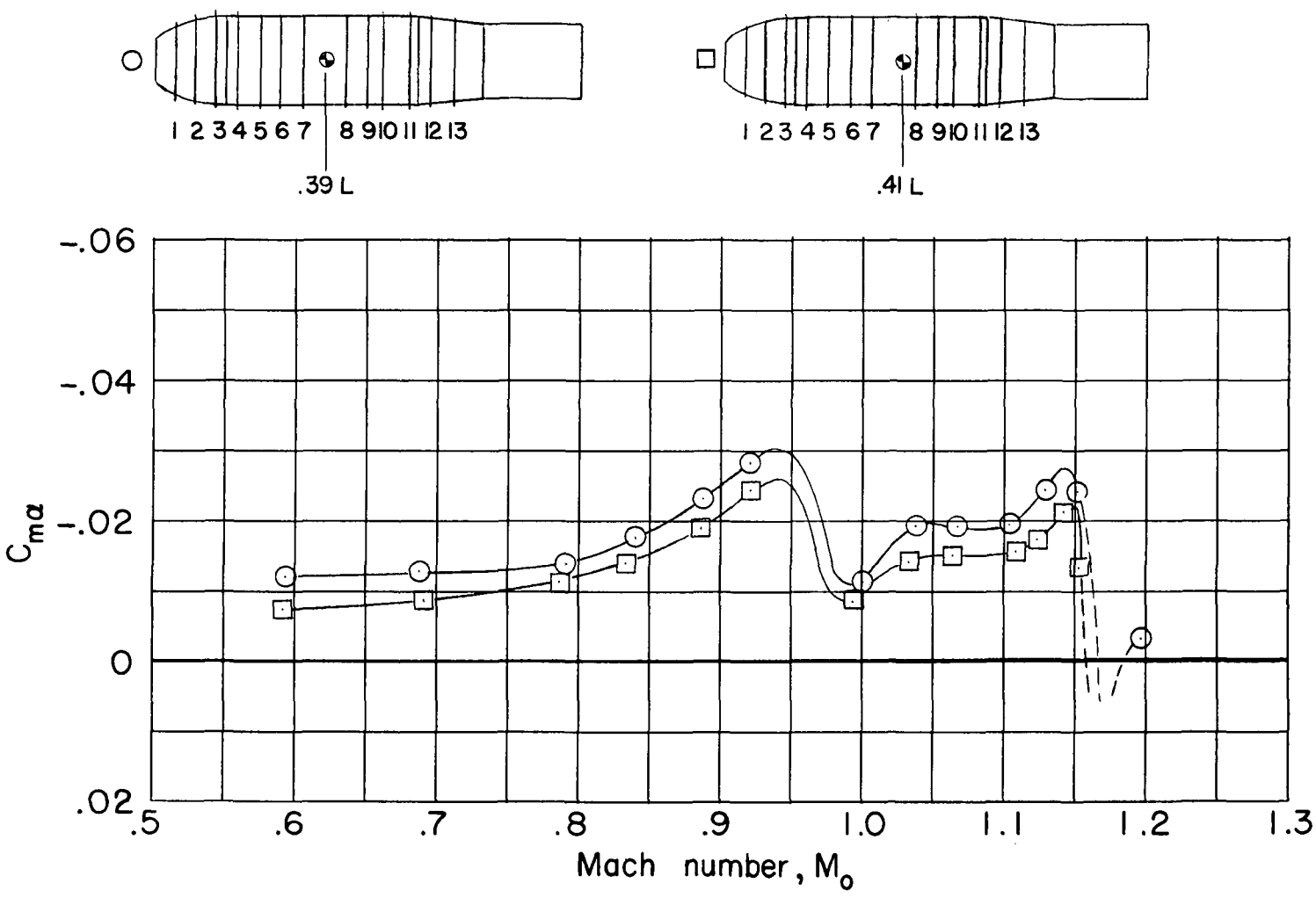

(b) Static stability

Figure 14.- Concluded.

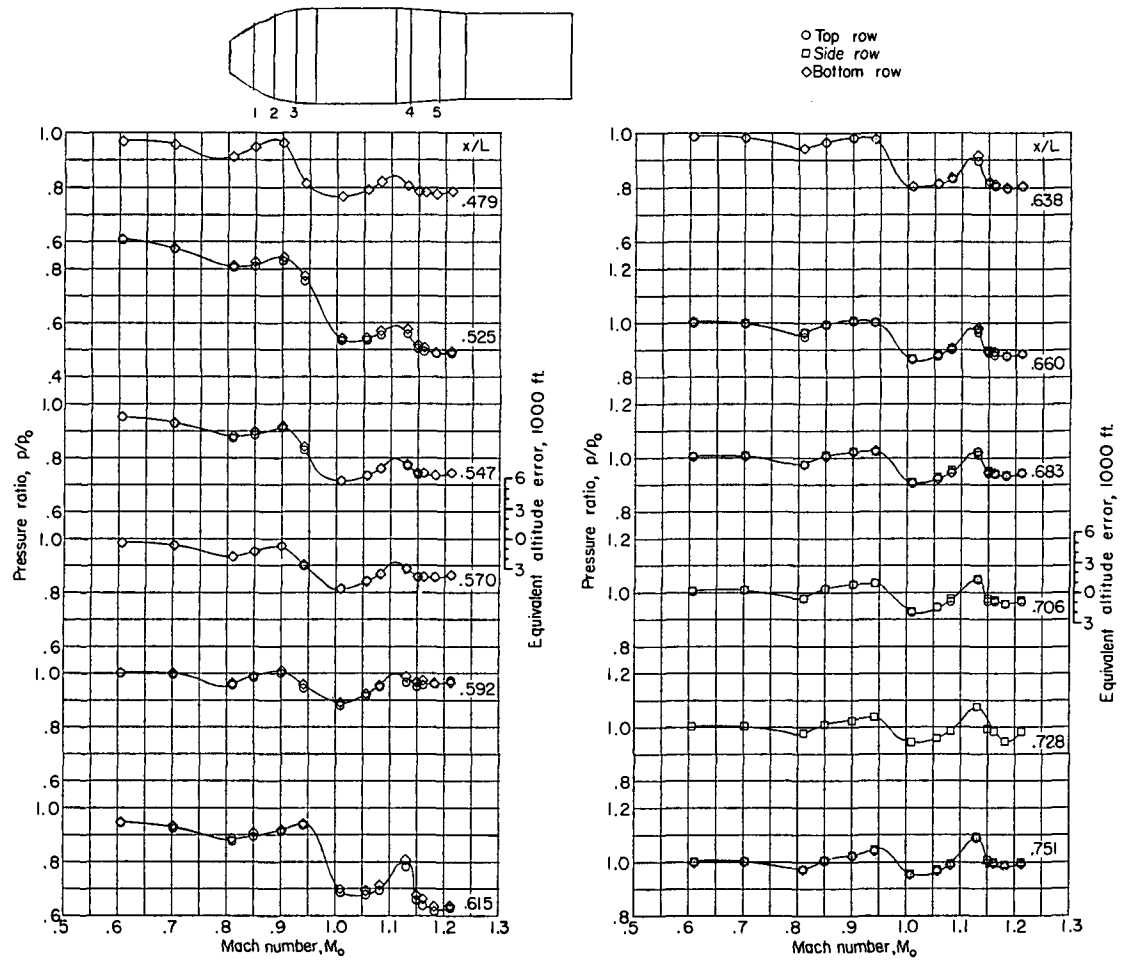

(a) $\alpha = 0^{\circ}$.

Figure 15.- The effect of Mach number and angle of attack on local static pressure ratios on the TX-14 afterbody.

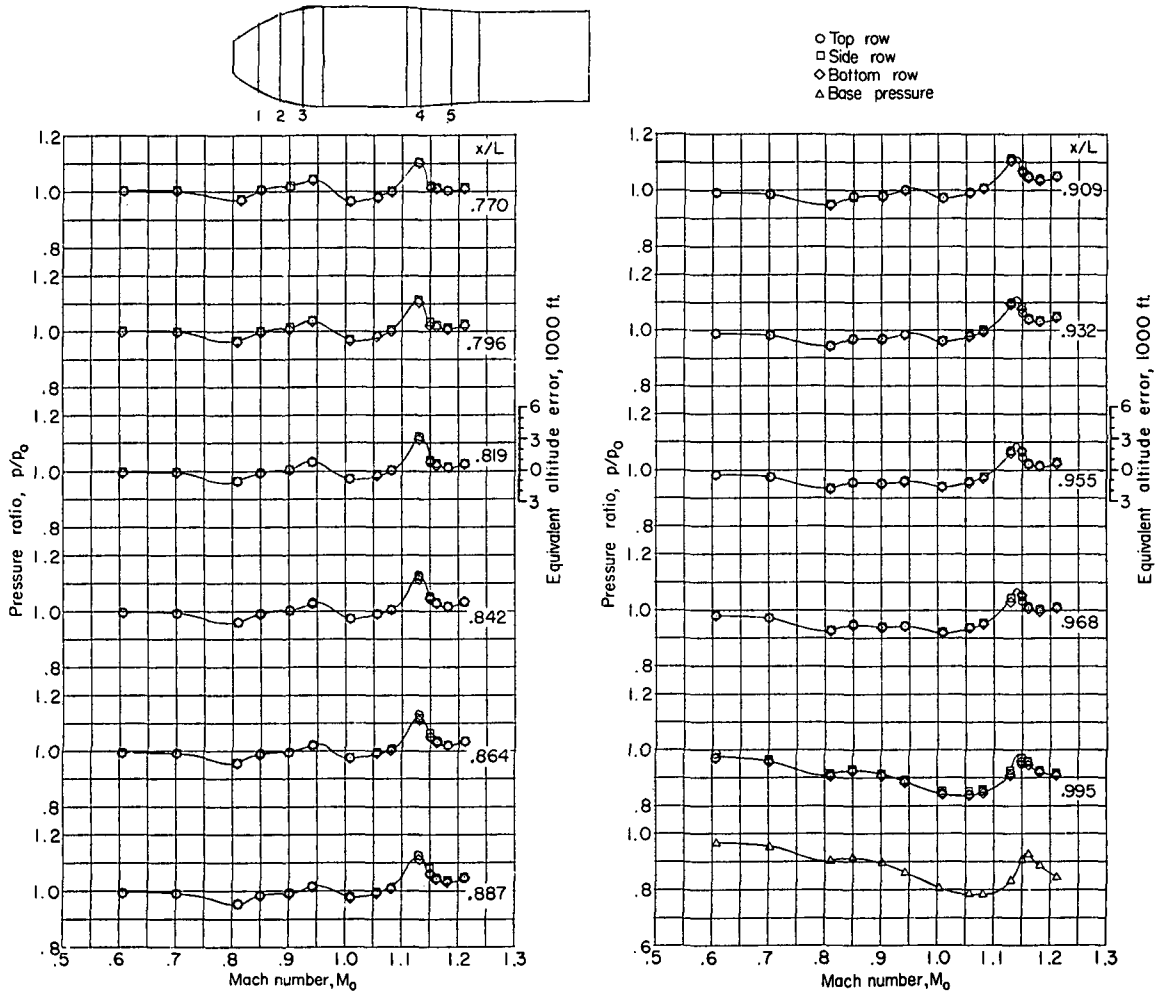

(a) $\alpha = 0^{\circ}$. Concluded.

Figure 15.- Continued.

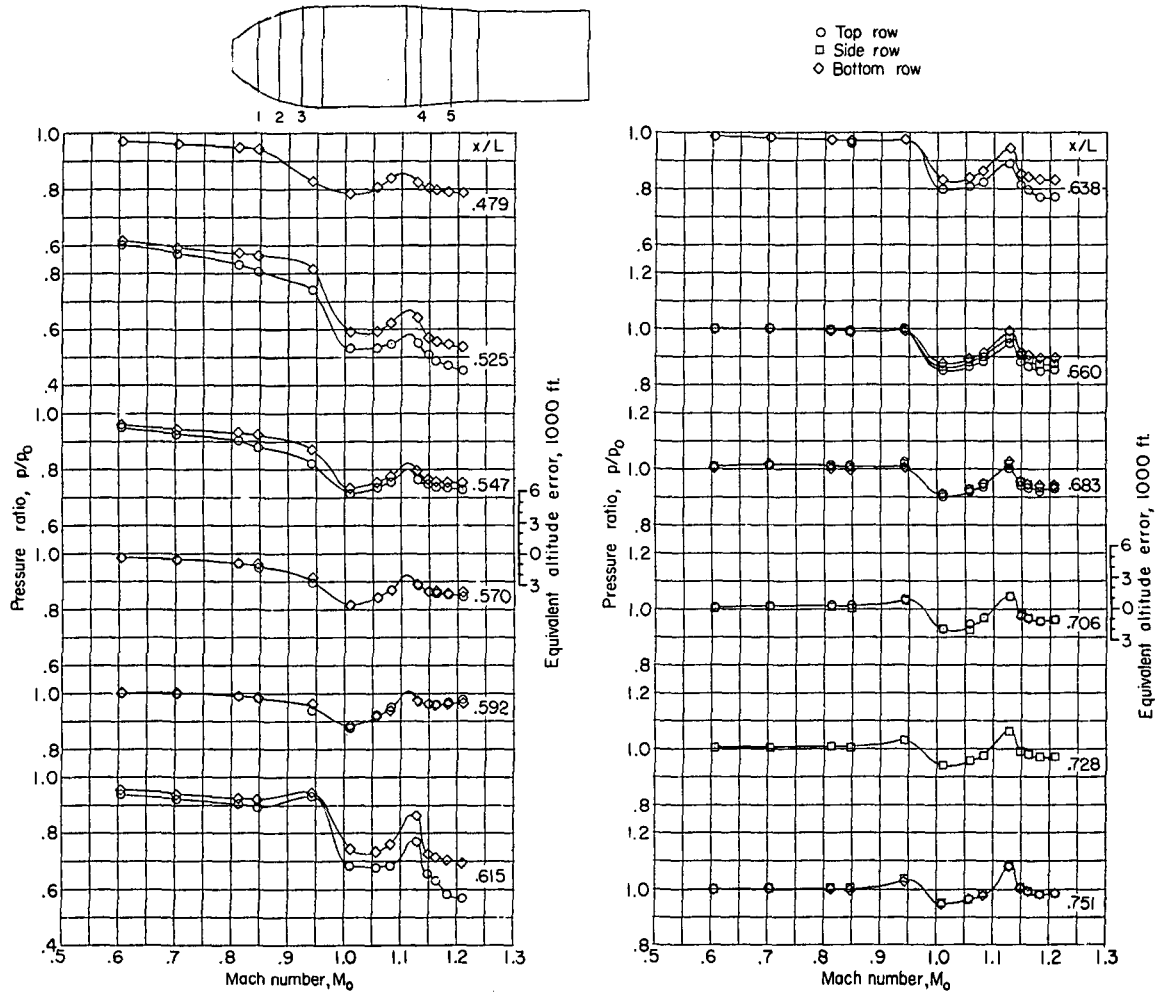

(b) $\alpha = -2^{\circ}$.

Figure 15.- Continued.

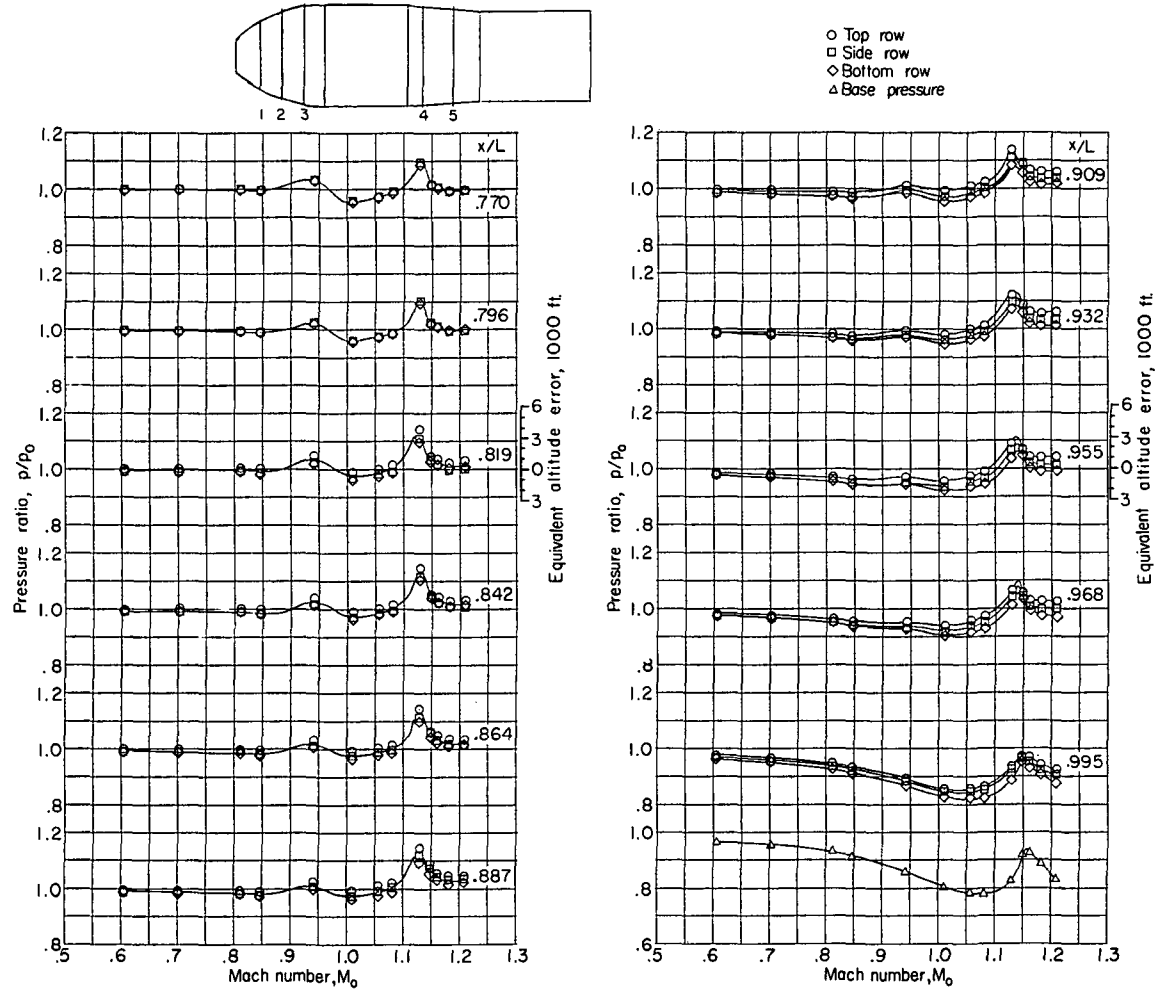

(b) $\alpha = -2^{\circ}$. Concluded.

Figure 15.- Continued.

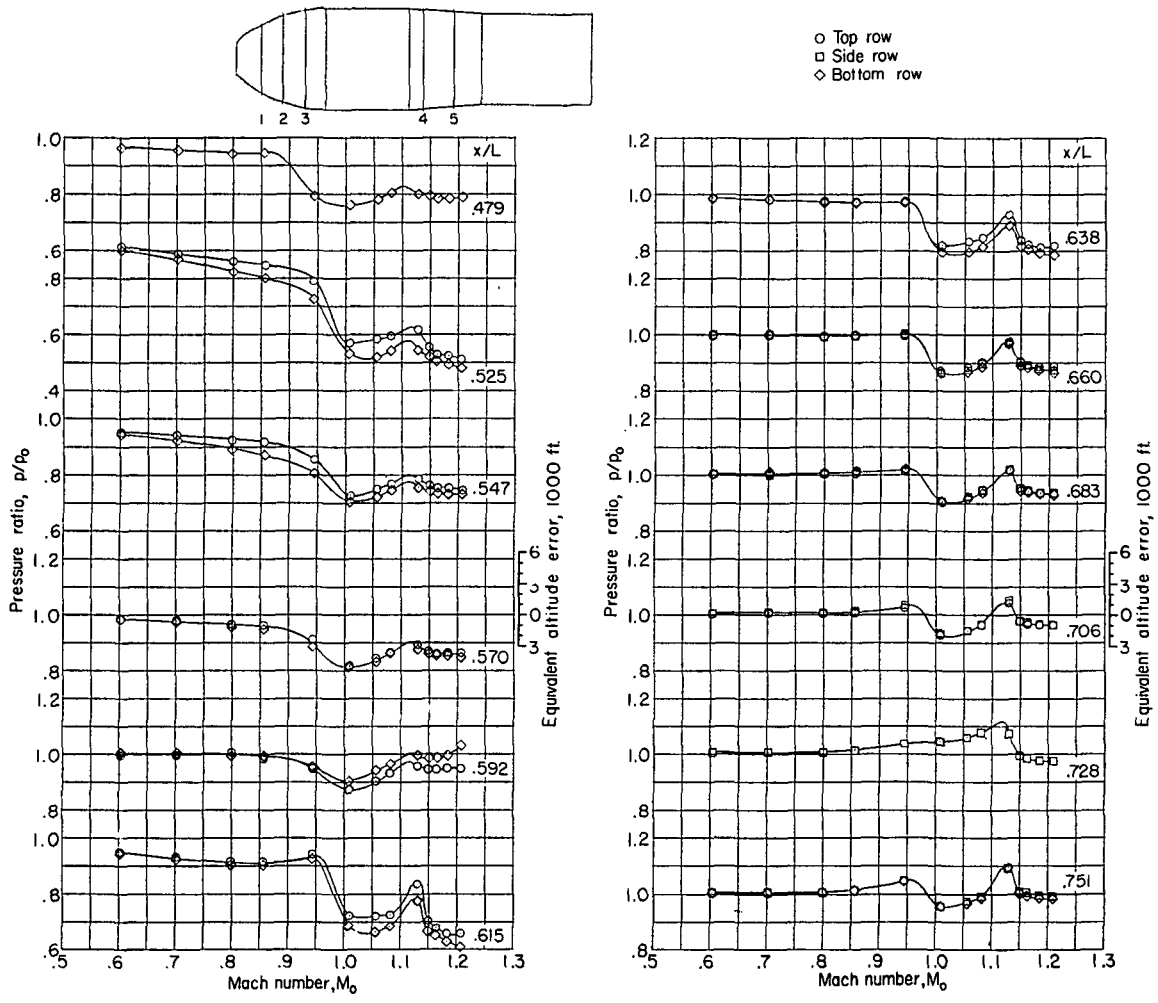

(c) $\alpha = +2^{\circ}$.

Figure 15.- Continued.

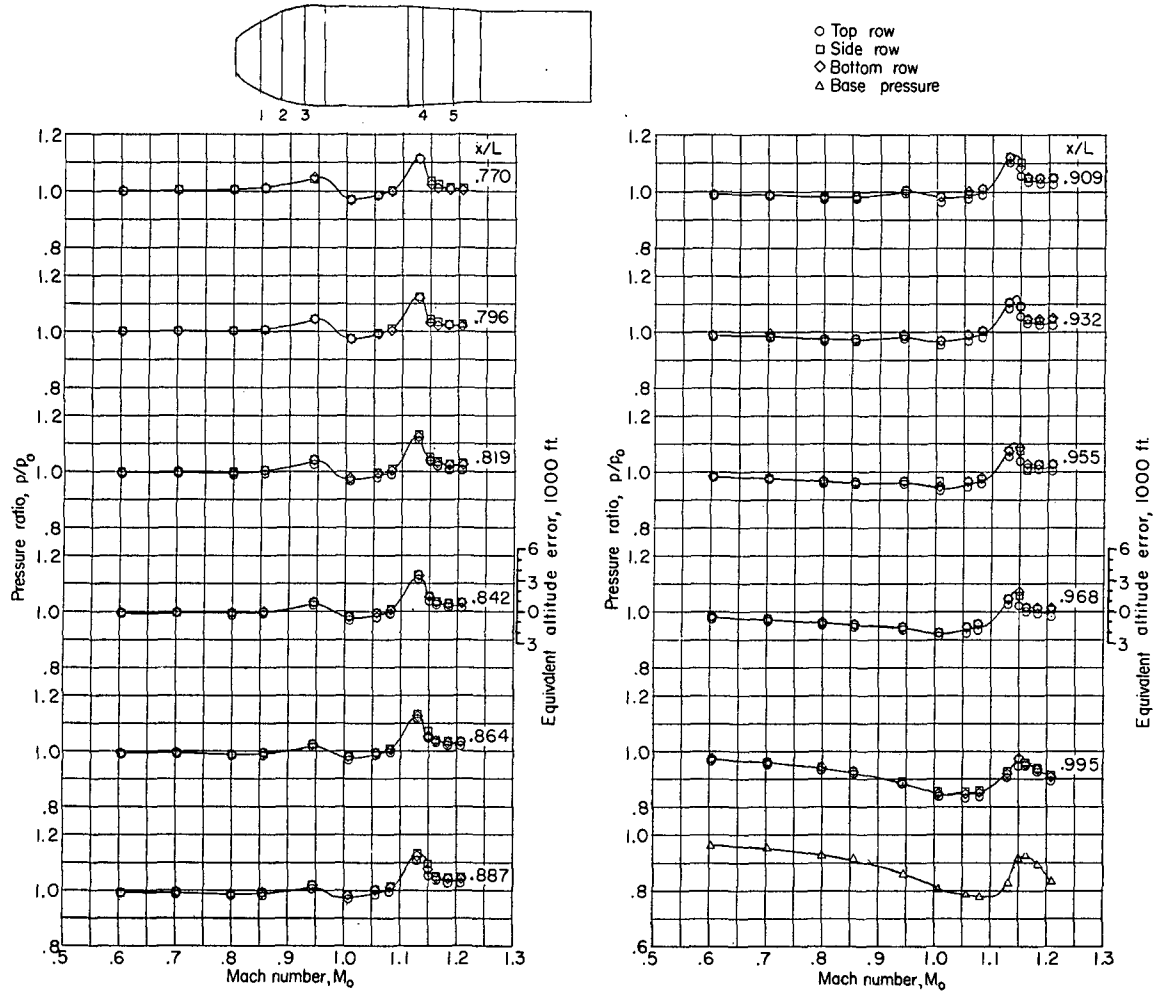

(c) $\alpha = +2^{\circ}$. Concluded.

Figure 15.- Concluded.

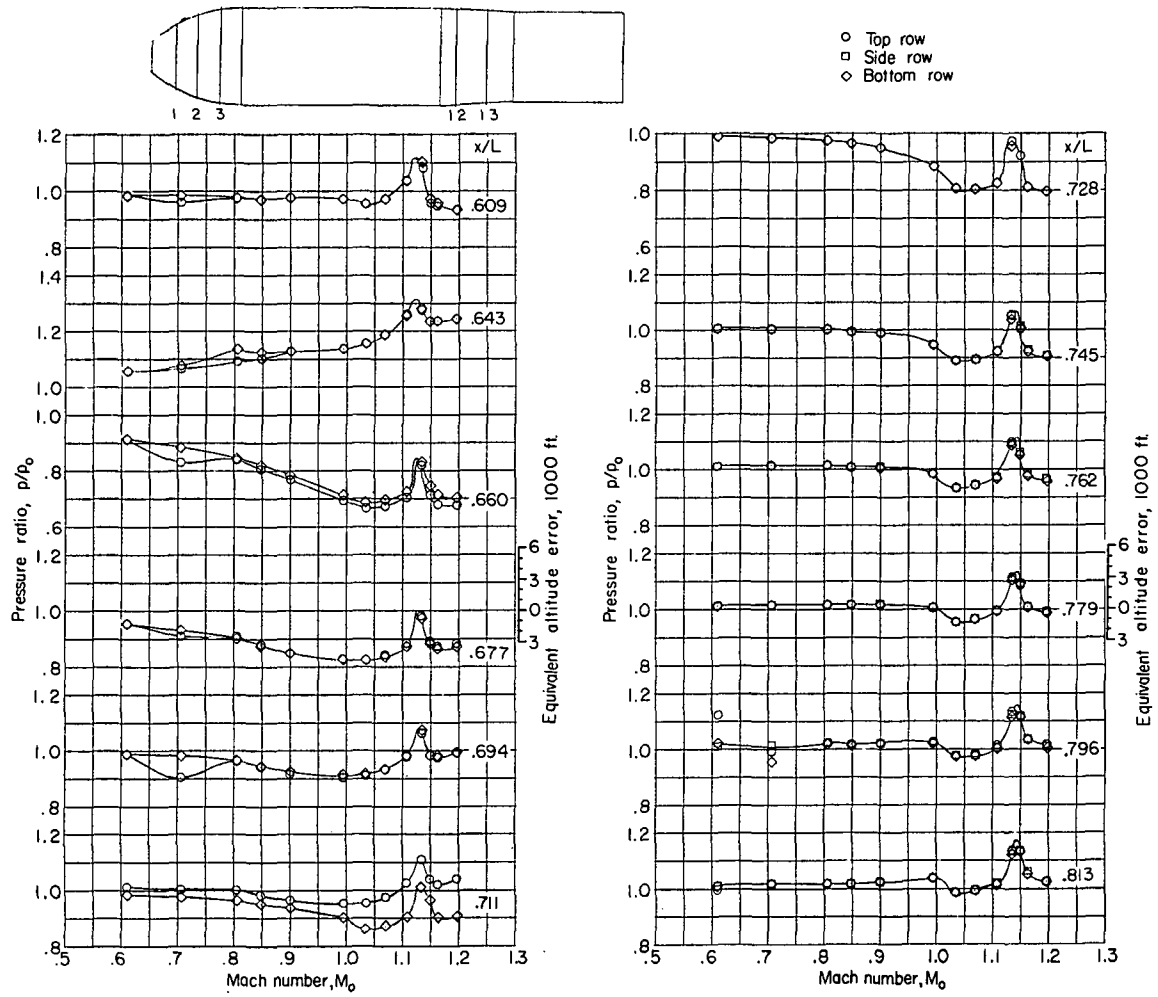

(a) $\alpha = 0^{\circ}$.

Figure 16.- The effects of Mach number and angle of attack on local static pressure ratios on the afterbody of the TX-16 with large bands and fins.

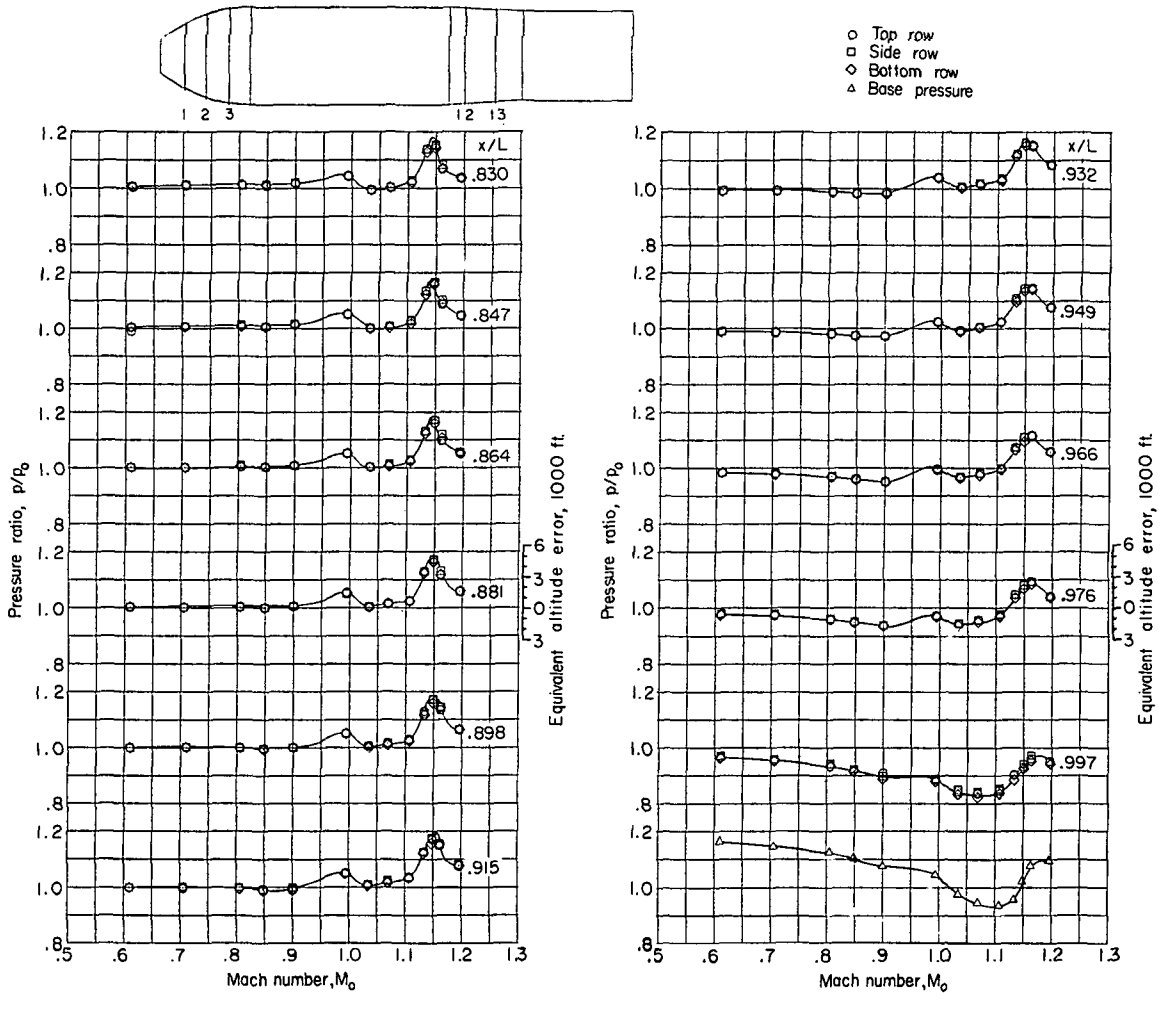

(a) $\alpha = 0^{\circ}$. Concluded.

Figure 16.- Continued.

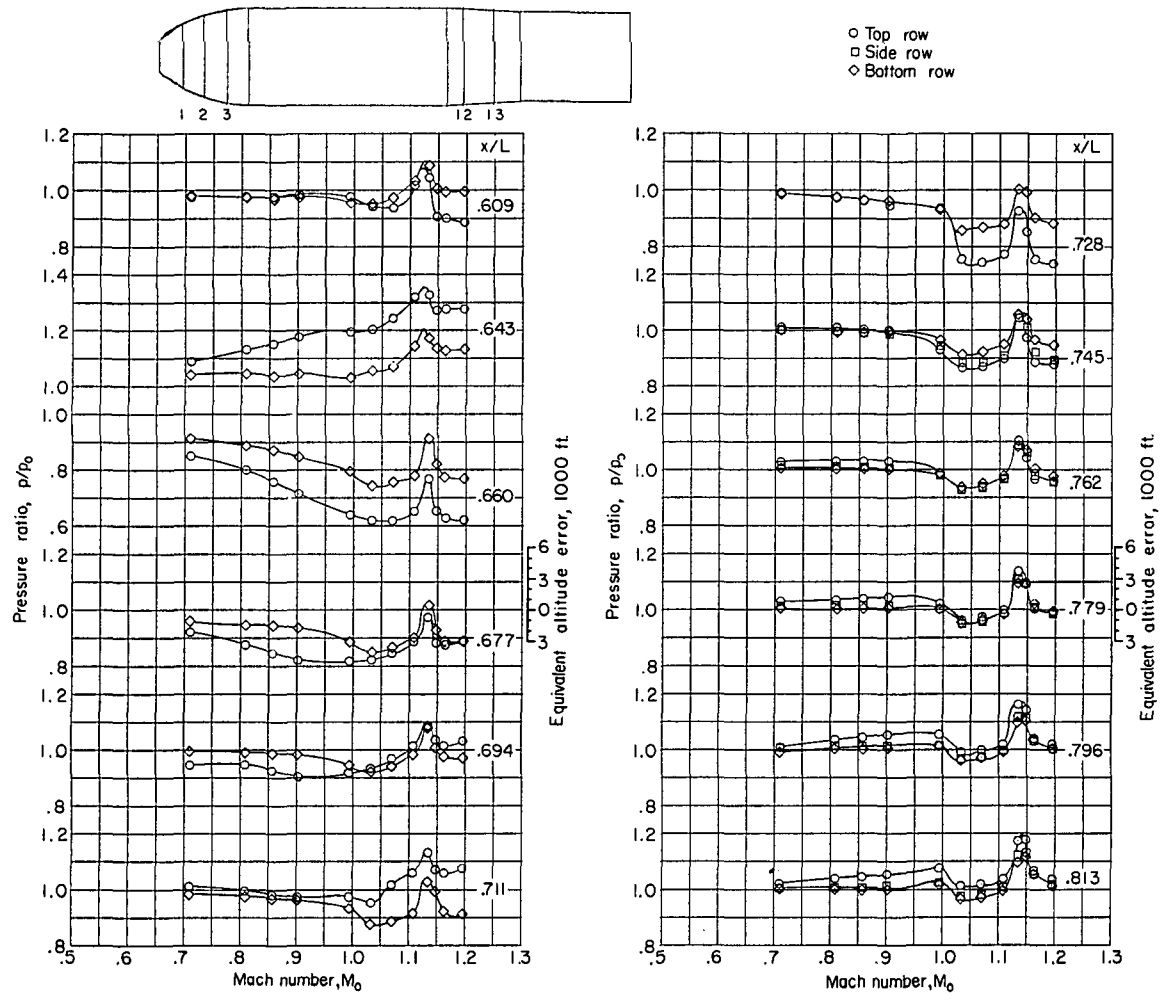

(b) $\alpha = -4^{\circ}$.

Figure 16.- Continued.

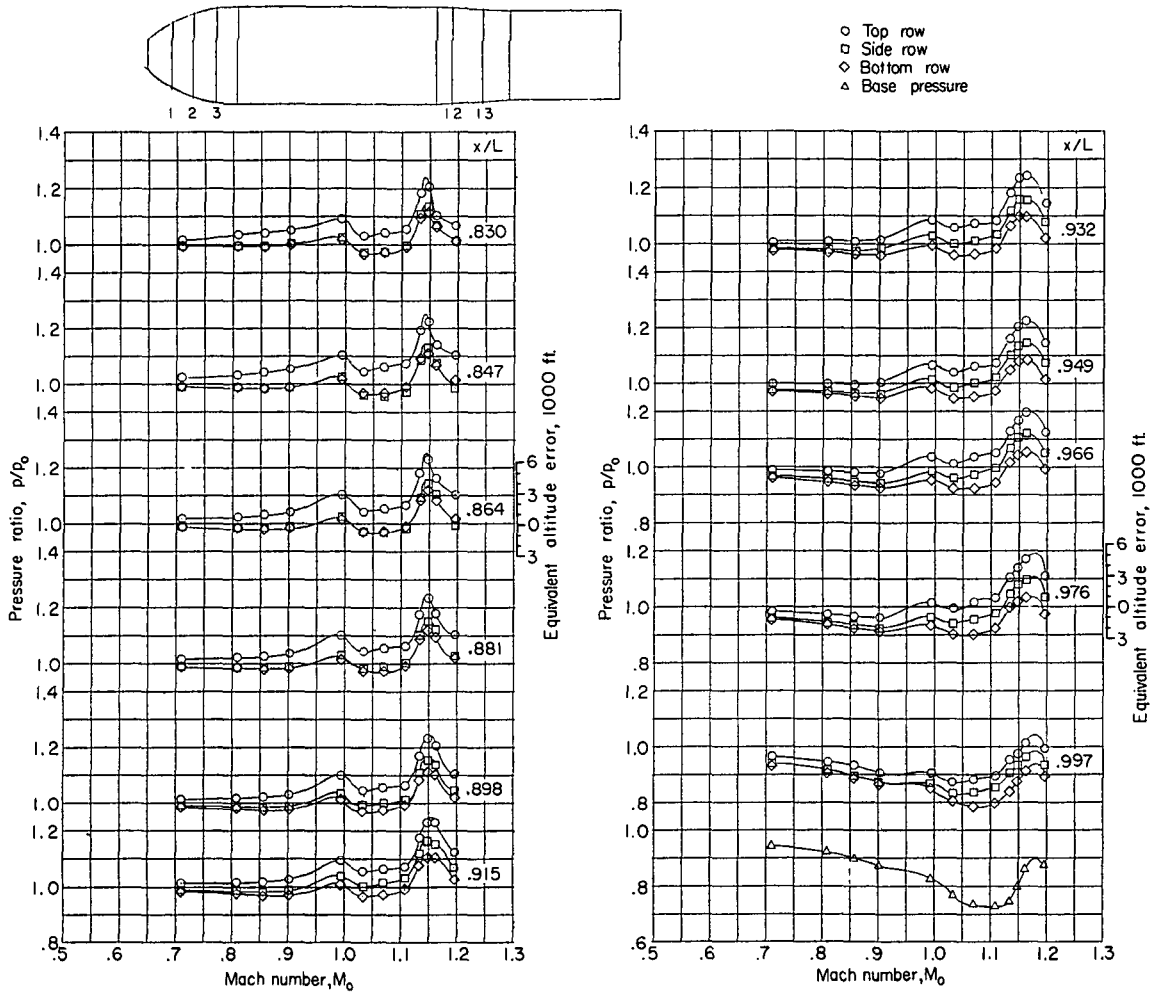

(b) $\alpha = -4^{\circ}$. Concluded.

Figure 16.- Continued.

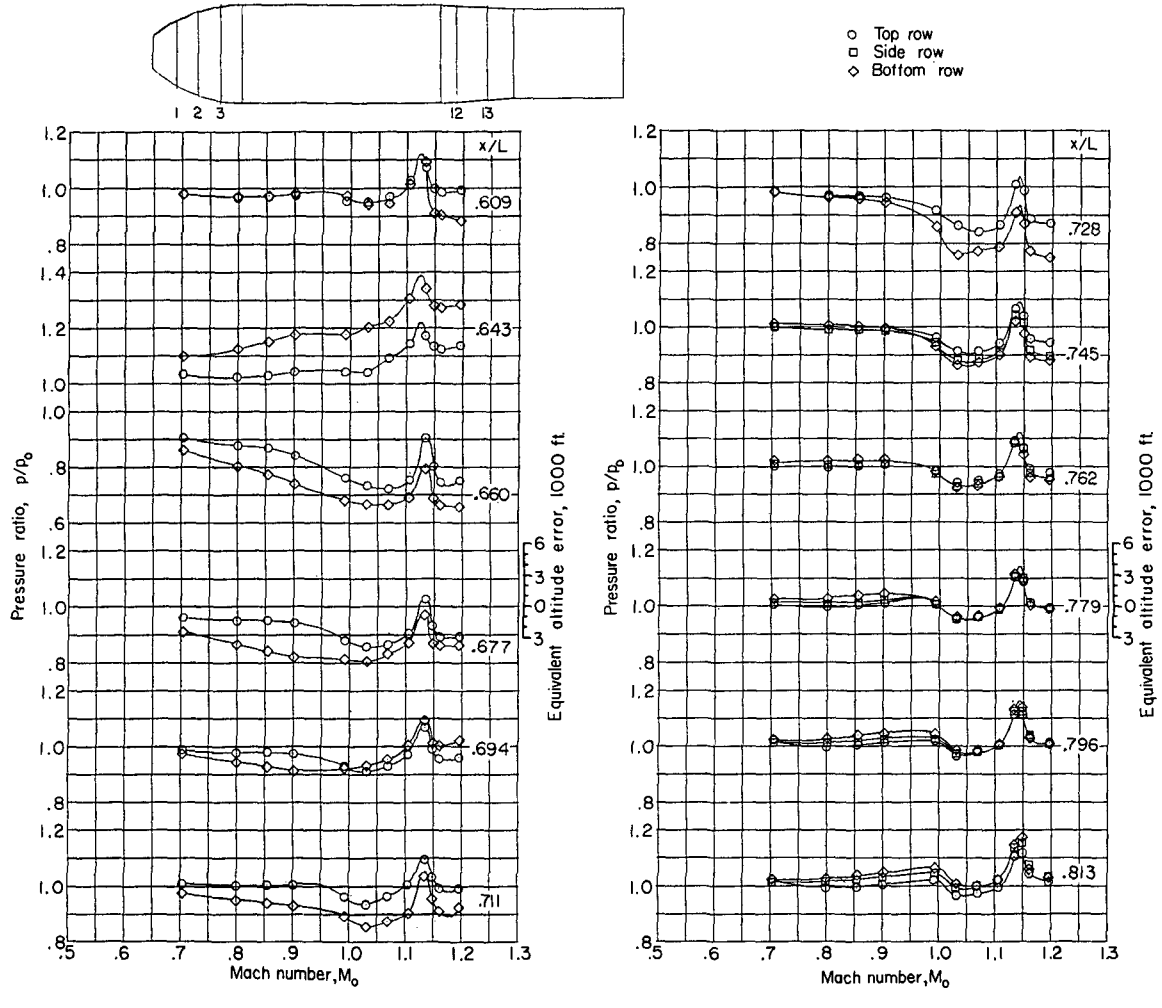

(c) $\alpha = +4^{\circ}$.

Figure 16.- Continued.

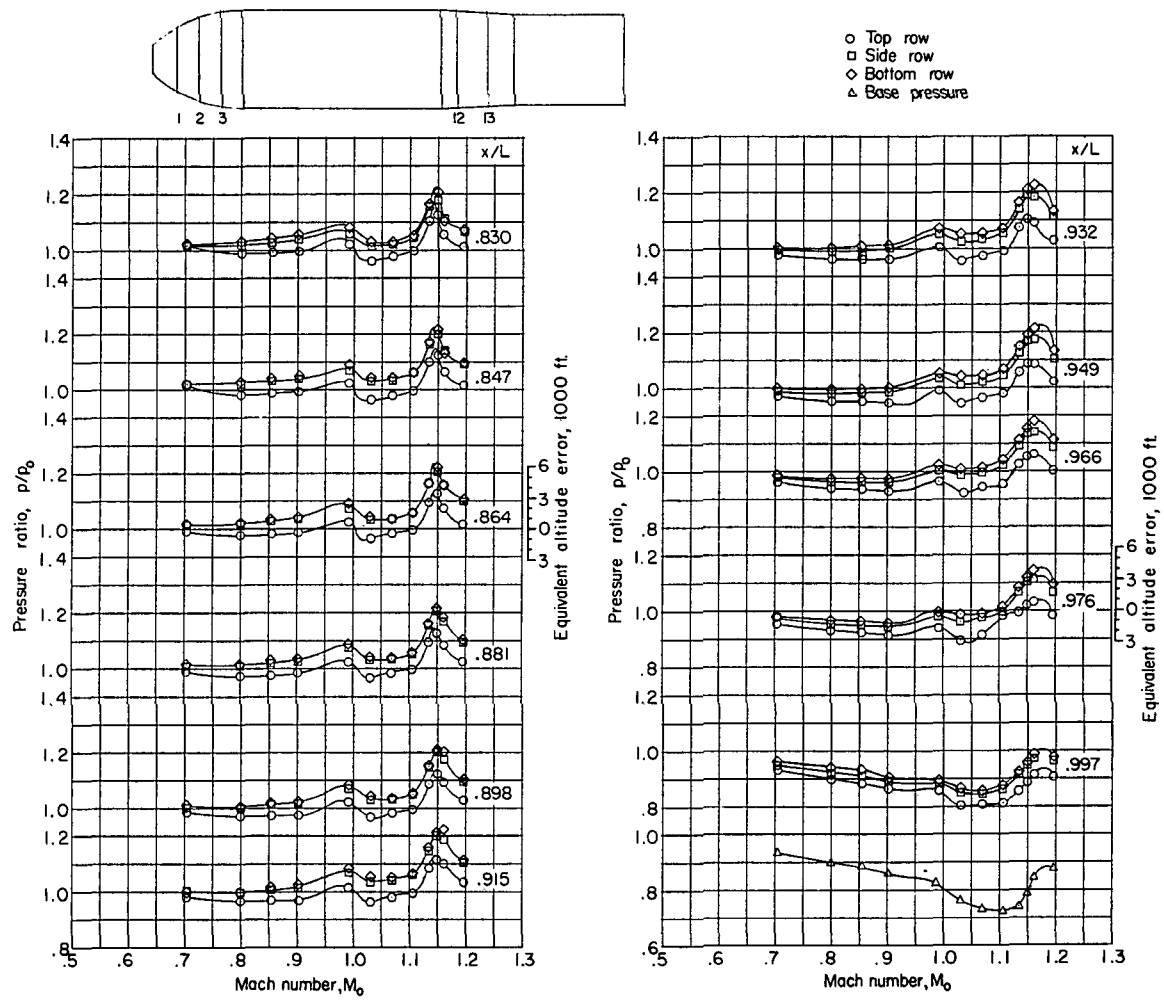

(c) $\alpha = +4^{\circ}$. Concluded.

Figure 16.- Continued.

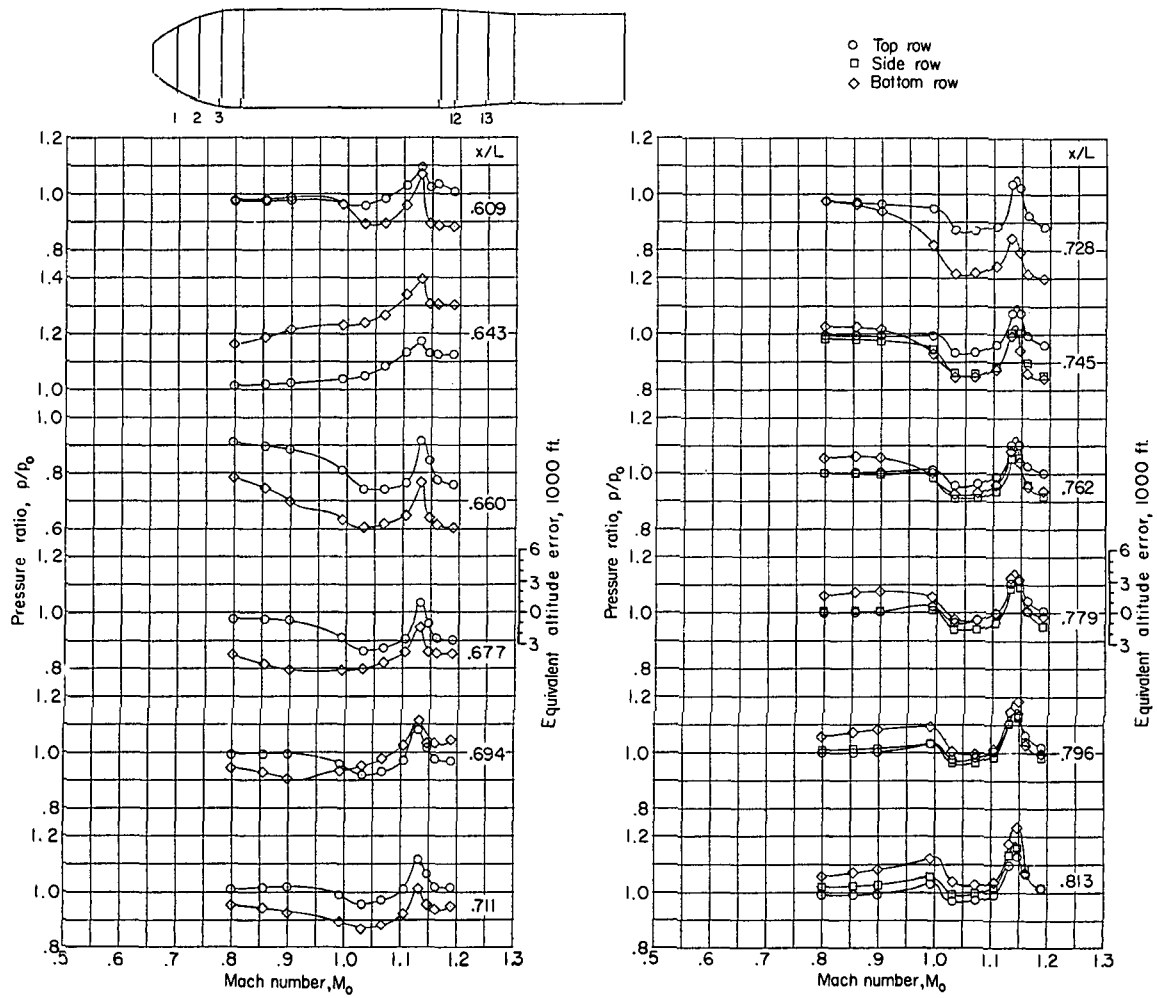

(d) $\alpha = +8^{\circ}$.

Figure 16.- Continued.

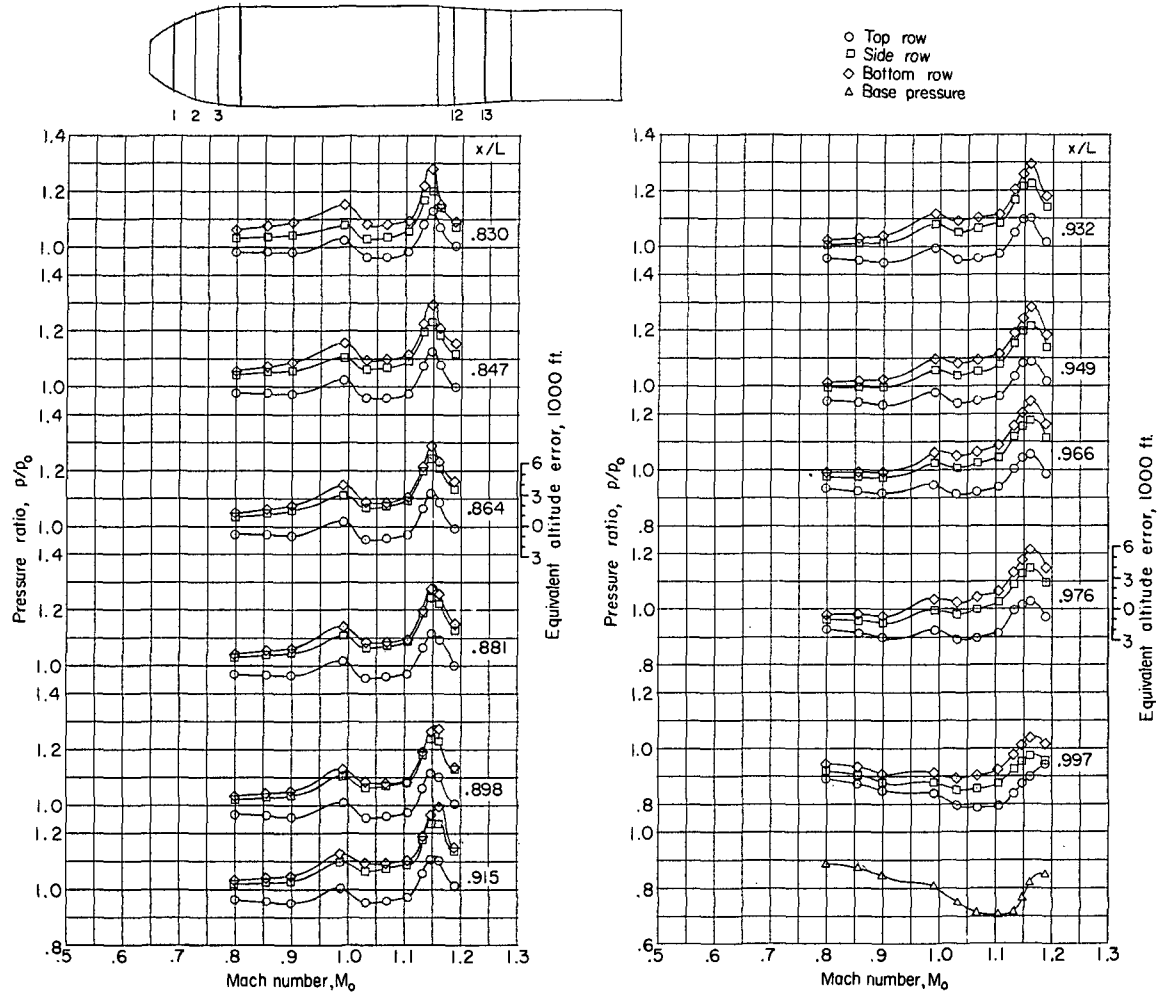

(d) $\alpha = +8^{\circ}$. Concluded.

Figure 16.- Continued.

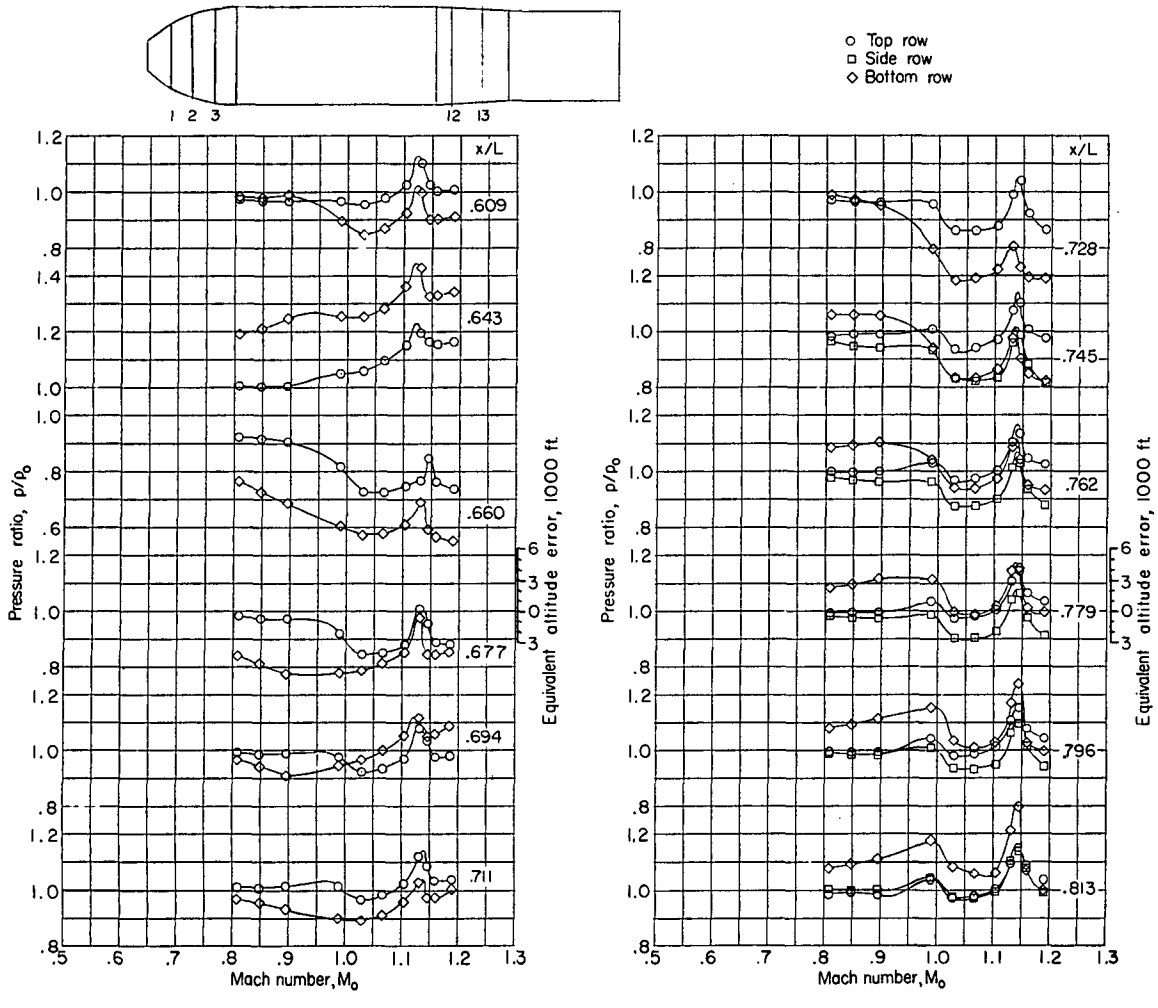

(e) $\alpha = +12^{\circ}$.

Figure 16.- Continued.

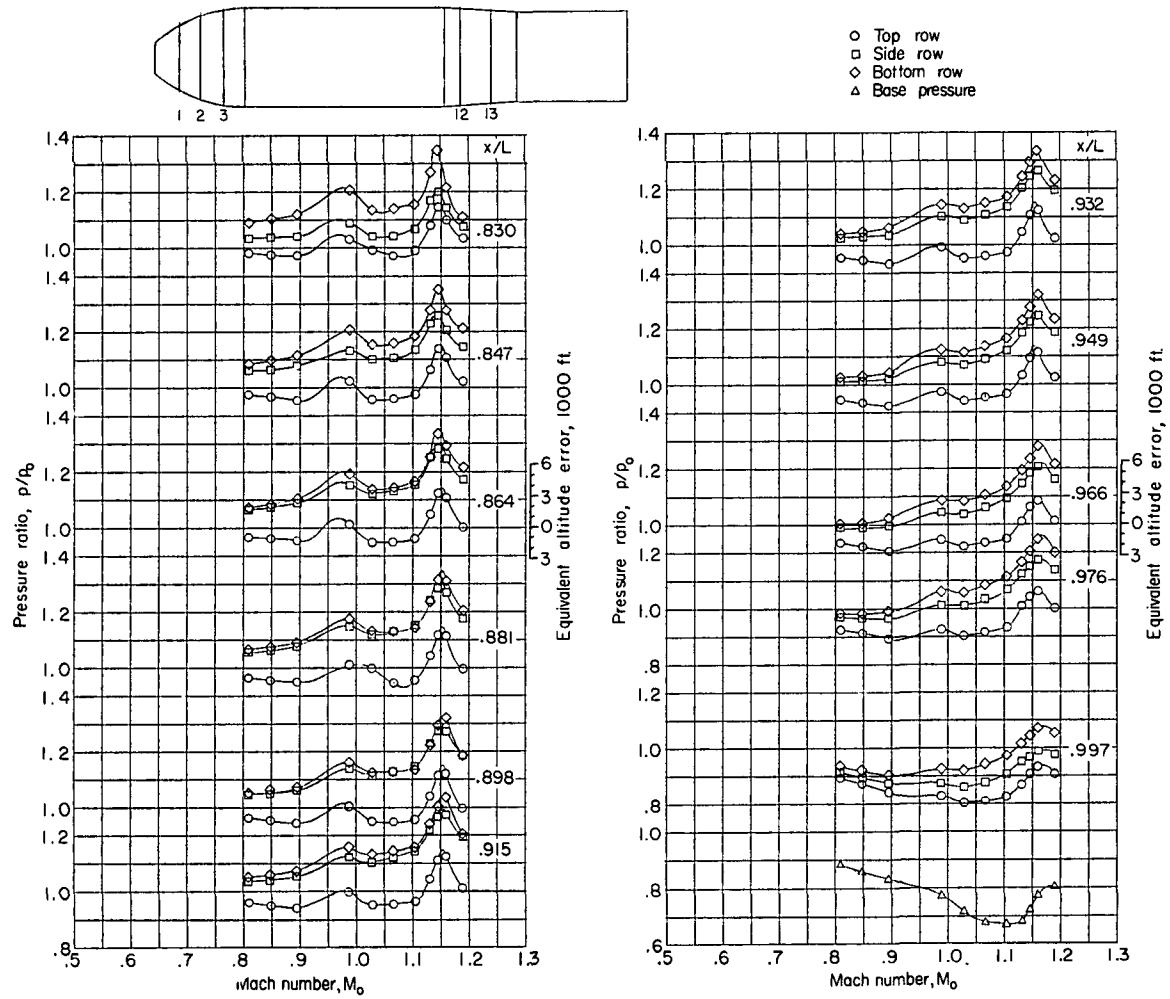

(e) $\alpha = +12^{\circ}$. Concluded.

Figure 16.- Concluded.

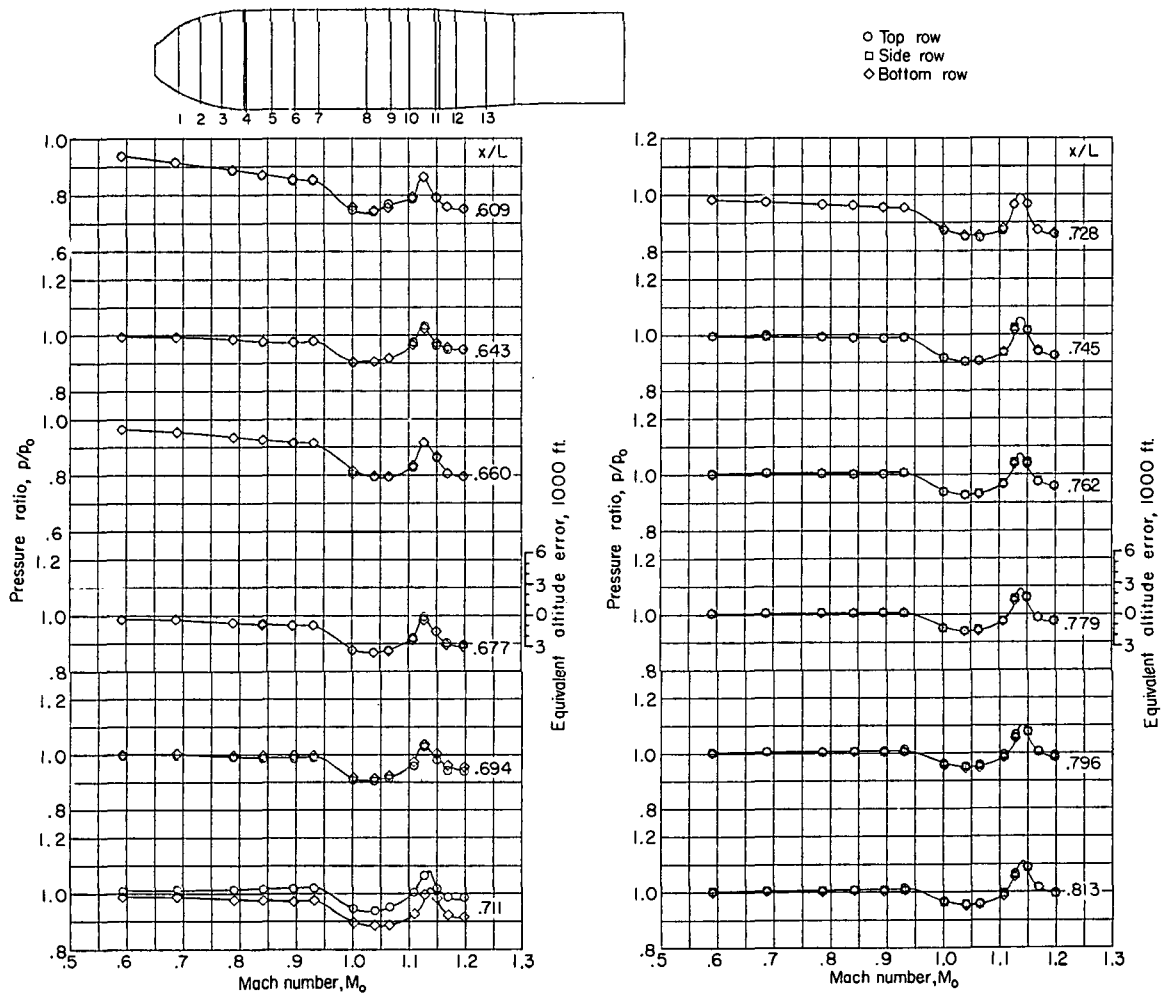

(a) $\alpha = 0^{\circ}$.

Figure 17.- The effects of Mach number and angle of attack on local static pressure ratios on the afterbody of the TX-16 with large bands and small fins.

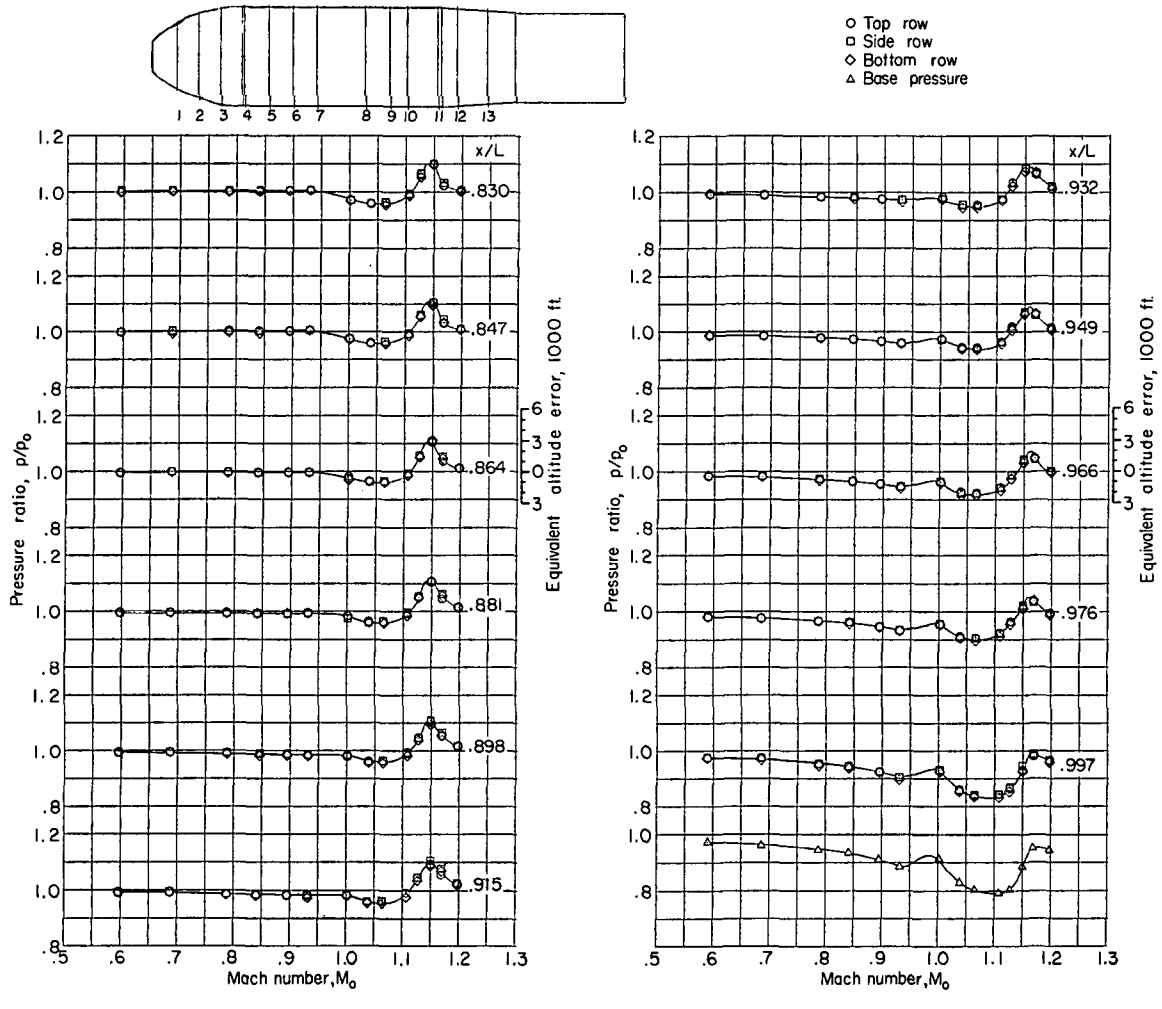

(a) $\alpha = 0^{\circ}$. Concluded.

Figure 17.- Continued.

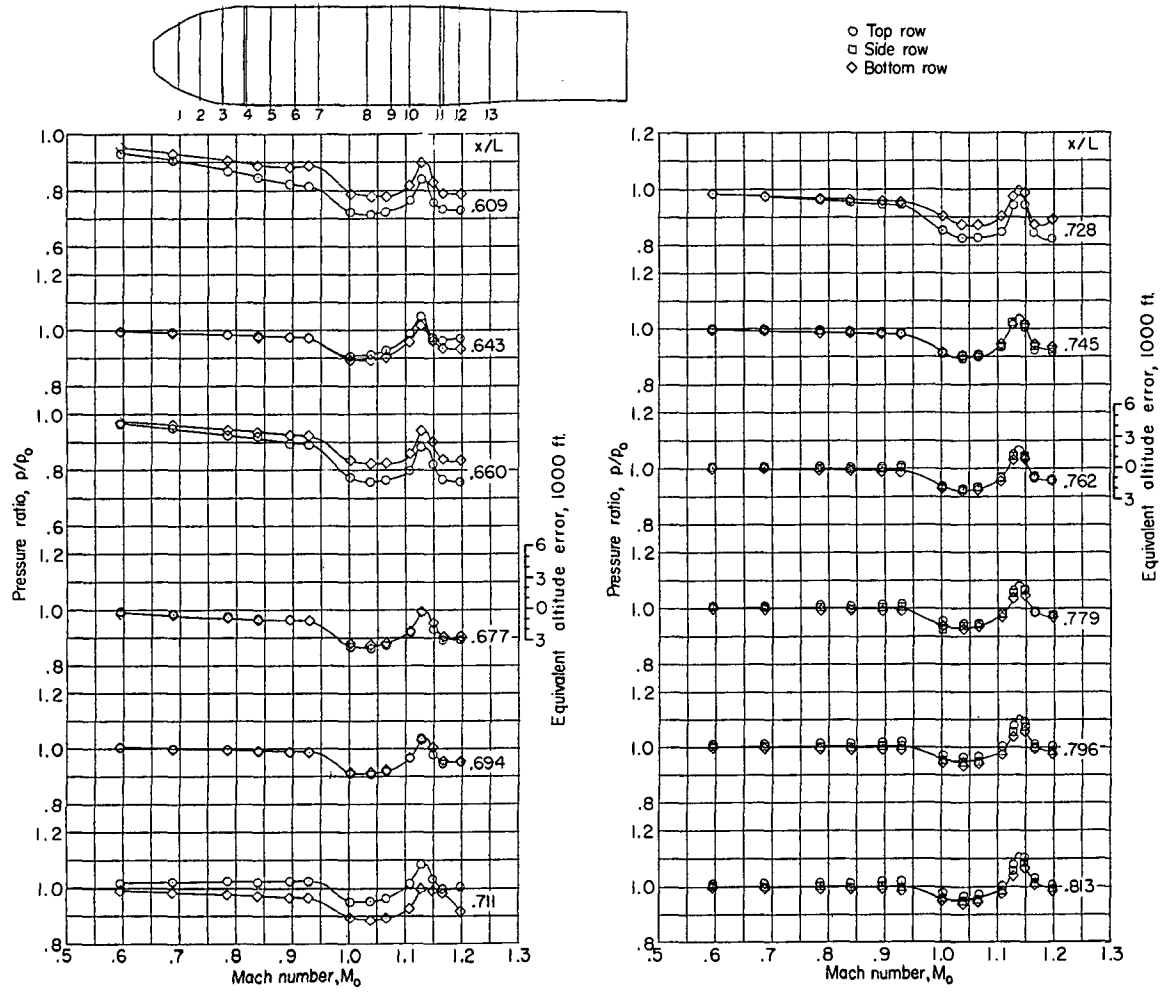

(b) $\alpha = -2^{\circ}$.

Figure 17.- Continued.

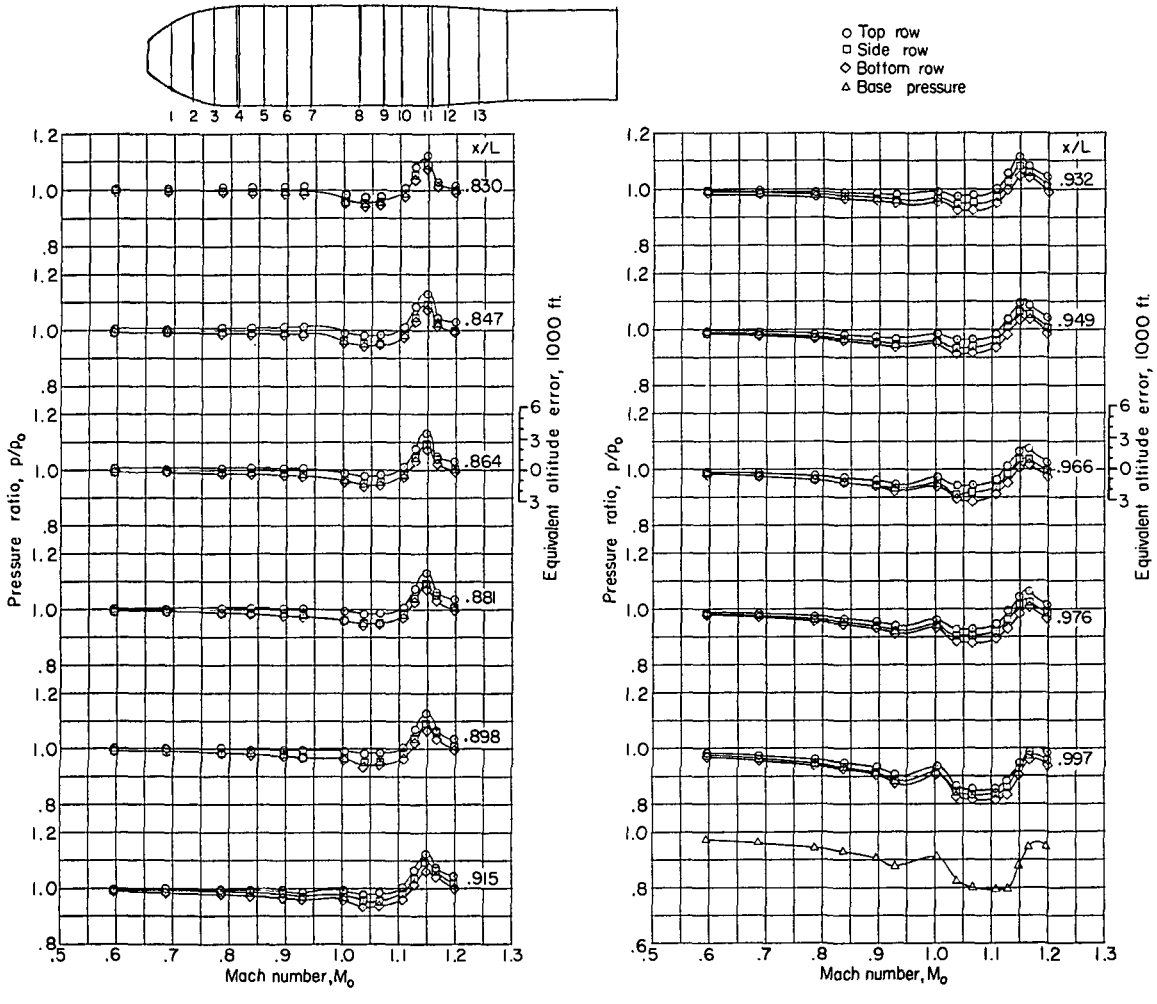

(b) $\alpha = -2^{\circ}$. Concluded.

Figure 17.- Continued.

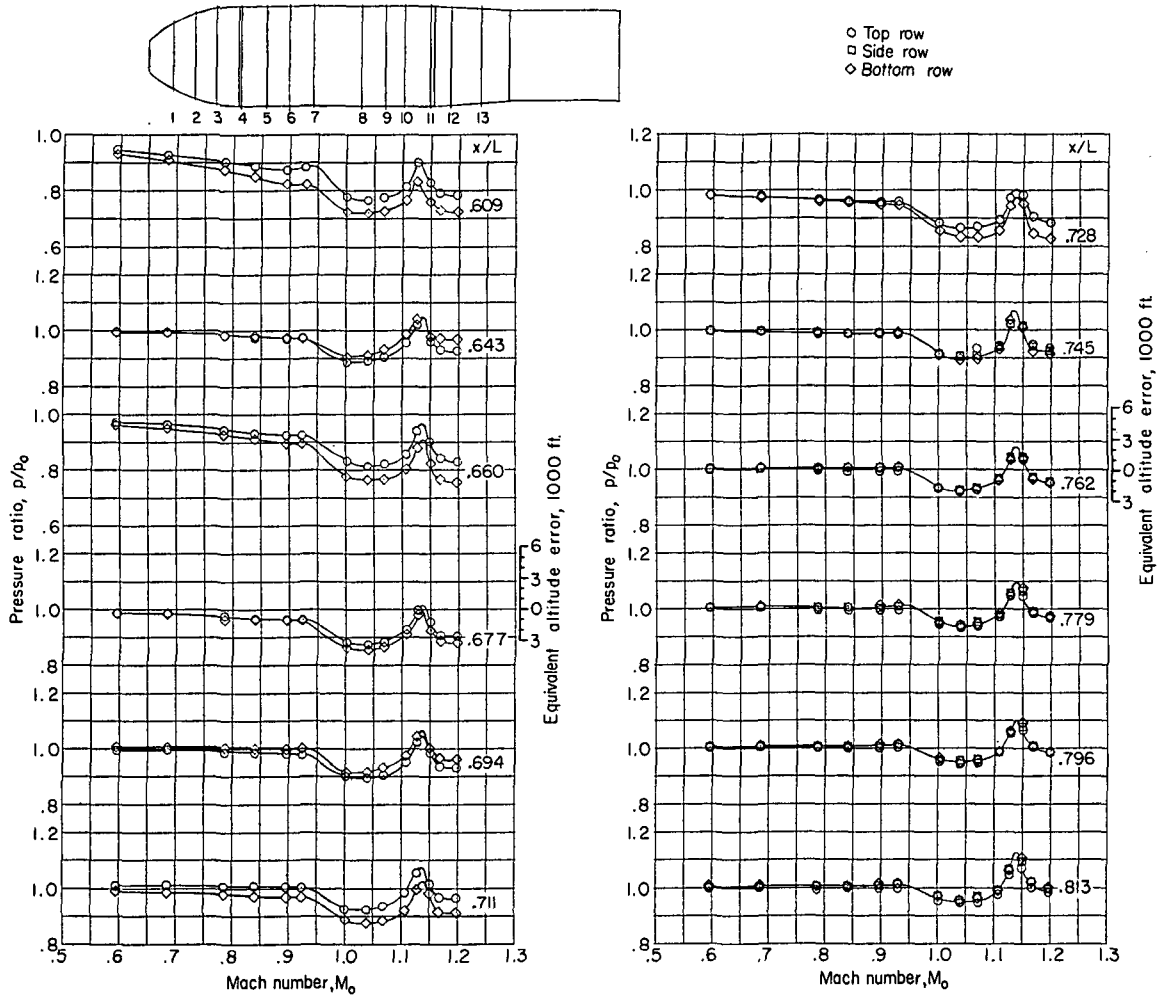

(c) $\alpha = +2^{\circ}$.

Figure 17.- Continued.

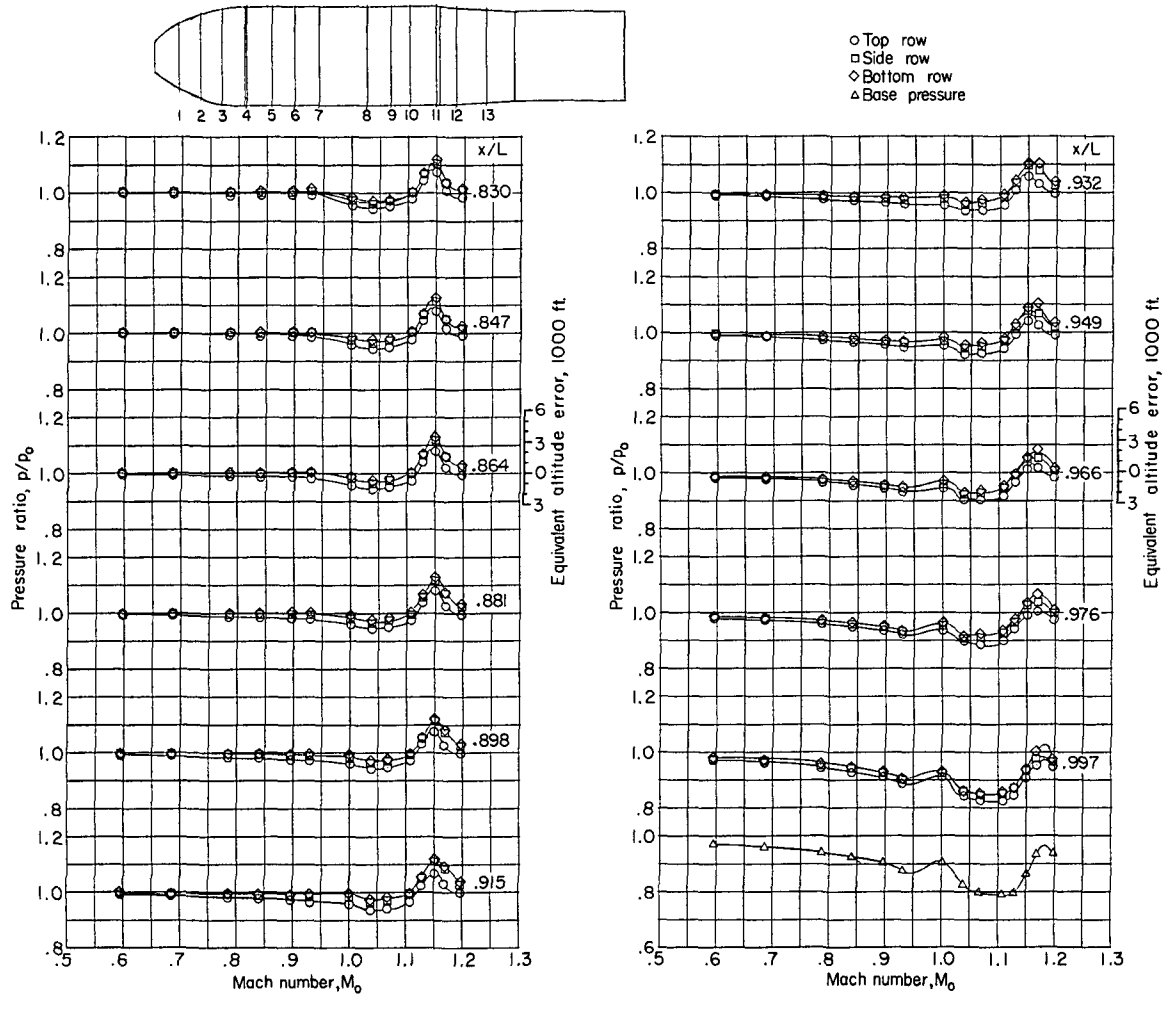

(c) $\alpha = +2^{\circ}$. Concluded.

Figure 17.- Concluded.

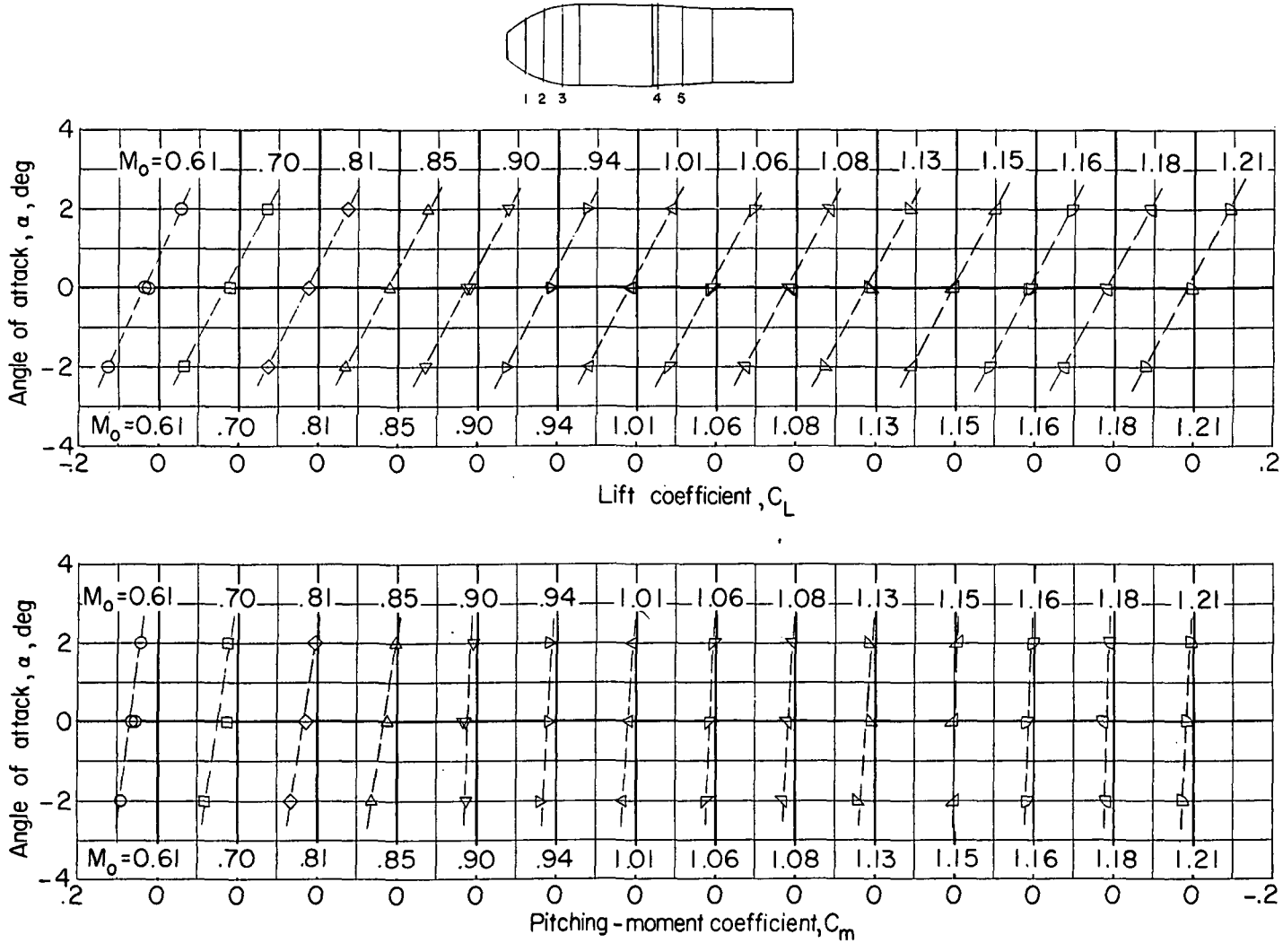

Figure 18.- Variation of the lift and pitching-moment coefficients with angle of attack for the TX-14.

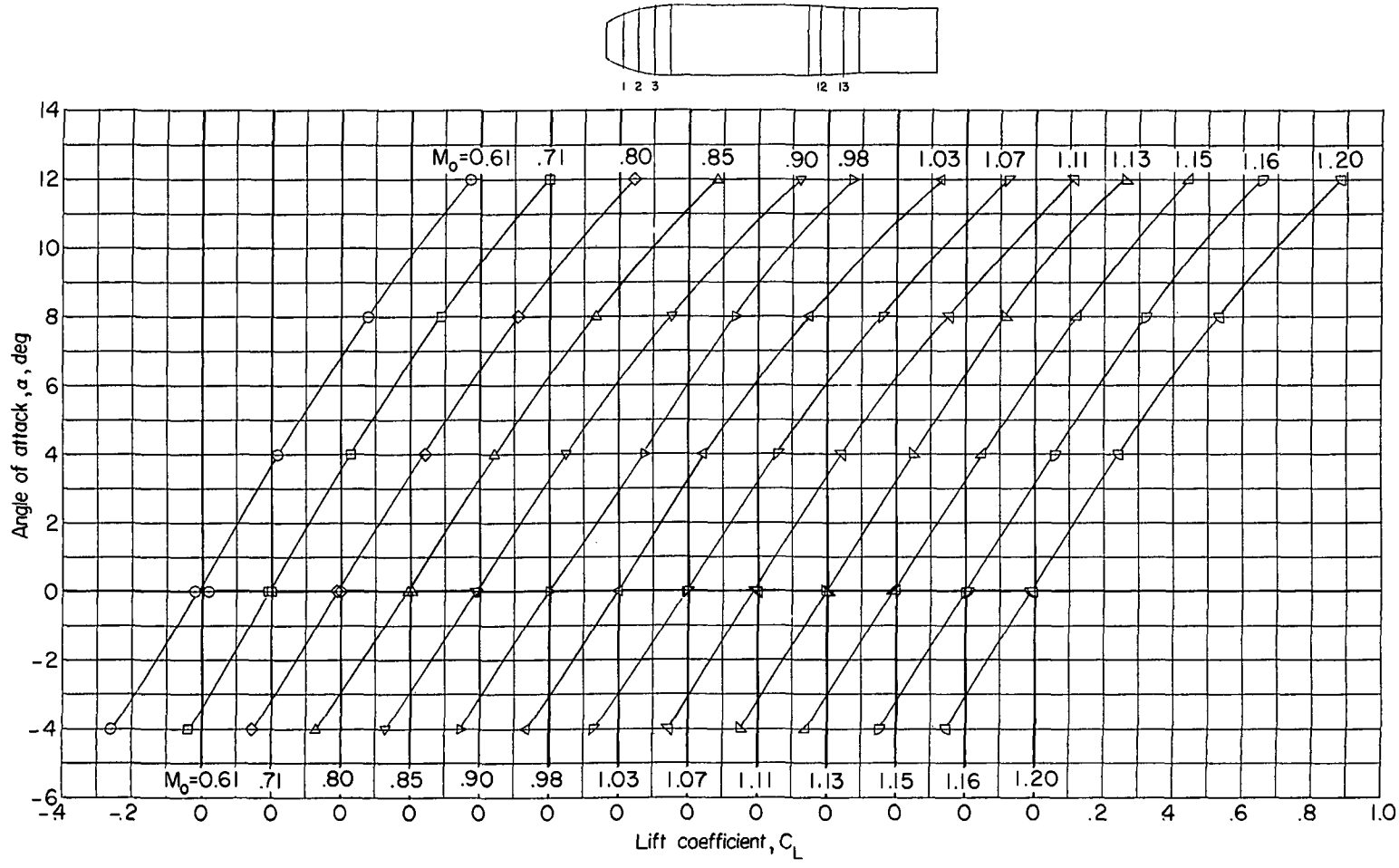

(a) Lift coefficient.

Figure 19.- Variation of the lift and pitching-moment coefficients with angle of attack for the TX-16 with large bands and fins.

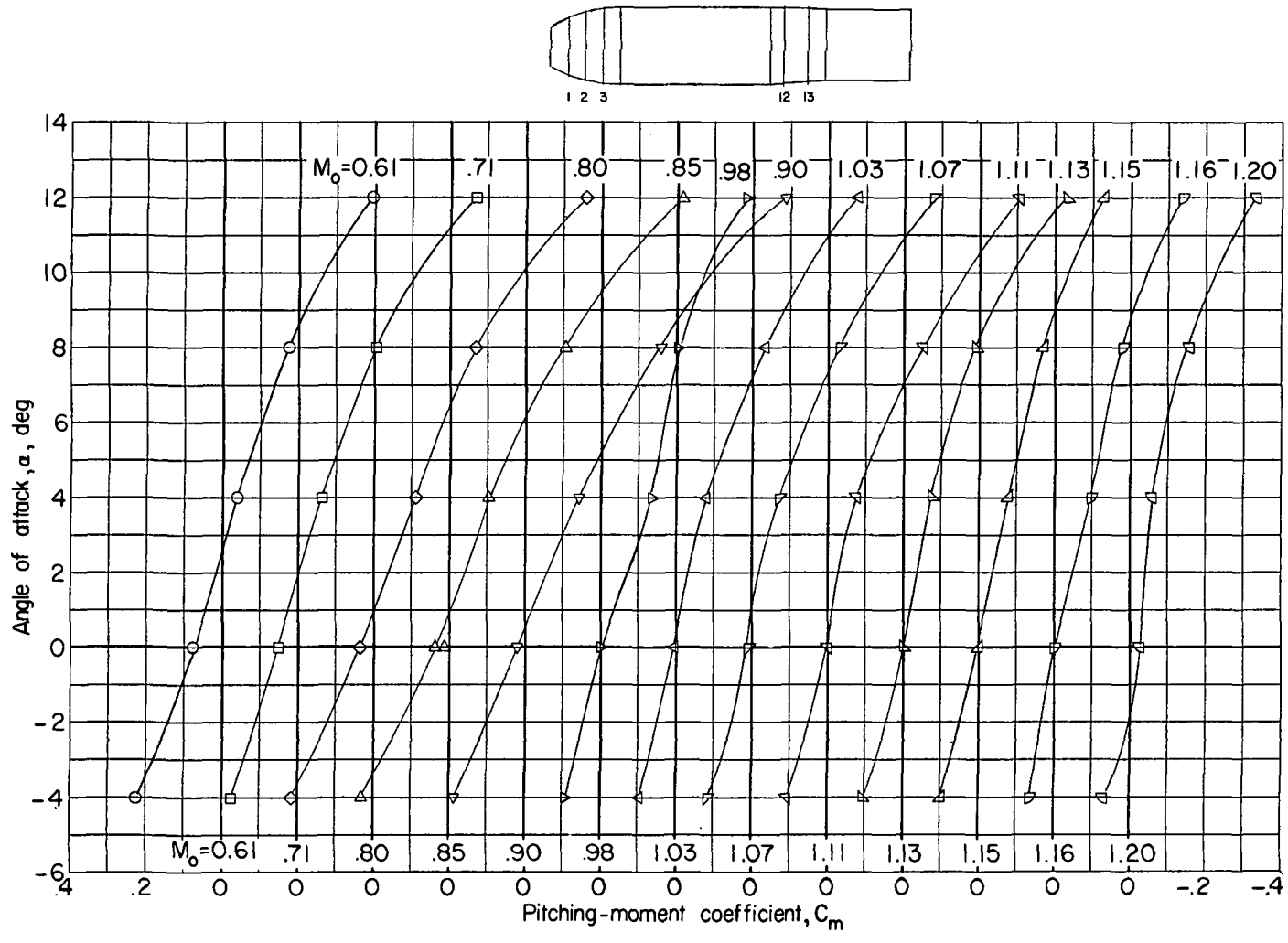

(b) Pitching moment.

Figure 19.- Concluded.

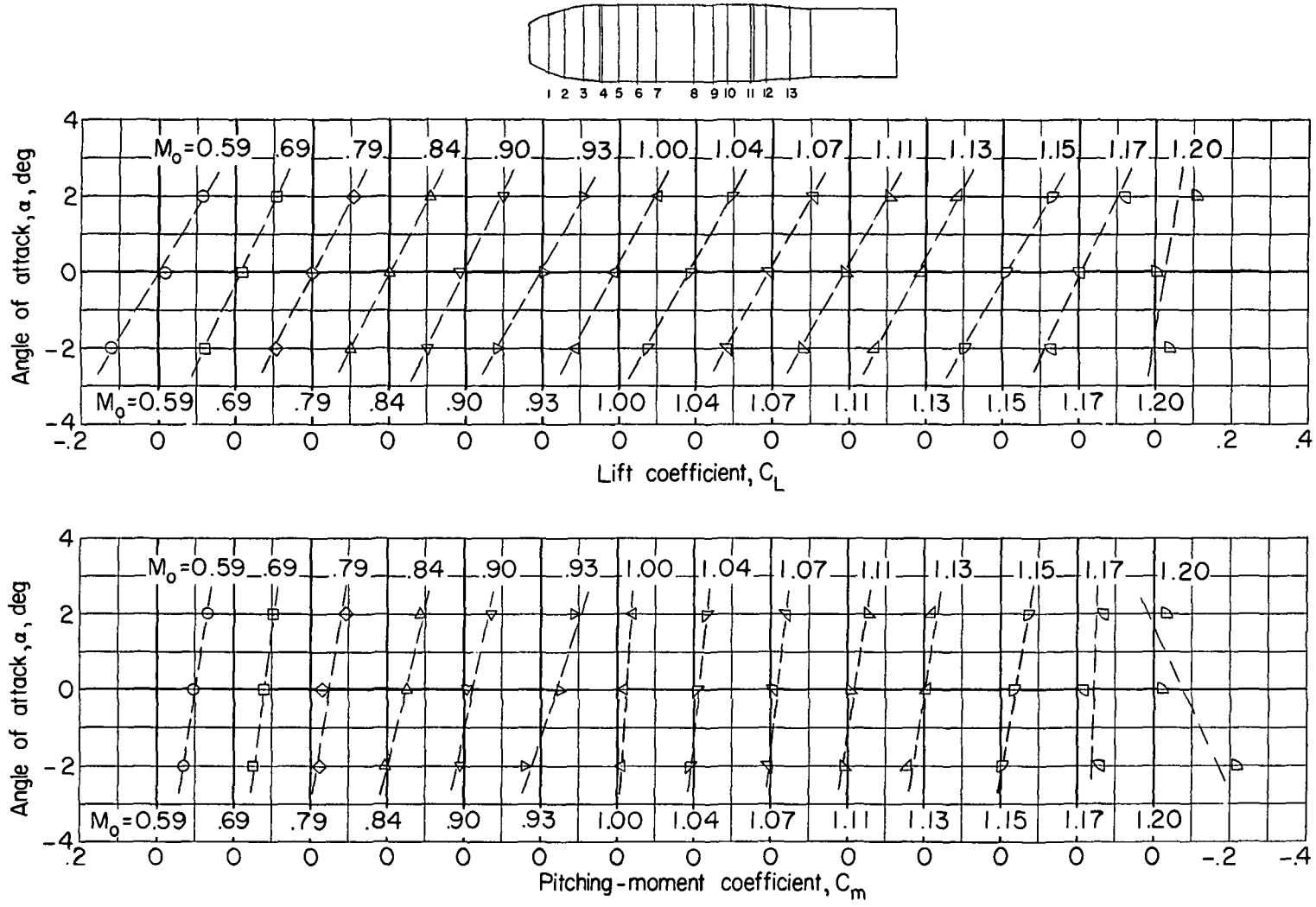

Figure 20.- Variation of the lift and pitching-moment coefficients with angle of attack for the TX-16 with large bands and small fins.

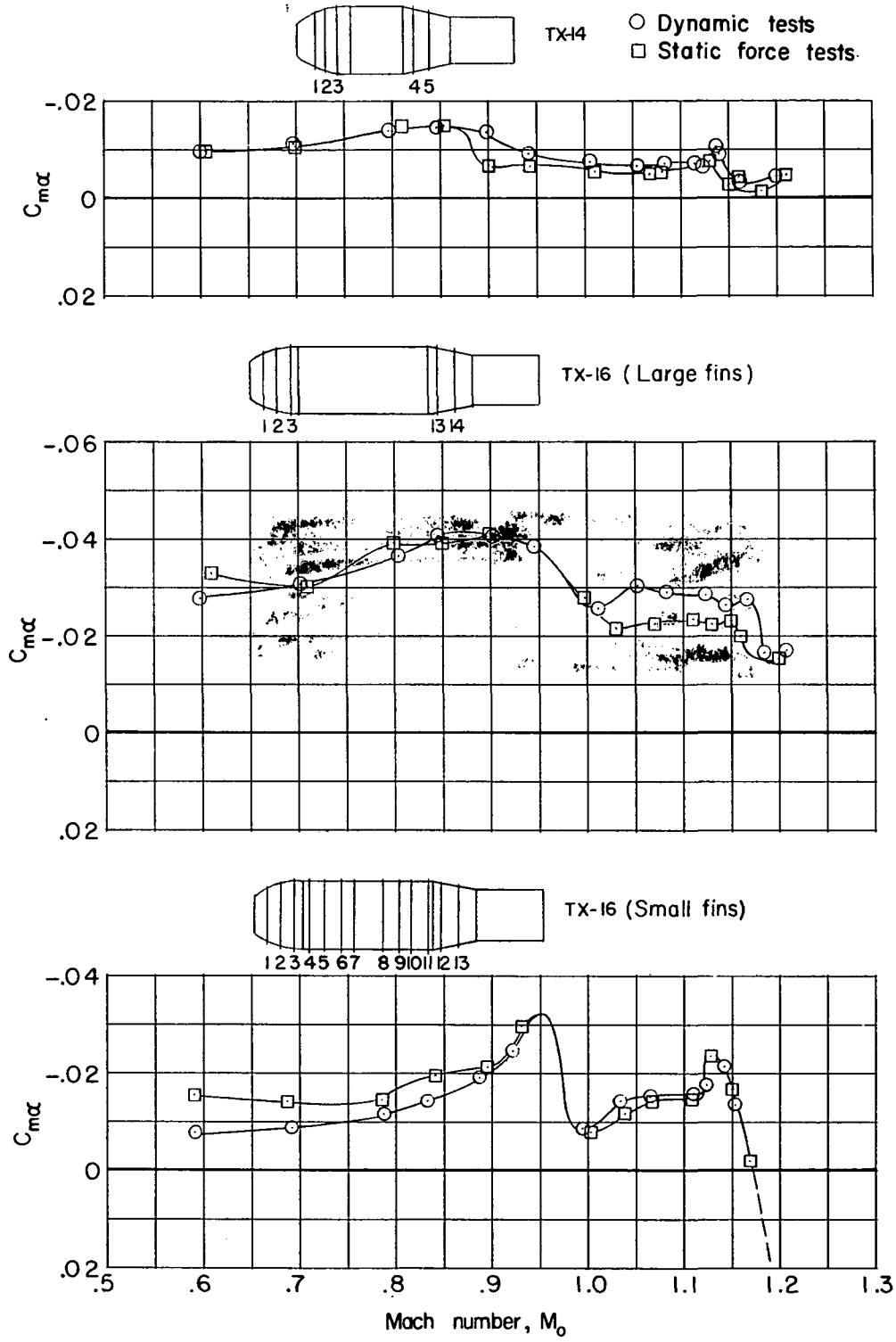

Figure 21.- Comparisons of the static stability parameter C_{m_α} about the 0.408L center of gravity as obtained from dynamic and static tests for the TX-14 and TX-16.